Assessment of Ventricular Function using Gated Blood Pool Planar and - SPECT Imaging: A Phantom Study

by

Hané Pieters

A dissertation submitted in fulfilment of the requirements in respect of the

Master's Degree (MMedSc) in Medical Physics

in the Department of Medical Physics in the Faculty of Health Sciences at the University of the Free State.

Submission Date:

5 December 2023

Supervisor: Dr JA van Staden

Co-Supervisors: Dr H du Raan and Dr FCP du Plessis

DECLARATION

I, Hané Pieters, declare that the Master's Degree research dissertation or interrelated, publishable manuscripts/published articles, that I herewith submit for the Master's Degree qualification in Medical Physics at the University of the Free State is my independent work, and that I have not previously submitted it for a qualification at another institution of higher education.

I hereby declare that I am aware that the copyright is vested in the University of the Free State. All royalties regarding intellectual property that were developed during and/or in connection with the study at the University of the Free State will accrue to the University.

This research was approved by the Health Sciences Research Ethics Committee; initial ethics clearance number: UFS-HSD2021/1792-0001. The study did not contain any human or animal subjects.

Date of submission: 5 December 2023

Signature: H Pieters

ACKNOWLEDGEMENTS

I thank the Lord for this opportunity and the blessings bestowed upon me throughout my life. I trust in His unwavering support and appreciate the daily strength and encouragement He provides.

"Keep vigilant watch over your heart; that's where life starts." Proverbs 4:23 MSG

Dr J van Staden, Dr H du Raan, and Dr F du Plessis, I cannot express my gratitude enough. Thank you for serving as exceptional supervisors, mentors, and role models. Under your guidance, my knowledge and passion for research have significantly grown. Your support and hard work have been invaluable, and I will forever appreciate it.

Dear family and soon-to-be extended family, I want to express my deepest gratitude for the endless encouragement and steadfast support. I take great pride in being a part of such a loving and supportive family. Mom and Dad, your assistance in helping me reach my dreams means the world to me. There has never been a shortage in the love you have for your children. My appreciation for both of you is beyond words.

I extend my gratitude to the Department of Nuclear Medicine, Universitas Academic Hospital and to the Department of Nuclear Medicine, Klerksdorp/Tshepong Hospital Complex. Thank you to everyone who assisted me with my studies. I appreciate all of you. Secondly, thanks to Mr Albert van Eck from the Division of High-Performance Computing at the University of the Free State, for the use of the high-performance cluster and his technical support. I extend a final thank you to Prof Charles Herbst for his invaluable programming assistance.

My Medical Physics friends, old friends, and new friends thank you for your ongoing support and love. Your encouragement has been a source of strength through it all.

To my fiancé, Sean. Thank you! Thank you for being there from the beginning to the end. Thank you for your endless support and daily encouragement. Thank you for being my all-in-one. And most of all, thank you for your boundless love every day.

TABLE OF CONTENTS

ABSTRACT

In the field of Nuclear Medicine, Gated Blood Pool (GBP) investigations are essential in offering vital insights into cardiac function, specifically the Left Ventricular Ejection Fraction (LVEF). The evaluation of ventricle volume changes during the end-diastolic (ED) and end-systolic (ES) phases plays a critical role in detecting, diagnosing, and managing various cardiac diseases. While the longstanding preference for Gated Blood Pool Planar (GBP-P) methods lies in their validation, non-invasiveness, and straightforward application, challenges such as anatomical overlap and the need for background correction persist.

The theoretical superiority of three-dimensional (3D) analogues, specifically Gated Blood Pool SPECT (GBP-S) studies, promises to overcome GBP-P challenges by offering true volumetric representation without the need for background correction. However, this transition introduces complexity in algorithms and processing software needed for GBP-S studies. Accuracy and precision in determining LVEF is paramount in both GBP-P and GBP-S methods to avoid misdiagnosis, improper treatment, or negligence. Rigorous testing and comparison to known or true values are imperative for validating GBP processing software programs to meet set standards.

A key advancement in validating these software programs is the use of digital hybrid phantoms, notably the advanced 4D-XCAT model. The model, blending voxelised and mathematical elements, mimics human anatomy and physiology. Paired with the Monte Carlo (MC) code, SIMIND, these 4D-XCAT models can be used to simulate clinically realistic GBP images, generating a database for testing, and validating various GBP software packages. Importantly, this approach avoids radiation exposure to patients and researchers and enhances the reliability of outcomes by providing benchmark input parameters for software evaluation.

The primary aim of this investigation was to assess ventricular function using MC-simulated GBP-P and GBP-S images of digital patient phantom studies based on 4D-XCAT models with varying cardiac volumes and functions. The aim was achieved by considering three objectives. Firstly, a Monte Carlo simulated cardiac phantom for planar and SPECT studies was validated. The modelled gamma camera was verified using routine quality control procedures outlined by the National Electrical Manufacturers Association (NEMA). Furthermore, 3D cardiac phantoms were printed and imaged according to GBP-P and GBP-S imaging guidelines. Simulated images of these phantoms were generated using the MC code SIMIND and compared to the gamma camera-acquired images. The successful verification of these simulated images led to the next step, namely verifying the use of the 4D-XCAT model in image simulations. By simulating GBP-P and GBP-S studies of a single 4D-XCAT model, the study demonstrates excellent agreement between known and calculated ventricular parameters, confirming the reliability of the 4D-XCAT model in simulating cardiac imaging.

Building on the successful simulation of the 4D-XCAT model, the second objective involved the creation of a comprehensive database comprising 64 clinically realistic GBP patient models. GBP-P simulated images from these models were utilised to evaluate four commercially available GBP-P processing software programs. The study yielded a strong correlation

between calculated LVEF values and known values, thereby affirming the reliability and accuracy of the GBP-P processing software.

Lastly, the research was extended to include clinically realistic GBP-S studies as part of the third objective. The phase focused on assessing the commercially available GBP-S processing software, Quantitative Blood Pool SPECT (QBS), from Cedars-Sinai. GBP-S images of the 4D-XCAT GBP database were simulated according to established imaging guidelines. The study assessed the accuracy of QBS in terms of LV volumes and EF values for two different reconstruction techniques and found a strong correlation between the calculated and known LV volumes and EF values. This paved the way for future multi-centre studies to validate other GBP-S processing software packages.

Key terms: Nuclear Medicine, gated blood pool studies, ejection fraction, ventricular function, end-diastolic volumes, end-systolic volumes, stereolithography printing, validating processing software, Quantitative Blood Pool SPECT (QBS), Monte Carlo simulations, digital 4D-XCAT phantom.

ABBREVIATIONS AND ACRONYMS

The abbreviations and acronyms used in this study are listed below in alphabetical order.

2D	Two-dimensional
3D	Three-dimensional
4D	Four-dimensional
^{99m}Tc	Technetium-99m
AN	Alfanuclear
ANOVA	Analysis of variance
Bkg	Background
BMI	Body Mass Index
CMR	Cardiac Magnetic Resonance
Cps	Counts per second
CT	Computed Tomography
CV	Coefficient of Variation
EC	Echocardiography
ECG	Electrocardiogram
ED	End-diastolic
EDV	End-diastolic volume
EF	Ejection Fraction
ES	End-systolic
ESV	End-systolic volume
FBP	Filtered back projection
FWHM	Full Width at Half Maximum
FWTM	Full Width at Tenth Maximum
GBP	Gated Blood Pool
GBP-P	Gated Blood Pool Planar
GBP-S	Gated Blood Pool SPECT
GE-X	Xeleris by General Electric
ICC	Interclass Correlation Coefficient

IR	Iterative reconstruction
LA	Left Atrium
LAO	Left anterior oblique
LEHR	Low energy high resolution
LV	Left Ventricle
LVEF	Left Ventricular Ejection Fraction
MC	Monte Carlo
MCAT	Mathematical Cardiac-Torso
mCi	millicurie
MBq	Megabecquerel
MPI	Myocardial Perfusion Imaging
M-TT	Tera-Tomo from Mediso
MUGA	Multigated Acquisition Scan
NaI(Tl)	Sodium Iodide crystal doped with Thallium
NCAT	NURBS-based Cardiac-Torso
NEMA	National Electrical Manufacturers Association
NMISA	National Metrology Institute of South Africa
NURBS	Nonuniform Rational B-splines
OSEM	Ordered-subsets expectation maximization
PET	Positron Emission Tomography
PMTs	Photo Multiplier Tubes
QBS	Quantitative Blood Pool SPECT
RA	Right Atrium
RBCs	Red blood cells
ROI	Region of Interest
RV	Right Ventricle
RVEF	Right ventricular ejection fraction
SIMIND	SIMulation of Imaging Nuclear Detectors
SM	Siemens
SPECT	Single-Photon Emission Computed Tomography
4D-XCAT	4D Extended Cardiac-Torso

CHAPTER 1 - INTRODUCTION

Table of Contents

1. Nuclear Medicine

Nuclear Medicine comprises a multifaceted domain encompassing diagnostic and therapeutic divisions in medical science. It employs radionuclides for diagnosing, staging, treating diseases, and monitoring disease response. This thesis focuses extensively on the diagnostic facet, delving into the intricate world of Nuclear Medicine cardiac studies. A Nuclear Medicine study involves administering a compound labelled with a small amount of radioactivity [1]. When labelled with a radioactive isotope, these compounds are referred to as "radiotracers". The chemistry behind radiotracers ensures the targeted absorption of the tracer within specific organs or regions, ranging from bones and kidneys to the cardiac muscle and blood pool. The radioactive isotope of choice for diagnostic Nuclear Medicine emits photons (e.g. gamma rays), which special medical imaging devices, e.g. gamma cameras, can detect. One of the main characteristics of a radiotracer is its ability to investigate the components of a homeostatic system without influencing the functionality of the system [2].

George de Hevesy laid the foundation of the radiotracer in 1913 by labelling non-radioactive lead with a radioactive isotope of radium. In 1923, he applied this principle to investigate plant and animal physiology using radium-labelled lead [1]. The first human study utilising radiotracers was performed in 1927 by Blumgart and Weiss [1] to assess cardiovascular performance using Bismuth-214. In the 1950s, Hal Anger developed the Anger camera, the predecessor of all single-photon imaging systems [1,3]. Paul Harper and colleagues paved the road for Nuclear Medicine imaging using Technetium-99m (^{99m}Tc) for thyroid imaging in 1964 [1]. The modern era started in the 1970s when Kuhl and colleagues developed single-photon emission computed tomography (SPECT), and Phelps and colleagues developed positron emission tomography (PET) [1].

The SPECT gamma camera (illustrated in Figure 1.1) is the primary imaging instrument used in Nuclear Medicine. It consists of various components, including photomultiplier tubes (PMTs), a large area sodium iodide scintillation crystal doped with thallium (NaI(Tl)), a light guide between the PMTs and the scintillation crystal, and a high-density material (e.g. lead) collimator [1]. Most of the photons emitted by the patient due to the administered radioactivity and not aligned with the holes of the collimator are absorbed by the collimator. The photons passing through the collimator holes are absorbed in the NaI(Tl) crystal, causing scintillation light emission. These light photons strike the PMTs and generate electrical signals [4], which are subsequently amplified by the preamplifiers. The amplified product is then converted into electrical signals by the analogue-to-digital converter, carrying information about the energy and position of the photons emitted by the patient [5]. Through a positioning circuit, the output of each PMT serves a dual purpose: firstly, defining

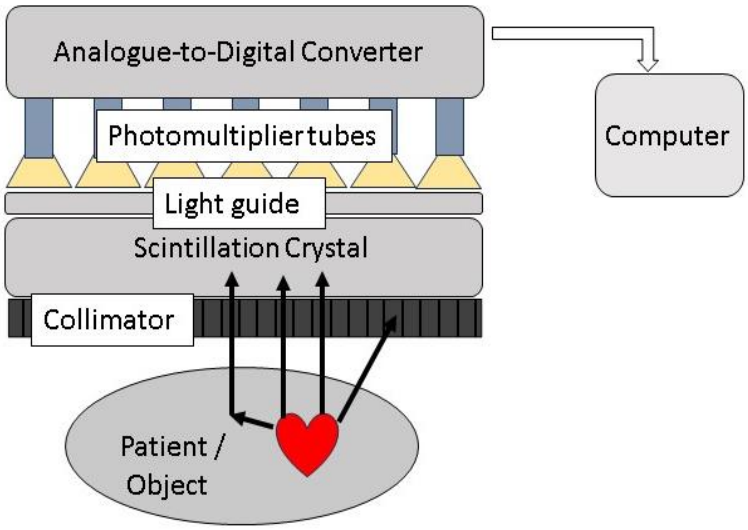

Figure.1.1: Basic gamma camera illustration

the X and Y coordinates of the gamma-ray interaction site in the detector. Simultaneously, the PMT outputs are summed to create the energy pulse. This pulse, representing the energy characteristics of the detected gamma rays, is then subjected to pulse height analysis. An image is formed on a computer, allowing for further image manipulation.

Clinical images are crucial in providing diagnostic and quantitative information contributing to patients' well-being. Therefore, ensuring optimal gamma camera performance is of paramount importance. The National Electrical Manufacturers Association (NEMA) has developed a series of standards and guideline publications [6], establishing consistent criteria for measuring and reporting performance parameters. This documentation undergoes periodic review with updates every five years [6]. The range of tests includes, but is not limited to, spatial resolution, sensitivity, and energy resolution. Spatial resolution measures the gamma camera's ability to accurately resolve radioactive sources separated by a small distance [6]. The sensitivity of a gamma camera, measured as the count rate per specific activity [6], is essential from a statistical perspective, as maximum sensitivity ensures that a maximum number of photons are detected within a given measuring time [1]. Meanwhile, energy resolution characterises the gamma camera's ability to accurately identify photopeak events that differ in small amounts of energy [6]. As described by NEMA, the results of these tests should meet or exceed the specifications set by the manufacturer [6]. Following a quality control program using the tests defined by NEMA will ensure optimal performance of the gamma camera, guaranteeing that the results obtained from the gamma camera and reported by a Nuclear Medicine specialist are reliable and accurate.

The clinical tests acquired with a gamma camera assist specialists in diagnosing patients, describing the functionality of some organs, and justifying specific procedures such as surgery or initiating chemotherapy.

2. Cardiac Ejection Fraction Assessment

Cardiac function evaluation in medicine is a comprehensive process that involves assessing the heart's ability to pump blood effectively. One of the key parameters used in this evaluation is ventricular ejection fraction (EF). EF quantifies the percentage of blood ejected from the ventricle with each contraction, providing critical insight into overall cardiac performance. The EF is calculated as a percentage in terms of end-diastolic volume (EDV) and end-systolic volume (ESV).

$$\mathrm{EF} = \frac{\mathrm{EDV} - \mathrm{ESV}}{\mathrm{EDV}} \times 100 \qquad (1)$$

Several imaging modalities can be used to evaluate ventricular function to calculate the EF; these may vary in accuracy, ease of use, availability, reliability, and cost-effectiveness [7]. The left ventricular ejection fraction (LVEF) may be determined by cardiac magnetic resonance (CMR) imaging, two- and three-dimensional echocardiography (2D- and 3D EC), and computed tomography (CT). Nuclear imaging studies such as gated blood pool (GBP) (planar and SPECT) and SPECT myocardial perfusion (MPI) studies [7–12] are particularly useful in assessing global and regional ventricular function. An advantage of three-dimensional studies is that volume information is available, and the superimposition of structures is avoided, allowing for more accurate left and right ventricular EF (LVEF and RVEF) calculations [7,13]. Recently, first-pass radionuclide angiography with PET has become an alternative to other LVEF-assessing methods [14]. Table 1.1 presents the main advantages and disadvantages of some of these imaging modalities [8,9,12].

Table.1.1: Advantages and disadvantages of different imaging modalities used to calculate ventricular ejection fraction.

IMAGING MODALITIES	Advantages	Disadvantages
CMR	– May be considered as the gold standard. – Volumetric. – Few assumptions are made to obtain the LV volume cavity. – High contrast resolution. – High signal-to-noise ratio. – Lack of ionising radiation. – High reproducibility.	– Implanted devices are contraindications. – Costly. – Low availability. – Breath-holding techniques are required for the patients (otherwise image quality may deteriorate).
2D EC	– Lack of ionising radiation. – Portable units. – Inexpensive.	– Operator dependent. – Poor image quality.
3D EC	– Lack of ionising radiation. – Portable units. – Inexpensive. – Volumetric. – Less variable and more accurate compared to 2D EC.	– Semi-automated processing software is operator-dependent. – Poor image quality. – Breathing motion may cause artefacts.
CT	– Few assumptions are made to obtain the LV volume cavity. – Images can be obtained within a single breath hold. – Volumetric.	– Makes use of ionising radiation. – Iodinated contrast may cause an allergic reaction. – High contrast and spatial resolution are dependent on the contrast bolus timing.
MPI	– Volumetric. – Myocardial function and perfusion may be done in one test. – Software automatically determines the volume cavity.	– A gated study, which means it is susceptible to problems due to arrhythmias. – Ionising radiation is used.
GBP-P	– Processing software can be manual, semi-automated or fully automated. – No breath-holding techniques required. – No geometric assumptions of the LV volume are required. – No absolute contraindications for this study.	– Ionising radiation is used. – Due to the gated study, arrhythmias may reduce the accuracy of the EF value. – Background calculation is required due to overlapping anatomy. – Poor labelling of the red blood cells may occur, which will also degrade the EF accuracy.
GBP-S	– Volumetric. – Background subtraction is not required. – Processing software can be manual, semi-automated or fully automated. – No breath-holding techniques required. – No geometric assumptions of the LV volume are required.	– Ionising radiation is used. – Due to the gated study, arrhythmias may reduce the accuracy of the EF value. – Poor labelling of the red blood cells may occur, which will also degrade the EF accuracy. – Processing software may be complicated.

CMR – Cardiac Magnetic Resonance; 2D EC – Two-Dimensional Echocardiography; 3D EC – Three-Dimensional Echocardiography; CT – Computed Tomography; MPI – Myocardial Perfusion Imaging; GBP-P – Planar Gated Blood Pool; GBP-S – SPECT Gated Blood Pool

In Nuclear Medicine, Anger's groundbreaking invention of the gamma camera initialised the potential of blood pool imaging. With the evolvement in radiotracers, Nuclear Medicine Cardiology today can be used to accurately diagnose and manage various cardiac conditions e.g., coronary artery disease and cardiomyopathy using SPECT and PET myocardial imaging [15].

Some chemotherapy drugs used for specific cancer treatments in patients are associated with dose-related cardiac muscle cell injury and death, leading to left ventricular dysfunction and heart failure [16,17]. Monitoring the change in LVEF for these patients is thus vital as it remains the basis for identifying cardiotoxicity [17]. LVEF is routinely calculated before and during chemotherapy. Baseline LVEF values are around 50%; therefore, if the LVEF before chemotherapy is below 50% or decreases by 10% during chemotherapy, the treatment will be suspended [18–23]. Accurate calculation of the LVEF value is thus extremely important. Early detection of a low LVEF value or changes in the value between chemotherapy sessions may lead to the prevention of further patient complications [18,21,24–26]. Currently, a 'golden standard' method for measuring LVEF has not been universally accepted [9].

This study will primarily focus on GBP planar (GBP-P) and SPECT (GBP-S) studies using ^{99m}Tc-labelled red blood cells and will be discussed in more detail below.

3. Gated Blood Pool Studies

In the 1970s, the concept of using electrocardiography with cardiac imaging was introduced [18,27]. The QRS complex of the electrocardiogram (ECG) signal provides information regarding the different phases of the heart with the principal peak, the R-wave, corresponding to the heart's end-diastolic (ED) phase [28]. The correspondence of the ED and end-systolic (ES) phases with the ECG signal is illustrated in Figure 1.2. Gating the cardiac cycle means it is divided into short intervals and images are synchronised with the different phases of the heart's contraction and relaxation cycle [19,23]. The R-wave is the trigger that represents the start of a new cycle [19]. Each interval corresponds to a different phase of the cardiac cycle, so an illusion of a beating heart can be viewed in cinematic display [19]. Without gating these studies, a blurred image due to cardiac wall motion will be observed [19].

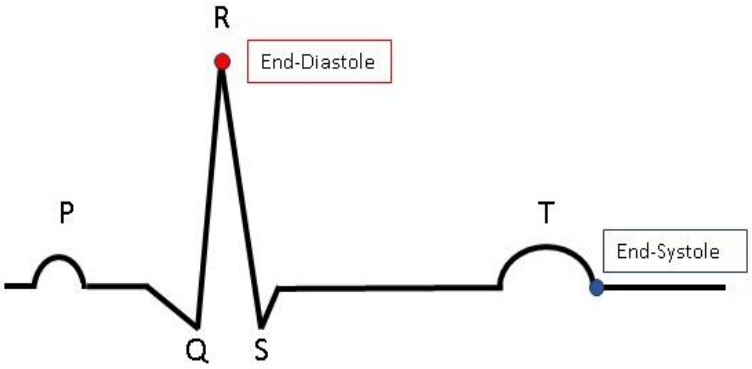

Figure 1.2: The QRS complex of the ECG signal provides necessary information such as the end-diastolic and end-systolic phases of the heart.

GBP studies are also known as radionuclide angiography, radionuclide ventriculography, or multigated acquisition scans (MUGA). This relatively simple and non-invasive study is commonly used to evaluate myocardial wall motion and ventricular function [21,29–35]. GBP studies also play a key role in detecting, diagnosing, and managing various cardiac diseases, including chronic heart failure, myocardial infarction, monitoring cardiotoxicity, coronary artery disease and dilated cardiomyopathy [7,19,21,31,33,35–37].

Effectively evaluating and interpreting imaging data relies heavily on key parameters such as image acquisition, reconstruction, processing, and quantification [38]. The accurate measurement of EF is of high importance, and inaccurate EF values not only risk misdiagnosis

but can potentially lead to fatal outcomes for patients. Over time there have been notable improvements in processing software that have led to semi-automated and automated processing, which reduces the operator's dependability. While semi-automated processing has introduced a level of automation, manual intervention is still required. This may include tasks such as selecting the LV or adjusting the regions of interest (ROI) selected by the processing software. The manual intervention after selecting automated processing may be beneficial, as the ROI may be adjusted according to the ventricles if the automated process falls short.

3.1. Planar Gated Blood Pool Studies

For LVEF calculation, GBP-P studies are acquired with the patient positioned supine and the detector in the left anterior oblique position. A minimum of 16 time-frames per R-R interval is required, but a higher framing rate (32 frames/R-R interval) is preferred [36]. Image duration is typically 10 – 15 minutes to ensure adequate counting statistics.

In GBP-P studies, there is an overlap of anatomical structures, that may affect the LVEF accuracy due to activity contribution from surrounding structures filled with activity such as the right ventricle (RV). Notably, the calculation of RVEF is often omitted due to the overlap between the right atrium and RV in the left anterior oblique view [39,40]. Given the absence of volumetric information in 2D images, Equation 2 below is used to calculate the EF for GBP-P studies.

To derive the ED and ES frames, a time activity curve is generated over the heart. Counts for ED and ES are obtained from selected ROIs positioned over the ventricle during their respective phases, while the background (Bkg) counts are obtained from an ROI adjacent to the ventricle. The EF calculation for GBP-P studies mandates background correction to account for surrounding tissue (over and underlying) such as lung and soft tissues containing radioactive-labelled red blood cells. Careful consideration is given to prevent interference from structures with high counts, such as the aorta, ensuring an accurate correction without artificially elevating background values. Other factors that may cause errors in the calculation of the LVEF include low count densities and the partial volume effect [41].

$$\mathrm{EF} = \frac{(\mathrm{ED\ counts} - \mathrm{Bkg\ counts}) - (\mathrm{ES\ counts} - \mathrm{Bkg\ counts})}{(\mathrm{ED\ counts} - \mathrm{Bkg\ counts})} \times 100 \qquad (2)$$

The selection of ED and ES ROIs can be carried out either manually or automatically. Automatic edge detection commonly employs a zero crossing, second derivative edge tracking algorithm [42]. In this process, edges are systematically sought radially outward from the ventricle centre.

3.2. SPECT Gated Blood Pool Studies

Tomographic imaging methods play an increasingly crucial role in the modern era of medical diagnostics. The growing significance of these methods is underscored by advancements in techniques and the expanding scope dedicated to their application [38]. GBP-S imaging can address many of the shortcomings and challenges of GBP-P studies. GBP-S is a 3D analogue of GBP-P studies offering the advantages of tomographic imaging. Wright et al [43] reported improved repeatability of EF calculation obtained due to ideal ventricle separation, direct

volume calculation, and eliminating the need for background correction; thus, making use of Equation 1. Another significant advantage of GBP-S studies is that they enable simultaneous assessment of biventricular function [44]. Since the RV function evaluation is clinically relevant, it may improve the management of the patient [44]. Despite all the advantages, GBP-S studies have not yet replaced GBP-P studies in many institutions.

During image acquisition of GBP-S studies, the patient assumes a supine position with arms raised above the head. The heart, located to the left side of the middle mediastinum between thoracic vertebrae T5-T8, is imaged using a 180° rotation orbit ranging from 45° right anterior oblique to 45° left posterior oblique in a non-circular trajectory. The imaging process predominantly adopts a step-and-shoot mode, utilising a 64 × 64 matrix and a pixel size in the order of 6.4mm, and acquiring at least 64 projections as outlined by Hesse et al [36,45]. To effectively capture the contracting cycle of the heart, the R-R cycle is divided into eight or preferably 16 intervals, and gated images are acquired at each projection angle. More time-frames per projection provide a better temporal resolution. The overall acquisition time is kept between 20 to 30 minutes ensuring sufficient count statistics for acceptable image quality.

Processing of the GBP-S images involves reconstructing the acquired projection data to generate 3D representations of the heart at each gated phase of the cardiac cycle. Image reconstruction can be performed through Filtered Back Projection (FBP) using a modified Ramp filter [29,32,44]. Alternatively, an Iterative Reconstruction (IR) algorithm, such as the Ordered Subset Expectation Maximisation (OSEM) algorithm, can be employed with a pre-selected number of iterations and subsets, as well as post-filtering of images.

FBP is an analytical image reconstruction method and is often used for GBP-S processing [46,47]. The method is simplistic and quick and is also known for its computational efficiency [46,47]. In short, acquired projection data undergoes mathematical filtering, using a modified Ramp filter in the frequency domain. The filtered frequency information is then inversely transformed to generate filtered projection images, which are then backprojected for the different projection angles creating an accurate representation of the initial object (patient/phantom) [1,46,47]. A disadvantage of FBP is that the reconstructed images appear noisy [1,46].

IR methods are known for their ability to effectively reduce noise, minimise image artefacts and enhancement of spatial resolution, and therefore can provide more accurate quantitative measurements of radioactivity. One of these methods, OSEM, makes use of multiple iterations to obtain an accurate estimation of the initial object [46–48]. The iterations include calculations by forward-projected data based on a previous iteration and comparing the current image estimate with the raw acquisition [1,46,47]. The iterative process is repeated until the difference between the reconstructed estimate and the raw acquisition data reaches a certain convergence criterion, indicating an accurate or sufficiently stable solution [1,46]. The drawback is that IR methods are computationally more intensive than FBP methods [1,46]. However, with the improvement in computational speed and the introduction of OSEM, IR methods have replaced FBP to a large extent in SPECT image reconstruction in Nuclear Medicine [1].

After reconstruction of the GBP-S studies, the reconstructed image datasets are re-orientated into short-axis slices by manually selecting left ventricular symmetry axes. Subsequently, the images undergo quantitative analysis, providing crucial information about the ED and ES volumes, as well as the EF of the ventricles. Quantitative Blood Pool SPECT (QBS) software, which forms part of the Cedar-Sinai Cardiac Suite, developed by QUAD, is one such processing software package that is commercially available [49].

The sophisticated QBS algorithm, described in detail by Van Kriekinge and colleagues [50,51] was initially developed for automatic quantitative measurements of the LVEF [50]. Later, it was expanded to encompass the calculation of right ventricular volume and EF values [51]. The software uses short-axis gated data image sets and operates in three concise steps. It uses phase analysis to differentiate the left and right ventricles from surrounding structures, extracts the LV endocardial surface, and subsequently extracts the RV endocardial surface, aided by the LV endocardium. The algorithm employs phase-based structure discrimination by generating a three-dimensional data set, utilising cosine transform coefficients of the Time-Activity Curve. The resultant voxel values accentuate the ventricular periphery and atrial regions. The LV and RV components are delineated from a binary mask generated through thresholding and morphologic operations. LV endocardial surface extraction uses a three-dimensional extension of an orientation-based template mechanism, addressing challenges in delineation posed by partial volume effects in SPECT. The RV surface is similarly extracted, with the LV guiding the process. The resulting surfaces compute endocardial volumes and EF values at each interval of the gated data set. QBS has the option to process GBP-S studies completely automatically or semi-automatic with manual adjustments guiding ventricular delineation.

The accuracy and reliability of the EF values determined by different processing software packages must be tested extensively before being used clinically. A significant challenge is evaluating these processing software packages (and possibly improving them) without putting patients or volunteers at risk [52] due to the radiation concern. A further challenge arises from the inability to obtain the precise cardiac volumes necessary for calculating LVEF values from patient data. To resolve these problems, the use of phantoms has been investigated.

4. Phantoms and Simulations

When assessing diagnostic imaging techniques such as GBP studies, using a phantom serves a dual purpose. Not only does it mitigate radiation hazards, but also enhances the reliability of outcomes, providing the option of controlled known input parameters that serve as a valuable benchmark for evaluation [53]. Physical phantoms are specially constructed items that facilitate non-invasive imaging methods and can be used to evaluate the performance of different medical imaging devices and procedures [54]. Several phantom types reflect the evaluation of multiple imaging tasks, including geometrical accuracy, dose algorithm accuracy, image quality, machine- and patient-quality assurance, improvement of irradiation techniques, and the performance of required calibrations [55]. Initially, hollow cylinders containing hollow spheres were used to mimic activity distributions in clinical studies [38]. With the availability of 3D printers, manufacturing clinically realistic physical phantoms has become more accessible. This includes anthropomorphic phantoms with detailed structures such as organs and tumour lesions [38,56].

However, the use of physical phantoms can be limited due to the fixed size and geometry of the phantom. 3D-printed phantoms are expensive, and they reflect a crude representation of the human body [54]. However, a trade-off between anthropomorphism, the complexity of motion and the reproducibility of the motion does exist [56]. Using physical phantoms for calibration purposes can be costly and time-consuming. Furthermore, it is challenging to use phantoms in dynamic and ECG-gating procedures [57].

Digital phantoms, as a substitute for physical phantoms, can be used to create a virtual model of a patient's anatomy and physiology [52]. Imaging data of the digital phantom can be simulated using Monte Carlo (MC) simulations through an accurate computerised model of the physics of the imaging process and a modelled gamma camera.

Nuclear Medicine imaging is well suitable for MC modelling techniques due to the stochastic nature of radiation absorption, transport, and detection processes [58]. The benefits of MC simulations encompass evaluating the performance of an existing detector system, investigating the development of new detector systems, and enabling the assessment of image corrections and reconstruction algorithms [5,58]. The MC code, SIMulation of Imaging Nuclear Detectors (SIMIND) [59], has been extensively utilised for Nuclear Medicine applications. SIMIND emulates a clinical SPECT gamma camera and simulates both planar and SPECT images, performing a range of calculations and measurements common in Nuclear Medicine imaging [60]. SIMIND is frequently used to precisely assess imaging system designs, such as collimators, reconstruction algorithms, and scattering corrections. X-ray CT data is often used to generate voxelised phantoms which can be incorporated in SIMIND simulations [61–64].

Research trials may therefore be conducted entirely on a computer. One of the benefits of using such experiments is that the phantom's exact composition is established, providing a "gold standard" by which to test and refine imaging devices and techniques. The user knows exactly what the simulated images should represent in terms of phantom volumes, shapes, and motion extent. However, for simulation results to be credible, realistic models of human anatomy and cardiac and respiratory motions are required.

Extensive work has been undertaken to develop realistic digital computerised phantoms because of their significant potential in imaging research. Digital phantoms can be classified into three categories: voxelised, mathematical, and hybrid phantoms [58,65]. Voxelised phantoms rely on segmented image data (such as CT data) and thus provide a precise model of patient anatomy [52,65]. However, voxelised phantoms are based on fixed geometries (obtained for a specific patient), posing challenges in modelling anatomical variations or motion [52,65]. In contrast, mathematical phantoms use equations to describe the phantoms and structures inside the body of the phantom. These equations allow for alterations in the size and motion of structures like organs in patient phantoms [65]. Mathematical phantoms, though, have limitations in realistically modelling human anatomy [52,65]. Conversely, hybrid phantoms, offer an advantage by integrating characteristics from both voxelised and mathematical phantoms. Segmented patient data is primarily used to create the hybrid phantoms, but each anatomical entity is described using nonuniform rational B-splines (NURBS) or polygon meshes. NURBS surfaces can accurately model each structure in the body based on patient data [52]. Hybrid phantoms can thus be easily altered to model anatomical changes and motion, making them effective for use with MC simulations to mimic GBP studies, enabling the evaluation of patients' ventricular function.

Digital four-dimensional (4D) hybrid phantoms, such as the extended cardiac-torso (4D-XCAT) phantom proposed by Paul Segars, provide reproducible data and reliable outcomes [56]. The phantom was initially developed as the 4D Mathematical Cardiac-Torso (MCAT) phantom in the 1990s, encompassing male and female anatomies [65]. It aimed to improve the original MIRD-5 model used for radiation dosimetry [65]. While the 4D-MCAT model found success in imaging research, especially SPECT and PET imaging, it still had limitations in terms of geometrical design, resulting in a less realistic model of human anatomy [65].

To create a more advanced computational phantom, the 4D NURBS-based cardiac-torso (NCAT) model was designed [52,65]. NURBS surfaces were used to shape the organs using the 3D Visible Human CT dataset [66] as the foundation [52,65]. The 4D-NCAT model was developed with a focus on enhancing realism in both human anatomy and physiology [65,67], incorporating features such as cardiac beating and respiratory motion. A limitation of this model was that it is based on a single male dataset and confined to the torso region [52,65].

To overcome the limitations of the 4D-NCAT model, the 4D-XCAT was developed. This model included highly detailed whole-body male and female anatomies, based on the high-resolution Visible Male and Female anatomical datasets [56,65,66–69]. With enhanced anatomical detail and the availability of whole-body anatomies for both genders, the 4D-XCAT model became applicable to a broader range of medical imaging applications [65,68]. Further improvements to this model included the integration of a physiologically based, finite-element mechanical model of the heart [69]. Developed within the framework of the Living Heart Project [70] , this model emulates the comprehensive function of the heart across various aspects [69]. This includes electro-mechanical excitation and contraction throughout the cardiac cycle, along with a model for the blood flow and its impact on cardiac function [69]. Figure 1.3 provides a summarised timeline of the model's evolution, from the original MIRD model to 4D-XCAT [52,69]. The timeline is based on the MIRD pamphlet number 5 publication [71], and the respective publications of the models by W.P. Segars and his colleagues [4,52,72].

The 4D-XCAT boasts an unmatched level of detail and anatomical realism and contributes to the usefulness of digital phantoms [67,68]. Comprising a diverse population of male and female anatomies that vary based on age, height, and weight [67–69], this model introduces phantom variability, offering the opportunity to build a comprehensive database with multiple models. Such models prove invaluable for extensive testing of software packages, particularly in the context of GBP studies. The known cardiac chamber volumes and EF values for each model establish a gold standard, facilitating the evaluation of software packages.

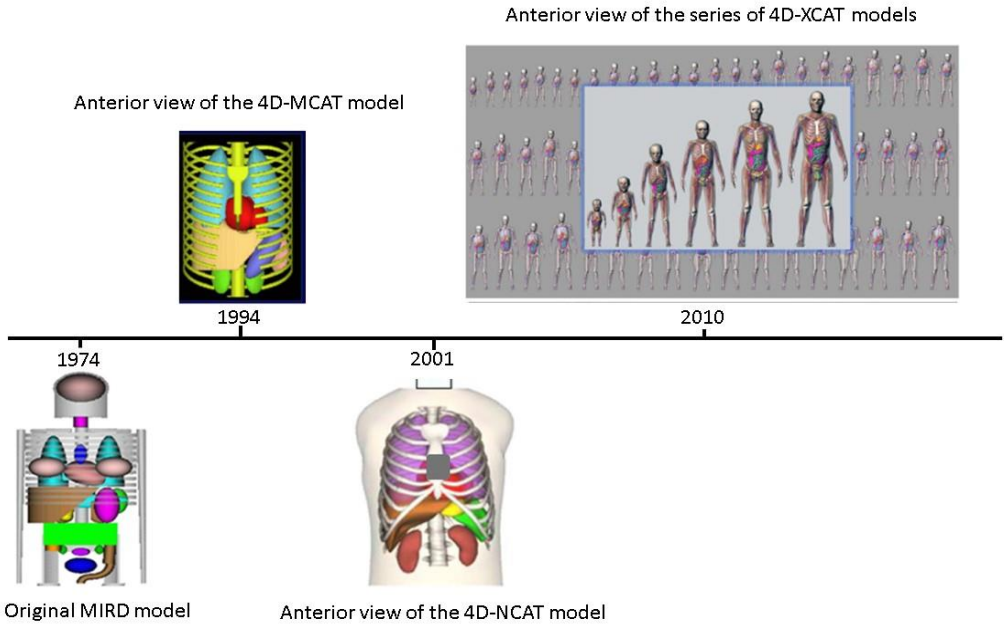

Figure 1.3: Anterior views of the models that led to the development of the 4D-XCAT phantom [65,69]

5. Dissertation Rationale

Ensuring the reliability of any imaging technique or processing software is crucial before its application in a clinical setting. Rigorous testing and verification are essential to confirm the benefits to the patient and to guarantee accurate, reliable, and reproducible results. In the context of GBP studies, ensuring accurate EF values necessitates volumetric information on the cardiac chambers, which is not readily available with human study groups. In recent times the use of phantoms, especially digital human phantoms, enables researchers to test and validate the software packages without posing a radiation hazard to patients or themselves. These phantoms, with known volumetric parameters, can be considered the gold standard.

The intention of this study was thus to adjust parameters such as the heart size and volumes during the cardiac cycle, to generate a comprehensive database of GBP studies encompassing various EF values. The database of studies was simulated for both planar and SPECT studies enabling a comparison of the reliability and reproducibility of not only different software packages but also for the comparison between planar and SPECT studies. Should SPECT studies prove to be more accurate and reliable, GBP-S may replace GBP-P studies at the Universitas Academic Hospital in Bloemfontein, South Africa.

6. Aim of Study

The study aimed to assess ventricular function using GBP-P and GBP-S imaging in simulated patient models with varying cardiac volumes and functions and to test the accuracy, reliability, and reproducibility of commercial software packages.

The following objectives were considered:

I. Validating MC simulated cardiac phantoms for the evaluation of GBP-P and GBP-S studies.
II. Assessing the accuracy of four commercial GBP-P software packages by generating a digital phantom database of GBP-P studies with known LVEF values.
III. Assessing the accuracy of a commercial software package for processing GBP-S studies using the GBP-S generated database with known left ventricular volumes and EF.

7. Summary of Chapters

Articles 1 to 3, summarised below, form the basis of Chapters 2 to 4.

Note to readers: *The referencing styles of the articles (Chapters 2 and 3) are according to the journals' referencing guidelines in which they were submitted/published. Their referencing style is not the same as that of Chapter 1 and the complete bibliography.*

<u>Article 1: Validation of a Monte Carlo simulated cardiac phantom for planar and SPECT studies.</u>

Gated blood pool (GBP) scintigraphy (planar and SPECT), using ^{99m}Tc pertechnetate labelled red blood cells, is commonly used to evaluate the ventricular function of patients thanks to its excellent reproducibility measures. This work aimed to validate MC simulated cardiac phantoms for the evaluation of GBP-P and GBP-S studies. The validation process commenced with a comparison of the gamma camera system performance criteria measurements (energy resolution, spatial resolution, and sensitivity) with the corresponding values obtained through MC simulations. Furthermore, the accuracy of both measured and simulated volumes of two

stereolithography-printed cardiac phantoms (based on 4D-XCAT phantoms) was assessed. The final step involved validating the simulated GBP-P and GBP-S XCAT studies by comparing the calculated LVEF and LV volume values (EDV and ESV) with known parameters, comprehensive validations have been documented in a published manuscript in *Physica Medica* [73], with the front page of the article provided in Appendix A for reference.

Article 2: Assessment of Planar Gated Blood Pool Processing Software using a Simulated Patient Phantom Database.

GBP-P radionuclide imaging serves as a valuable tool for the non-invasive assessment of LVEF. Serial cardiac imaging can be performed to monitor the potential decline in LVEF among patients undergoing cardiotoxic chemotherapy. Consequently, accurate LVEF determination is of paramount importance. Although commercial software programs have significantly improved the reproducibility of LVEF calculation, concerns have arisen regarding the accuracy of these software programs. This study aimed to assess the accuracy of LVEF determination using four commercial software programs. The goal was achieved by generating a database of 64 GBP-P studies utilising the digital hybrid phantom, 4D-XCAT. This database contains models with a range of known LVEF values. The processed values obtained from the commercial software packages were compared against the known values, to ascertain accuracy. The findings of this research have been compiled into a manuscript submitted to *Heliyon* as evidenced by the acknowledgement of submission in Appendix B.

Article 3: Assessment of SPECT Gated Blood Pool Processing Software using a Simulated Patient Phantom Database

The importance of GBP studies is evident as it is a non-invasive procedure that provides valuable information. Gated SPECT studies could replace planar studies as the preferred technique mainly due to their ability to provide volumetric information through tomographic imaging. While GBP-S studies have multiple advantages over planar studies, they have not yet replaced GBP-P studies, primarily due to the complexity of the processing software and the cost thereof. This study aimed to assess the accuracy of Cedar Sinai's GBP-S processing software package, QBS, employing a fully automated approach. Utilising a simulated GBP-S database the studies were reconstructed and processed automatically using QBS. The results of this research constitute a manuscript ready for publication and are currently undergoing finalisation before submission.

8. References

1. Cherry SR, Sorenson JA, Phelps ME. *Physics in Nuclear Medicine*. 4th ed. Elsevier Saunders; 2012.

2. Vallabhajosula S, Killeen RP, Osborne JR. Altered Biodistribution of Radiopharmaceuticals: Role of Radiochemical/Pharmaceutical Purity, Physiological, and Pharmacologic Factors. *Semin Nucl Med*. 2010;40(4):220-241. doi:10.1053/j.semnuclmed.2010.02.004

3. Tapscott E. Nuclear Medicine Pioneer, Hal O. Anger, 1920 - 2005. *J Nucl Med Technol*. 2005;33(4). Accessed August 22, 2023. https://tech.snmjournals.org/content/33/4/250

4. Segars WP, Tsui BMW. (2001) *DEVELOPMENT AND APPLICATION OF THE NEW DYNAMIC NURBS-BASED CARDIAC-TORSO (NCAT) PHANTOM*. PhD Thesis. University of North Carolina. Accessed July 20, 2022. https://deckard.duhs.duke.edu/~wsegars/xcat/segars_NCAT_dis.pdf

5. Ljungberg M, Strand SE, King MA. *Monte Carlo Calculations in Nuclear Medicine*. 2nd ed. (Webster JG, Walz-Flannigan A, Tabakov S, Ng KH, eds.). Taylor & Francis Group; 2013.

6. NEMA Standards Publication. *Standard for Performance Measurements of Gamma Cameras*.; 2018. Accessed January 22, 2023. https://www.nema.org/standards/view/performance-measurements-of-gamma-cameras

7. Hacker M, Hoyer X, Kupzyk S, et al. Clinical validation of the gated blood pool SPECT QBS® processing software in congestive heart failure patients: Correlation with MUGA, first-pass RNV and 2D-echocardiography. *International Journal of Cardiovascular Imaging*. 2006;22:407-416. doi:10.1007/s10554-005-9031-1

8. Man SC, van der Wall EE, Swenne CA. Gated SPECT: What's the ideal method to measure LVEF? *International Journal of Cardiovascular Imaging*. 2008;24(8):807-810. doi:10.1007/s10554-008-9359-4

9. Foley TA, Mankad S V, Anavekar NS, et al. Measuring Left Ventricular Ejection Fraction-Techniques and Potential Pitfalls. *Citation: European Cardiology*. 2012;8(2):108-122. doi:https://doi.org/10.15420/ecr.2012.8.2.108

10. Daly CA, Abbasi S, Kwong RY. Cardiac Imaging. In: McManus LM, Mitchell RN, eds. *Pathobiology of Human Disease: A Dynamic Encyclopedia of Disease Mechanisms*. Elsevier Inc.; 2014:4019-4045. doi:10.1016/B978-0-12-386456-7.07611-5

11. Pellikka PA, She L, Holly TA, et al. Variability in Ejection Fraction Measured by Echocardiography, Gated Single-Photon Emission Computed Tomography, and Cardiac Magnetic Resonance in Patients with Coronary Artery Disease and Left Ventricular Dysfunction. *JAMA Netw Open*. 2018;1(4). doi:10.1001/jamanetworkopen.2018.1456

12. Scatteia A, Silverio A, Padalino R, et al. Non-invasive assessment of left ventricle ejection fraction: Where do we stand? *J Pers Med*. 2021;11(11). doi:10.3390/jpm11111153

13. Marwick TH. Ejection Fraction Pros and Cons: JACC State-of-the-Art Review. *J Am Coll Cardiol*. 2018;72(19):2360-2379. doi:10.1016/j.jacc.2018.08.2162

14. Verrecchia-Ramos E, Morel O, Retif P, Ben Mahmoud S. Innovative procedure for measuring left ventricular ejection fraction from 18F-FDG first-pass ultra-sensitive digital PET/CT images: evaluation with an anthropomorphic heart phantom. *EJNMMI Phys*. 2021;8(1). doi:10.1186/s40658-021-00387-2

15. Underwood SR. A history of nuclear cardiology in the UK. In: *A History of Radionuclide Studies in the UK: 50th Anniversary of the British Nuclear Medicine Society*. Springer International Publishing; 2016:53-62. doi:10.1007/978-3-319-28624-2_8

16. Chia PL, Chiang K, Snyder R, Dowling A. The utility of routine pre-chemotherapy screening with cardiac gated blood pool scan for patients at low risk of anthracycline toxicity. *Journal of Oncology Pharmacy Practice*. 2018;24(4):264-271. doi:10.1177/1078155217697487

17. Henriksen PA. Anthracycline cardiotoxicity: An update on mechanisms, monitoring and prevention. *Heart*. 2018;104(12):971-977. doi:10.1136/heartjnl-2017-312103

18. Giubbini R, Milan E. The time for radionuclide ventriculography resurrection is coming. *Journal of Nuclear Cardiology*. 2016;23(5):1139-1141. doi:10.1007/s12350-015-0245-x

19. Sachpekidis C, Sachpekidis V, Moralidis E, Arsos G. Equilibrium radionuclide ventriculography: still a clinically useful method for the assessment of cardiac function? *Hell J Nucl Med*. 2018;21:213-220.

20. Steyn R, Boniaszczuk J, Geldenhuys T. Comparison of estimates of left ventricular ejection fraction obtained from gated blood pool imaging, different software packages and cameras. *Cardiovasc J Afr*. 2014;25(2):44-49. doi:10.5830/CVJA-2013-082

21. Bresser P, de Beer J, de Wet Y. *A Study Investigating Variability of Left Ventricular Ejection Fraction Using Manual and Automatic Processing Modes in a Single Setting*.; 2015. doi:10.1016/j.radi.2014.10.002

22. Fair JR, Heintz PH, Telepak RJ. Evaluation of new data processing algorithms for planar gated ventriculography (MUGA). *J Appl Clin Med Phys*. 2009;10(3):173-179. doi:10.1120/jacmp.v10i3.2977

23. Mitra D. Equilibrium radionuclide angiocardiography: Its usefulness in current practice and potential future applications. *World J Radiol*. 2012;4(10):421. doi:10.4329/wjr.v4.i10.421

24. Huang H, Nijjar PS, Misialek JR, et al. Accuracy of left ventricular ejection fraction by contemporary multiple gated acquisition scanning in patients with cancer: Comparison with cardiovascular magnetic resonance. *Journal of Cardiovascular Magnetic Resonance*. 2017;19(1). doi:10.1186/s12968-017-0348-4

25. Das GK, Chen Siew NG, Manap MA. Left ventricular ejection fraction by multigated acquisition scan using planar sodium iodide and cadmium-zinc-telluride cameras: a comparison with two-dimensional echocardiography. *Asia Ocean J Nucl Med Biol*. 2023;11(1):55-70. doi:10.22038/AOJNMB.2022.60392.1424

26. Bailey EA, Bailey DL. Results from an Australian and New Zealand audit of left ventricular ejection fraction from gated heart pool scan analysis. *Nucl Med Commun*. 2012;33(1):102-111. doi:10.1097/MNM.0b013e32834c2f0b

27. Kumar R. Multiple Gated Equilibrium Blood Pool Imaging (MUGA). In: Movahed A, Buscombe JR, Gnanasegaran G, Hall M, eds. *Integrating Cardiology for Nuclear Medicine Physicians*. Springer; 2009:344-353. doi:DOI 10.1007/978-3-540-78674-0

28. Germano G, Berman Daniels. Physics and technical aspects of gated myocardial perfusion SPECT. In: Germano G, Berman D, eds. *Clinical Gated Cardiac SPECT*. 2nd ed. Bleckwell Publishing; 2006:27-45.

29. Groch MW, Depuey EG, Belzberg AC, et al. Planar Imaging Versus Gated Blood-Pool SPECT for the Assessment of Ventricular Performance: A Multicenter Study. *J Nucl Med* 2001;42:1773-1779.

30. Bartlett ML, Srinivasan G, Barker WC, Kitsiou AN, Dilsizian V, Bacharach SL. Left ventricular ejection fraction: Comparison of results from planar and SPECT gated blood-pool studies. *Journal of Nuclear Medicine*. 1996;37:1795-1799.

31. Odagiri K, Wakabayashi Y, Tawarahara K, et al. Evaluation of right and left ventricular function by quantitative blood-pool SPECT (QBS): Comparison with conventional methods and quantitative gated SPECT (QGS). *Ann Nucl Med*. 2006;20(8):519-526. doi:10.1007/BF03026815

32. Harel F, Finnerty V, Ngo Q, Grégoire J, Khairy P, Thibault B. SPECT versus planar gated blood pool imaging for left ventricular evaluation. *Journal of Nuclear Cardiology*. 2007;14(4):544-549. doi:10.1016/j.nuclcard.2007.04.020

33. Xie BQ, Tian YQ, Zhang J, et al. Evaluation of left and right ventricular ejection fraction and volumes from gated blood-pool SPECT in patients with dilated cardiomyopathy: Comparison with cardiac MRI. *Journal of Nuclear Medicine*. 2012;53(4):584-591. doi:10.2967/jnumed.111.096057

34. Nicol A, Avison M, Harbinson M, Jeans S, Waddington W, Woldman S. Procedure guideline for planar radionuclide cardiac ventriculogram for the assessment of left ventricular systolic function. *Nucl Med Commun*. 2009;30:245-252. doi:10.1097/MNM.0b013e328321cdba

35. van Dijk JD. Dose-optimization in nuclear cardiac imaging, time for the next step? *Journal of Nuclear Cardiology*. 2019;26(6):1981-1983. doi:10.1007/s12350-018-1441-2

36. Hesse B, Lindhardt TB, Acampa W, et al. *EANM/ESC Guidelines for Radionuclide Imaging of Cardiac Function*. Vol 35.; 2008. doi:10.1007/s00259-007-0694-9

37. Sibille L, Bouallegue F Ben, Bourdon A, Micheau A, Vernhet-Kovacsik H, Mariano-Goulart D. Comparative values of gated blood-pool SPECT and CMR for ejection fraction and volume estimation. *Nucl Med Commun*. 2011;32(2):121-128. doi:10.1097/MNM.0b013e32834155f1

38. Läppchen T, Meier LP, Fürstner M, et al. 3D printing of radioactive phantoms for nuclear medicine imaging. *EJNMMI Phys*. 2020;7:22. doi:10.1186/s40658-020-00292-0

39. Maddahi J, Berman DS, Matsuoka DT, Waxman AD, Forrester JS, Swan HJC. Right Ventricular Ejection Fraction During Exercise in Normal Subjects and in Coronary Artery Disease Patients: Assessment by Multiple-gated Equilibrium Scintigraphy. *American Heart Association*. 1980;62:133-149. doi:10.1161/01.cir.62.1.133

40. Marving J, H PF, Chrammer-jorgensen B, Gadsboll N, Flemming PH. Are right and left ventricular ejection fractions equal? *Circulation*. 1985;3:502-514. doi:10.1161/01.cir.72.3.502

41. Yang SN, Sun SS, Zhang G, et al. Left ventricular ejection fraction estimation using mutual information on technetium-99m multiple-gated SPECT scans. *Biomed Eng Online*. 2015;14:119. doi:10.1186/s12938-015-0117-2

42. Wagner R, Halama JR, Henkin RE, Dillehay GL, Sobotka PA. Errors in the determination of left ventricular functional parameters. *Journal of Nuclear Medicine*. 1989;30:1870-1874. https://www.researchgate.net/publication/20345997

43. Wright GA, Thackray S, Howey S, Cleland JG. *Left Ventricular Ejection Fraction and Volumes from Gated Blood-Pool SPECT: Comparison with Planar Gated Blood-Pool Imaging and*

Assessment of Repeatability in Patients with Heart Failure. *Journal of Nuclear Medicine*. 2003;44:494-498. http://www.sghms.ac.uk/depts/phs/staff/jmb/compsd.htm

44. Dercle L, Ouali M, Pascal P, et al. Gated blood pool SPECT: The estimation of right ventricular volume and function is algorithm dependent in a clinical setting. *Journal of Nuclear Cardiology*. 2015;22:483-492. doi:10.1007/s12350-014-0062-7

45. Hesse B, Tägil K, Cuocolo A, et al. EANM/ESC procedural guidelines for myocardial perfusion imaging in nuclear cardiology. *Eur J Nucl Med Mol Imaging*. 2005;32:855-897. doi:10.1007/s00259-005-1779-y

46. IAEA. Human Health Campus - 3D image reconstruction. Published 2016. Accessed November 29, 2023. https://humanhealth.iaea.org/HHW/MedicalPhysics/NuclearMedicine/ImageAnalysis/3Dimagereconstruction/index.html

47. Lyra M, Ploussi A. Filtering in SPECT image reconstruction. *Int J Biomed Imaging*. Published online 2011. doi:10.1155/2011/693795

48. Trevisan AC, Raed MD, Tumas V, et al. Comparison between OSEM and FBP reconstruction algorithms for the qualitative and quantitative interpretation of brain DAT-SPECT using an anthropomorphic striatal phantom: implications for the practice. *Research on Biomedical Engineering*. 2020;36(1):77-88. doi:10.1007/s42600-019-00034-x

49. Cedars-Sinai. QUAD - Quantitative Diagnostic Software Group. 2022. Accessed October 1, 2023. https://www.csaim.com/

50. Van Kriekinge D, Berman DS, Germano G. Automatic quantification of left ventricular ejection fraction from gated blood pool SPECT. *Journal of Nuclear Cardiology*. 1999;6:498-506. doi:10.1016/s1071-3581(99)90022-3

51. Daou D, Van Kriekinge SD, Coaguila C, et al. Automatic quantification of right ventricular function with gated blood pool SPECT. *Journal of Nuclear Cardiology*. 2004;11(3):293-304. doi:10.1016/j.nuclcard.2004.01.008

52. Segars WP, Sturgeon G, Mendonca S, Grimes J, Tsui BMW. 4D XCAT phantom for multimodality imaging research. *American Association of Physicists in Medicine*. 2010;37:4902-4915. doi:10.1118/1.3480985

53. De Bondt P. *Evaluation of Cardiac Volumes by New Scintigraphic Techniques*. Degree of doctor in medical sciences. University of Ghent; 2005.

54. Akhavanallaf A, Fayad H, Salimi Y, et al. An update on computational anthropomorphic anatomical models. *Digit Health*. 2022;8. doi:10.1177/20552076221111941

55. Filippou V, Tsoumpas C. Recent advances on the development of phantoms using 3D printing for imaging with CT, MRI, PET, SPECT, and ultrasound. *Med Phys*. 2018;45:e740-e760. doi:10.1002/mp.13058

56. Eiben B, Bertholet J, Menten MJ, Nill S, Oelfke U, McClelland JR. Consistent and invertible deformation vector fields for a breathing anthropomorphic phantom: A post-processing framework for the XCAT phantom. *Phys Med Biol*. 2020;65(16). doi:10.1088/1361-6560/ab8533

57. Lee C, Lodwick D, Hasenauer D, Williams JL, Lee C, Bolch WE. Hybrid computational phantoms of the male and female newborn patient: NURBS-based whole-body models. *Phys Med Biol*. 2007;52(12):3309-3333. doi:10.1088/0031-9155/52/12/001

58. Zaidi H. Relevance of accurate Monte Carlo modeling in nuclear medical imaging. *Med Phys*. 1999;26:574-608. doi:10.1118/1.598559

59. Ljungberg M, Strand SE. A Monte Carlo program for the simulation of scintillation camera characteristics. *Comput Methods Programs Biomed*. 1989;29:257-272. doi:https://doi.org/10.1016/0169-2607(89)90111-9

60. Ljungberg M. The SIMIND Monte Carlo Program – Medical Radiation Physics, Lund. Published 2020. Accessed December 4, 2021. https://simind.blogg.lu.se/

61. Bahreyni Toossi MT, Islamian JP, Momennezhad M, Ljungberg M, Naseri SH. SIMIND Monte Carlo simulation of a single photon emission CT. *J Med Phys*. 2010;35:42-47. doi:10.4103/0971-6203.55967

62. Ljungberg M, Larsson A, Johansson L. A New Collimator Simulation in SIMIND based on the Delta-Scattering Technique. *IEEE Trans Nucl Sci*. 2004;52(5):3584-3588. doi:10.1109/TNS.2005.858252

63. Morphis M, van Staden JA, du Raan H, Ljungberg M. Modelling of energy-dependent spectral resolution for SPECT Monte Carlo simulations using SIMIND. *Heliyon*. 2021;7(2). doi:10.1016/j.heliyon.2021.e06097

64. Ramonaheng K, van Staden JA, du Raan H. Validation of a Monte Carlo modelled gamma camera for Lutetium-177 imaging. *Applied Radiation and Isotopes*. 2020;163. doi:10.1016/j.apradiso.2020.109200

65. Segars WP, Ravin CE, Tsui BMW. MCAT to XCAT: The Evolution of 4-D Computerized Phantoms for Imaging Research: Computer models that take account of body movements promise to provide evaluation and improvement of medical imaging devices and technology HHS Public Access. *Proc IEEE Inst Electr Electron Eng*. 2009;97(12):1954-1968. doi:10.1109/JPROC

66. National Library of Medicine. The National Library of Medicine's Visible Human Project. Accessed February 22, 2023. https://www.nlm.nih.gov/research/visible/visible_human.html

67. Segars WP, Tsui BMW, Cai J, Yin FF, Fung GSK, Samei E. Application of the 4D XCAT Phantoms in Biomedical Imaging and Beyond. *IEEE Trans Med Imaging*. 2018;37(3):680-692. doi:10.1109/TMI.2017.2738448.Application

68. Segars WP, Bond J, Frush J, et al. Population of anatomically variable 4D XCAT adult phantoms for imaging research and optimization. *Med Phys*. 2013;40(4). doi:10.1118/1.4794178

69. Segars WP, Veress AI, Sturgeon GM, Samei E. Incorporation of the Living Heart Model into the 4D XCAT Phantom for Cardiac Imaging Research. *IEEE Trans Radiat Plasma Med Sci*. 2019;3(1):54-60. doi:10.1109/TRPMS.2018.2823060

70. Living Heart Project | SIMULIA™ - Dassault Systèmes®. Accessed October 22, 2023. https://www.3ds.com/products-services/simulia/solutions/life-sciences-healthcare/the-living-heart-project/

71. Society of Nuclear Medicine and Molecular Imaging. Committee on Medical Internal Radiation Dose (MIRD). Accessed October 31, 2023. https://www.snmmi.org/AboutSNMMI/CommitteeContent.aspx?ItemNumber=12475

72. Tsui BMW, Terry JA, Gullberg GT. Evaluation of Cardiac Cone-Beam Single Photon Emission Computed Tomography using Observer Performance Experiments and Receiver Operating Characteristic Analysis. *Invest Radiol*. 1993;28(12):1101-1112. doi:10.1097/00004424-199312000-00004

73. Pieters H, Van Staden JA, Du Plessis FCP, Du Raan H. Validation of a Monte Carlo simulated cardiac phantom for planar and SPECT studies. *Physica Medica*. 2023;111(May). doi:10.1016/j.ejmp.2023.102617

CHAPTER 2 – ARTICLE 1

Validation of a Monte Carlo simulated cardiac phantom for planar and SPECT studies

This paper has been published in *Physica Medica*

(https://doi.org/10.1016/j.ejmp.2023.102617)

The front page of this article is shown in Appendix A

Table of Contents

1. Abstract

Purpose: This work aimed to validate Monte Carlo (MC) simulated cardiac phantoms for the evaluation of planar- and SPECT-gated-blood-pool (GBP-P and GBP-S) studies.

Methods: A comparison of gamma camera system performance criteria measurements (energy resolution, spatial resolution, sensitivity) with MC simulations was conducted. Furthermore, the accuracy of measured and simulated volumes of two stereolithography-printed cardiac phantoms (based on 4D-XCAT phantoms) was assessed. Finally, the simulated GBP-P and GBP-S XCAT studies were validated by comparing calculated left ventricular ejection fraction (LVEF) and ventricle volume values with known parameters.

Results: The simulated performance criteria compared well with measured values (energy resolution difference: 0.1±0.10%; spatial resolution (full width at half maximum) difference ≤0.5±0.8mm and system sensitivity difference ≤6.2±0.62cps/MBq). The measured and simulated cardiac phantoms were in good agreement; the left anterior oblique views compared well. This is supported by line profiles through these phantoms and on average, simulated counts were 5.8% lower than measured counts. The LVEF values calculated from the GBP-P and GBP-S simulated data differ from known values (2.8±0.64% and 0.8±0.52%). The differences between the known XCAT LV volumes and simulated GBP-S calculated volumes were -1.2 ±1.91ml and -1.5 ±0.96ml for the end-diastolic and end-systolic volumes.

Conclusion: The MC-simulated cardiac phantom has been validated successfully. Stereolithography printing allows researchers to create clinically realistic organ phantoms and is a valuable tool for validating MC simulations and clinical software. By conducting GBP simulation studies with various XCAT models, the user will be able to generate GBP-P and GBP-S databases for future software evaluation.

2. Introduction

Gated blood pool (GBP) scintigraphy (planar and SPECT), using ^{99m}Tc pertechnetate labelled red blood cells (RBCs), is commonly used to evaluate the ventricular function of patients due to excellent reproducibility measures [1,2]. Planar gated blood pool (GBP-P) imaging is often favoured over GBP SPECT (GBP-S) imaging due to the simplified acquisition and processing protocols [3]. GBP-P imaging is a well-established, highly repeatable, non-invasive technique to evaluate ventricular function, particularly the ejection fraction (EF) of the left ventricle (LV) [4,5].

However, a drawback of GBP-P studies is the overlap of anatomical structures resulting in the left ventricular ejection fraction (LVEF) not being calculated accurately due to activity contribution from the left atria (LA) and/or right ventricle (RV). Furthermore, the accuracy in determining the right ventricular ejection fraction (RVEF) is compromised due to the overlap between the right atrium (RA) and RV in the left anterior oblique (LAO) view [6,7]. The calculation of EF for GBP-P studies also requires a correction for background activity due to over-and underlying tissues such as lung and soft tissues containing radioactive-labelled RBCs. Low count densities and the partial volume effect are two further factors that may compromise the accuracy of LVEF calculations [8].

In contrast, GBP-S imaging can address many of the shortcomings and challenges of GBP-P studies. Wright et al. [5] reported improved repeatability of EF calculation obtained with GBP-S studies due to ideal ventricle separation and eliminating the need for background correction. Furthermore, GBP-S imaging is considered an "all-in-one" technique as it enables simultaneous assessment of biventricular volumes and functions [9]. Despite all the advantages, GBP-S studies have not yet replaced GBP-P studies for the calculation of EFs. This may be due to a lack of supportive evidence that ventricular volumes and EF values calculated from GBP-S studies are reliable. A significant challenge is assessing the accuracy of these parameters obtained from GBP-S studies without putting patients or volunteers at risk [10]. For this reason, using phantom studies to assess the accuracy of volume and EF values of GBP-S studies may be a viable alternative. The use of phantoms will not only minimise radiation hazards and costs but can also result in more reliable outcomes, as the volume and functional values obtained with phantom studies can be compared to the known input parameters[11].

With the availability of stereolithography 3D printers, manufacturing physical phantoms has become more accessible [12,13]. Stereolithography 3D printing technology has revolutionised the medical research industry by enabling the creation of highly accurate and clinically realistic organ models. These 3D printed phantoms provide researchers with a valuable tool for validating clinical software, allowing them to simulate real-life scenarios with greater precision and confidence. However, the use of physical phantoms for the evaluation of cardiac functions can be limited due to the fixed size and geometry of physical phantoms. Hybrid phantoms can address the limitations of physical phantoms and can be used to create a virtual model of a patient's anatomy and physiology [10]. These phantoms can be used with Monte Carlo (MC) simulations to accurately mimic GBP-P and GBP-S studies [14,15].

The 4D-XCAT phantom, developed by Segars et al., [10] is an example of a hybrid digital voxelised and mathematical phantom that uses Non-Uniform Rational B-Splines (NURBS) surfaces to generate organ shapes based on the 3D Visible Human Dataset [16]. NURBS surfaces are mathematical models that can precisely describe a wide range of 2D or 3D geometries. They provide a way to model complex shapes with smooth, curved surfaces and are widely used in fields that require a precise representation of digital shapes [17]. Patient motion (cardiac and respiratory) was added as the fourth dimension to the XCAT phantom [10] to ensure realistic clinical patient models.

De Bondt et al. [11] developed a physical phantom to assess the accuracy of EF and volume values obtained from gated cardiac scintigraphy data. This phantom was used to simulate variable RV and LV volumes. Recently, however, concerns have arisen regarding data credibility from physical phantom experiments in Nuclear Medicine because of differences in radioisotope regulation techniques, reproducibility, and individual differences in the phantoms [18]. Therefore, there is a tendency to replace actual phantom measurements with MC-simulated phantoms [19].

In the Nuclear Medicine department at our institution, many cancer patients undergo GBP studies to monitor cardiac function. It was decided to evaluate the calculated ventricular EF for both GBP-P and GBP-S studies using MC-simulated images of the 4D-XCAT phantom using different patient models. For this reason, a preliminary study was performed to validate the simulation procedure.

This study aimed to validate an MC-modelled gamma camera for the evaluation of planar and SPECT cardiac studies. This was done by verifying the SIMIND modelling of a gamma camera

for ^{99m}Tc by (i) comparing gamma camera performance criteria measurements with MC simulations and (ii) assessing the accuracy of the measured and simulated volumes of two 3D printed cardiac phantoms. Finally, the accuracies of a simulated GBP-P and GBP-S study obtained from the modelled gamma camera were verified by comparing the output parameters (EF and volume values) with the known input parameters of the 4D-XCAT phantom (further referred to as the XCAT phantom).

3. Materials and Methods

In this study, the Siemens Symbia T16 hybrid SPECT/CT dual-detector gamma camera (Siemens Medical Solutions, Inc. Hoffman Estates, IL., USA), available at our institute, fitted with low-energy high-resolution collimators, was used for all ^{99m}Tc image acquisitions and MC simulations. All the experimental and simulated images were obtained with a 15% energy window centred over the 140.5 keV photon peak of ^{99m}Tc. The ^{99m}Tc activity was measured using a Biodex Atomlab 500 radionuclide calibrator (Biodex Medical Systems, New York, NY, USA). The accuracy of the radionuclide calibrator was traceable to a secondary standard through the National Metrology Institute of South Africa (NMISA) in Cape Town, South Africa (±1.0%). The measured activity was contained in <0.2ml in a 1ml plastic syringe.

CT images of all experimental setups were acquired using the CareDose 4D protocol (CareDose, Siemens Medical Solutions, Germany) with a CT tube voltage of 130 kVp and an effective tube current of 15 mAs. The reconstructed transaxial CT data (512 × 512 image matrix; 0.98 mm/pixel; slice thickness of 1.0 mm) was used to create digital voxelised phantoms [20]. Source and density distributions were created from CT-derived or XCAT phantoms to use as input in the SIMIND MC code, version 6.2 [21,22,23].

SIMIND was used to create the virtual Siemens Symbia T16 gamma camera according to the specification sheet [22] and as described by Morphis et al. [24]. The gamma camera was simulated using a single detector (NaI crystal) fitted with a low-energy, high-resolution collimator. The photomultiplier tubes and electronics were mimicked by a layer of backscatter material [23]. The SIMIND ^{99m}Tc isotope file, based on the nuclear data available from the "Laboratoire National Henri Becquerel" [25] was used to model the ^{99m}Tc photons [26]. The simulations were performed on a high-performance cluster. All simulations were run only once for 70 million photons per projection to reduce the statistical uncertainty. The SIMIND MC simulation utilises variance reduction techniques, which result in the recording of weights rather than absolute counts during the simulation process. Consequently, the simulated images do not follow a Poisson distribution. To ensure the simulated images match the realism of typical gamma camera images in clinical settings, as recommended by Ljungberg [26,27], Poisson noise was incorporated during the simulation process.

All image acquisitions and processing were repeated three times; average and associated uncertainty values for results were reported.

3.1. Verification of the SIMIND Gamma Camera model

Simulations of SPECT models using ^{99m}Tc, described by Bahreyni Toossi et al. [23] and Dong et al. [28] for the Symbia gamma camera, were verified in this study. The gamma camera performance criteria stipulated by the National Electrical Manufacturers Association (NEMA) [29] were used as guidelines to ensure optimal MC modelling of the gamma camera with SIMIND. The specific tests selected for the verification were system energy resolution, system

spatial resolution, and system sensitivity, as proposed by Morphis et al. [24] and Ramonaheng et al. [20]. Experimental measurements of these tests were carried out on the gamma camera, and simulations of the same tests were performed with ^{99m}Tc as radionuclide, employing the experimental setup and simulations as described by Ramonaheng et al. [20]. The differences between the results obtained from the experimental measured (acquired) and simulated data were reported using equation 3.

$$\text{Difference} = \text{Measured} - \text{Simulated} \quad (3)$$

The system energy resolution, system spatial resolution, and system sensitivity images were simulated using the CT-derived voxelised digital phantoms with the same imaging parameters as for the experimental data measurements.

The performance criteria tests were evaluated as described by Ramonaheng et al. [20]. The measured and simulated energy spectra were compared visually and the energy resolution of the primary photo peak of ^{99m}Tc for both spectra was calculated. For the system spatial resolution, the full width at half and tenth maximum (FWHM, FWTM) values (expressed in mm) were calculated for the line sources without and with a scatter medium at three source-detector distances (50 mm, 100 mm and 150 mm). The measured and simulated system sensitivity values (petri-dish in air) were calculated and reported at a source-detector distance of 100 mm expressed in counts/s/MBq.

3.2. Verification of the simulated Cardiac Phantom

3.2.1. Stereolithography Printed Cardiac Phantom

The 4D-XCAT computer software program was used to construct end-diastolic (ED) and end-systolic (ES) phase images of the cardiac model. These images were based on an XCAT phantom male model (body mass index (BMI) = 24.38). The public domain software ITK-SNAP [30], was used to segment the images resulting in 3D templates of the ED and ES cardiac phases, which were printed using a Form 3 Formlabs stereolithography printer [31]. Each 3D cardiac phantom consists of four cardiac chambers (left and right atria and ventricles). Wall thicknesses were printed according to the segmentation obtained from the XCAT phantom. The XCAT models did not include the papillary muscles in the cardiac chambers and therefore these muscles were omitted in the printed phantoms. To ensure the stability of the phantom, limited support structures with a diameter of 0.45 mm were integrated into the printing process. The volumes of these chambers were validated by comparing them with the volumes of the XCAT model.

3.2.2. Cardiac Phantom imaging

The cardiac chambers of the two printed 3D phantoms were filled with a clinically relevant activity concentration of 159±8 MBq/L ^{99m}Tc (concentration at filling time) in water. This was corrected for decay to know the correct activity at the time of acquisition. The acquisitions were performed according to a GBP-S setup using international guidelines [32,33]. In brief, this entails 64 step-and-shoot projections covering a 180° arc using a 64 × 64 image matrix from the 45° right anterior oblique to the 45° left posterior oblique view, acquired for 25 seconds per projection. Since clinical GBP-S studies are not performed routinely at our institute, the optimal zoom factor should still be established. The simulated cardiac phantom should therefore be evaluated for different zoom factors. GBP-S studies were thus acquired

using three different zoom factors (1.23, 1.45, and 1.78). Furthermore, CT images of the printed phantoms were acquired as explained before.

3.2.3. Cardiac Phantom simulation

CT data acquired for both the ES and ED printed phantoms was used to create digital voxelised phantoms (source and density maps) to use for MC simulation. The above-mentioned SPECT studies of the ED and ES cardiac phantoms were simulated using the SIMIND code for the three different zoom factors. The simulations were performed as described previously for the performance criteria validation tests (Section 3.1). The acquisition parameters (image matrix size, pixel size, energy window settings, activity values, acquisition duration and zoom factor) for the simulation of the SPECT studies were the same as for the acquired (measured) data on the gamma camera.

3.2.4. Analysis and comparison of acquired and simulated SPECT Cardiac Phantom studies

To validate the printed cardiac phantoms, the individual chambers of the phantoms were filled with water and weighed to determine the precise volume of each chamber. These weighted volume values were compared with the known chamber volume values of the XCAT model.

The acquired and simulated SPECT studies of the ED and ES phantoms were reconstructed using the Siemens Syngo software available in the department (filtered back projection, Butterworth filter, cut-off frequency of 0.6 cycles.cm^{-1}, order of 5) with no attenuation or scatter corrections applied. The public domain Java image processing program, ImageJ [34], was used to determine the volume of each phantom. The area of the cardiac phantom in each of the reconstructed transaxial slices was determined using a predefined threshold value. These areas were added together and multiplied by the slice thickness to determine the phantom volume. This process was repeated for acquired and simulated data of all six studies (three different zoom factors for each of the ED and ES phantoms).

For further validation of the simulated SPECT images, image projections obtained at an LAO view for the acquired and simulated studies for each data set was identified. Line profiles were drawn mid-ventricular on the LAO views of the acquired and simulated studies and compared visually. The averages of the total counts over all projections for the acquired and simulated studies were also compared.

3.3. Verification of GBP-P and GBP-S XCAT Phantom simulation studies

An XCAT male model (BMI = 24.38) was used to simulate a GBP-P and a GBP-S study with SIMIND. These simulations mimicked gated planar and SPECT clinical studies of the XCAT model. The average activity biodistribution for the organs of interest used in the simulations was based on distributions reported in the Ultratag^{TM} RBC package insert [35]. These values were optimised by comparing the XCAT simulated images with anonymous GBP-P patient studies and the final values are shown in Table 2.1. The GBP-P and GBP-S simulations were performed using the modelled gamma camera as described for the performance criteria simulations (Section 3.1).

Table 2.1: Average activity biodistribution for the organs of interest.

Organ of interest	Percentage activity per organ
Cardiac (Bloodpool, arteries and veins)	44%
Muscle (Body and myocardium)	6%
Lungs	24%
Liver	13%
Spleen	13%

3.3.1. GBP-P simulated XCAT study

A GBP-P study, with the detector at a 45° angle, representing an LAO view and 32 frames per cardiac cycle, was simulated. The data was gated using the XCAT model's functional information. The simulations were performed using a 64 × 64 image matrix, a zoom factor of 2.67 (pixel size of 3.35 mm) for 9 million counts in the total study, as per clinical studies. The SIMIND output files (interfile format) were converted to Dicom format using in-house software. The Alfanuclear software IM512P [36] was used to import and process these files to determine the LVEF values.

3.3.2. GBP-S simulated XCAT study

A GBP-S study was simulated of the XCAT model using a similar SPECT acquisition protocol as described in section 3.2. Similar to the GBP-P study, the projection data was gated using the functional information associated with the XCAT model. In-house software was used to convert SIMIND output files to Dicom format and to import these to the Siemens Syngo database. The GBP-S study was reconstructed with the Siemens Syngo workstation as explained in section 3.2. The ventricles were segmented using the reconstructed data with the Cedars-Sinai quantitative blood pool SPECT software "QBS" [37] available on the Siemens Syngo workstation. Minor adjustments were made to the QBS contours to ensure that the entire ventricle is included. Left ventricular ES and ED volume and EF were obtained using QBS.

Due to the known XCAT cardiac ventricle volumes at the ED- and ES phases, the true LVEF was known for the XCAT model. The LVEF and volume values obtained from the XCAT GBP-P and GBP-S simulation studies were compared with the known values to determine the difference using equation 3. GBP-P and GBP-S calculations of the LVEF were repeated four times to obtain average LVEF values.

4. Results

4.1. Verification of the SIMIND Gamma Camera model

For the verification, energy spectra, system energy resolution, system spatial resolution, and system sensitivity were considered.

The measured and simulated energy spectra as well as the difference between the two spectra are shown in Figure 2.1. To calculate the energy resolution for the measured and simulated photopeaks (Table 2.2), a Gaussian function was fitted to the photopeak of each spectrum to obtain the FWHM values.

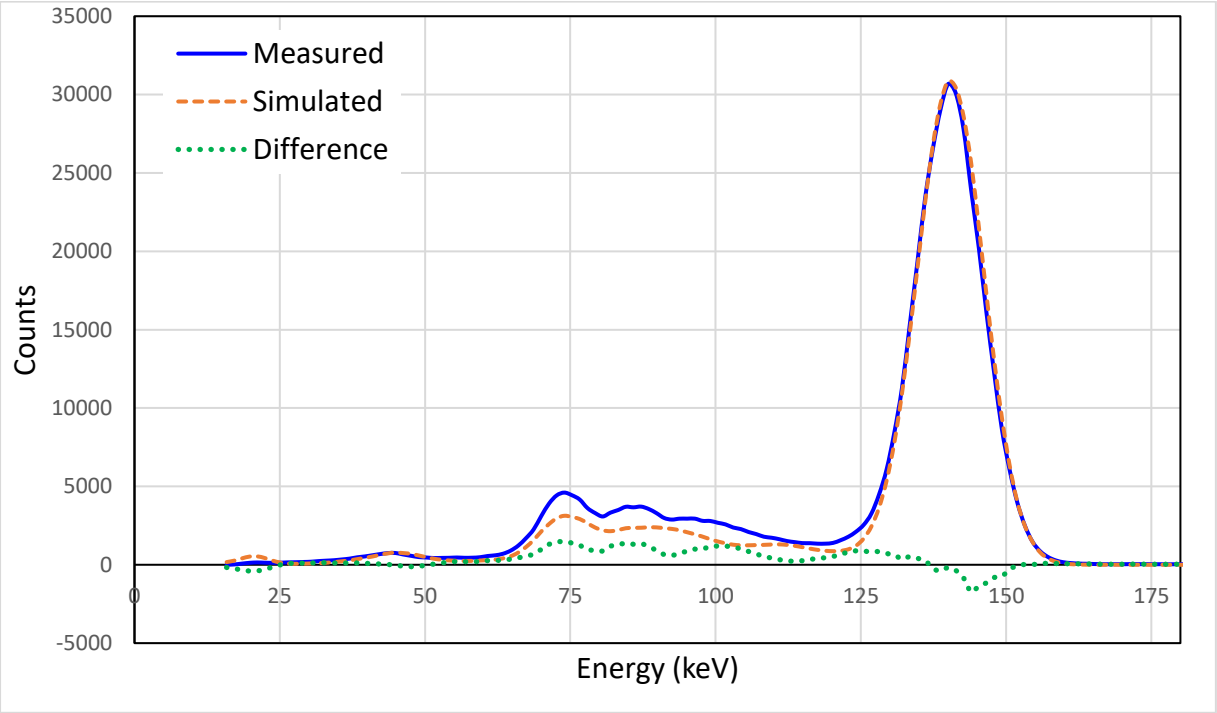

Figure 2.1. Measured (blue solid line) and simulated (orange, dashed line) 99mTc energy spectra. The green dotted line represents the difference between the measured and simulated energy spectra.

The results for the system energy resolution, system spatial resolution, and system sensitivity for both the measured and simulated data are shown in Table 2.2. Average and standard uncertainty values for the three measurements are reported. The simulations were not repeated, however, average and standard uncertainty values for the simulated resolution values were obtained by drawing line profiles at three different positions on the simulated images.

Table 2.2: Comparison of the measured and simulated performance criteria test results: system energy resolution, system spatial resolution, and system sensitivity. Average and standard uncertainty values are reported.

		Measured	Simulated	Difference
System Energy Resolution (%)		9.5 ± 0.01	9.4	0.1 ± 0.01
System Spatial Resolution (Without scatter)				
FWHM* (mm)	50 mm	5.6 ± 0.10	6.0 ± 0.01	-0.4 ± 0.10
	100 mm	7.6 ± 0.11	8.0 ± 0.04	-0.4 ± 0.12
	150 mm	9.8 ± 0.11	10.1 ± 0.01	-0.3 ± 0.11
FWTM* (mm)	50 mm	10.5 ± 0.18	11.0 ± 0.02	-0.5 ± 0.18
	100 mm	13.6 ± 0.18	14.1 ± 0.03	-0.5 ± 0.18
	150 mm	17.4 ± 0.14	17.5 ± 0.04	-0.1 ± 0.15
System Spatial Resolution (With scatter)				
FWHM* (mm)	50 mm	5.9 ± 0.06	6.1 ± 0.01	-0.2 ± 0.06
	100 mm	7.9 ± 0.06	8.1 ± 0.02	-0.2 ± 0.06
	150 mm	10.3 ± 0.09	10.3 ± 0.14	0.0 ± 0.16
FWTM* (mm)	50 mm	11.7 ± 0.14	11.3 ± 0.04	0.4 ± 0.15
	100 mm	15.2 ± 0.10	14.7 ± 0.05	0.5 ± 0.11
	150 mm	19.3 ± 0.10	18.3 ± 0.08	1.0 ± 0.13
System Sensitivity (cps/MBq)		97.8 ± 0.62	91.6	6.2 ± 0.62

*FWHM: full width at half maximum; FWTM: full width at tenth maximum

4.2. Verification of the simulated Cardiac Phantom

Figure 2.2(a) shows posterior views of the 3D printed cardiac phantoms. The phantoms represent the ED phase and ES phase of the heart. The structural support inserts and the printed myocardial thickness are visible in the cross-sectional printer diagram for the ES phantom in Figure 2.2(b).

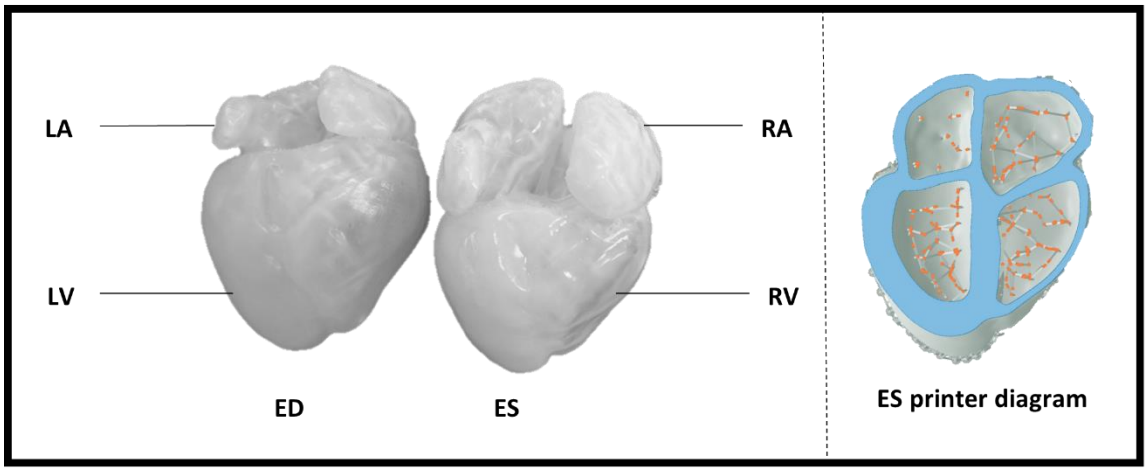

Figure 2.2. (a). 3D printed cardiac phantoms for the end-diastolic (ED) and end-systolic (ES) phases based on an XCAT male model (BMI: 24.83), posterior view. (b) Cross-section through the printer diagram of the ES cardiac phantom.

The known volumes of the XCAT phantom and the weighted volumes are listed in Table 2.3. The largest differences (32% and 26%) were obtained for the ED and ES RV volume. It should be noted that a part of the pulmonary trunk was included as part of the right ventricle in the printed phantom which will explain why the RV volume of the printed phantom exceeded that of the XCAT model. Smaller differences were obtained for the LV ED and ES volumes (5% and 3%), with the printed volume slightly exceeding the known XCAT volumes. The LA and RA (for ED and ES) printed volumes were less than the known XCAT volumes, which can be attributed to the added support structures included in the hollow chambers during the printing process. Since the atrial volumes are small in comparison to the ventricular volumes, the support structures may have a more notable contribution to these volume differences.

Table 2.3: Known XCAT model volumes and weighted printed phantom volumes for the atria and ventricles of the ED* and ES* cardiac phantoms. Average and standard uncertainty values are reported for weighted volumes.

Chamber	ED volume (ml)		ES volume(ml)	
	XCAT	Printed Phantom	XCAT	Printed Phantom
Left atrium	35.4	28.2 ± 0.99	65.6	57.3 ± 0.79
Right atrium	50.0	40.4 ± 0.75	88.1	76.2 ± 0.45
Left ventricle	136.0	142.8 ± 1.15	53.3	54.9 ± 0.43
Right ventricle	101.9	134.6 ± 1.57	60.8	76.4 ± 0.91
Total	324.2	346.0 ± 2.49	273.7	264.9 ± 1.66

*ED: end-diastolic; ES: end-systolic

The cardiac volumes obtained from the reconstructed SPECT data of the measured and simulated cardiac phantom studies, for the different zoom factors, are shown in Table 2.4.

Table 2.4: Measured and simulated cardiac volumes, reported for the different zoom factors.

Phantom	Zoom	Cardiac volume (ml)		Difference
		Measured	Simulated	
ED	1.23	356.4 ± 1.27	366.1 ± 2.27	-9.7 ± 2.60
	1.45	355.2 ± 1.44	362.9 ± 1.05	-7.7 ± 1.78
	1.78	346.0 ± 1.44	342.9 ± 0.93	3.1 ± 1.71
ES	1.23	265.1 ± 0.64	291.8 ± 0.38	-26.7 ± 0.75
	1.45	261.2 ± 1.21	292.9 ± 1.93	-31.7 ± 2.28
	1.78	266.1 ± 0.36	273.2 ± 2.40	-7.1 ± 2.43

*ED: end-diastolic; ES: end-systolic

A visual presentation of the LAO projection for the measured and simulated SPECT studies is shown in Figure 2.3 for both the cardiac phantoms, obtained with the three different zoom factors. Also shown are the averages of the total counts over all projections with the normalised line profiles.

The comparison of the average total counts between the measured and simulated projections showed that the simulated counts, on average, were 5.8% lower than the measured counts (with a range of 3.6% to 8.4%). This is consistent with the 6.3% underestimation of the simulated system sensitivity value, as shown in Table 2.2. Additional factors, such as phantom filling inconsistencies and the influence of geometric variations between the acquisition and simulation setup, may also impact the reported differences.

Phantom & Zoom	LAO view with count statistics		Mid-ventricular line profiles
	Measured	Simulated	
ED 1.23	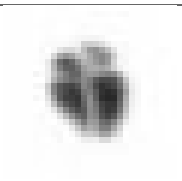 78187	 71618	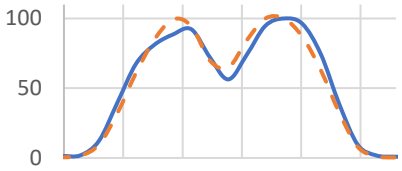
ED 1.45	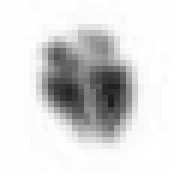 81261	 75275	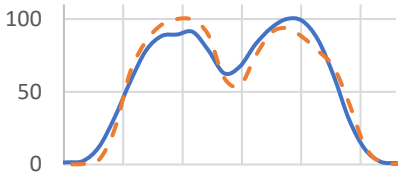
ED 1.78	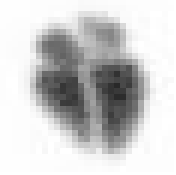 73584	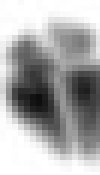 67931	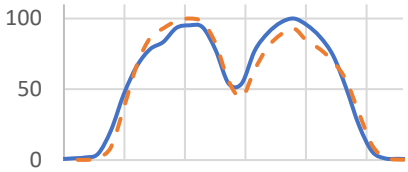
ES 1.23	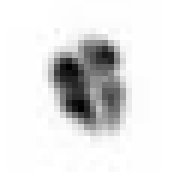 53126	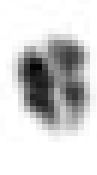 50951	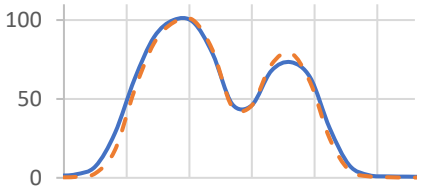
ES 1.45	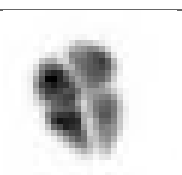 55669	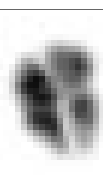 53674	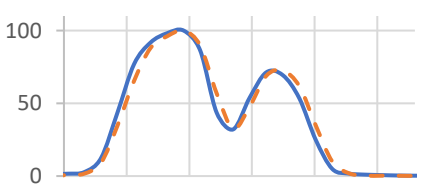
ES 1.78	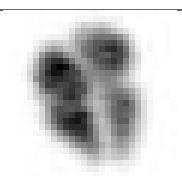 50869	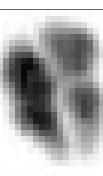 48967	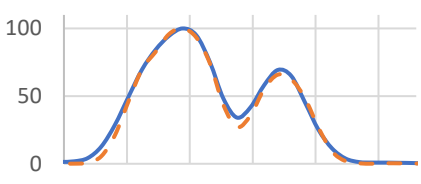

*LAO: left anterior oblique; ED: end-diastolic; ES: end-systolic

Figure 2.3. Visual comparison between the LAO* projection images of measured and simulated cardiac SPECT studies for the ED* and ES* 3D printed cardiac phantoms obtained with different zoom factors. Averages of the total counts over all the projections are reported below the different LAO views. Normalised mid-ventricular line profiles are shown for the measured (solid blue line) and simulated (dashed orange line) studies.

4.3. Verification of GBP-P and GBP-S XCAT Phantom simulation studies

4.3.1. GBP-P simulated XCAT study

The simulated GBP-P XCAT study (Figure 2.4) was processed using the Alfanuclear processing software. The average LVEF obtained for the GBP-P simulation compared well with the true XCAT LVEF and is shown in Table 2.5. As mentioned before, the true LVEF value was obtained from the known XCAT ED and ES volume values of the LV.

Table 2.5: Alfanuclear processed planar blood pool results of the simulated XCAT study.

	Known XCAT LVEF	Processed LVEF	Difference
LVEF (%)	48.1	45.3 ± 0.64	-2.8 ± 0.64

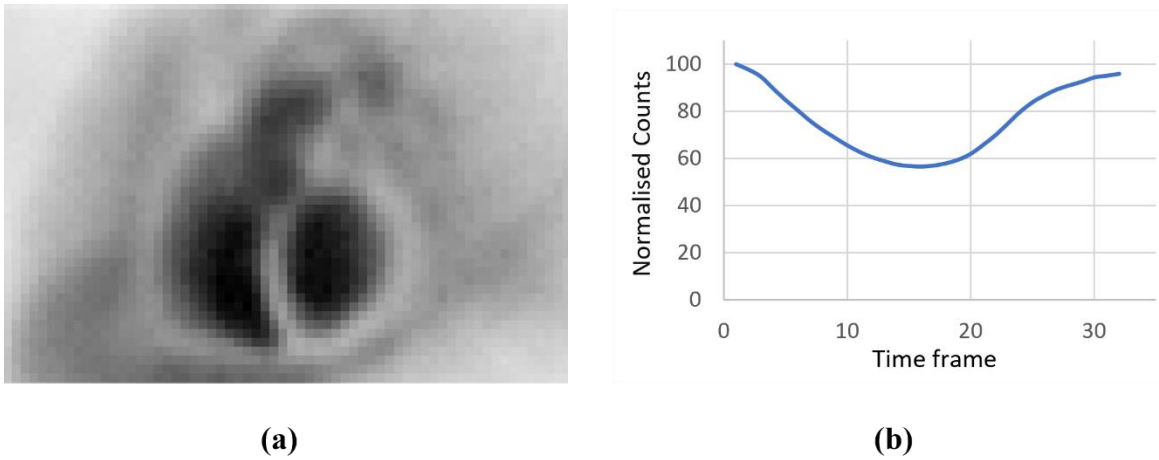

Figure 2.4. (a) Summed image of all gated frames in the planar gated blood pool study. (b) Left ventricular volume curve obtained for the planar gated blood pool study.

4.3.2. GBP-S simulated XCAT study

Figure 2.5 shows the LV and RV during the ED and ES phase, as well as an LV volume curve. The average and standard uncertainty of the LV ED and ES volume and EF values obtained after processing the GBP-S XCAT study are reported in Table 2.5 and compared to the known XCAT model values. The calculated LV volume and EF values of the XCAT model compare favourably to these true values.

Table 2.6: Quantitative SPECT blood pool results of the simulated XCAT study.

	Known XCAT value	Processed value	Difference
ED volume (ml)	136.5	137.7 ± 1.91	-1.2 ± 1.91
ES volume (ml)	70.8	72.3 ± 1.96	-1.5 ± 0.96
EF (%)	48.1	47.3 ± 0.52	0.8 ± 0.52

* ED: end-diastolic; ES: end-systolic; EF: ejection fraction

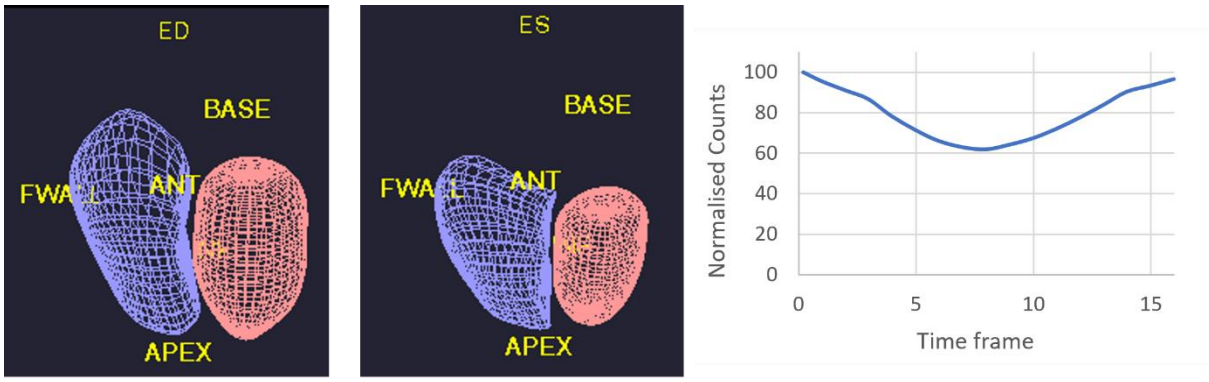

Figure 2.5. (a) End-diastolic (ED) and (b) end-systolic (ES) phases of the SPECT gated blood pool study. The blue mesh presents the right and the red mesh the left ventricle. (c) Left ventricle volume curve obtained for the SPECT gated blood pool study.

5. Discussion

As mentioned, MC simulations are excellent tools for the design of detector systems, for improving image quality and acquisition protocols, as well as for the assessment of processing software. However, the complexity of patients' anatomy and physiology has placed a significant demand on phantoms utilising MC simulation to mimic gamma camera acquisitions of patient images. This is also relevant for hybrid phantoms using MC simulations to mimic cardiac studies for the assessment of cardiac software. In this paper, a multistep validation process was conducted to confirm the accuracy of MC simulations of an XCAT phantom. These simulations involved comparing gamma camera data to MC simulations to validate the SIMIND modelling of a gamma camera, as well as verifying the correctness of the measured and simulated volumes of two 3D printed cardiac phantoms. These cardiac phantoms were based on an XCAT model. The accuracy of a simulated GBP-P and GBP-S study generated from the modelled gamma camera was confirmed in the last stage of the validation by comparing the output parameters (EF and volume values) from the simulated studies with the known input parameters of the XCAT phantom.

5.1. Verification of the SIMIND Gamma Camera model

The simulated performance criteria of the gamma camera compared well with the measured values. The system energy resolution resulted in a 0.1% difference between the measured and simulated results. Visually, these energy spectra were in good agreement with minor differences in the Compton region, which correlate with the results reported by Bahreyni Toossi et al. [23] and Morphis et al. [24]. These differences may be attributed to minor discrepancies between the measurement and simulation setup. Given that a 15% energy window is commonly used for imaging, it can be concluded that the difference in energy resolution between the measured and simulated data is unlikely to have a significant impact on the results of an imaging study.

The system spatial resolution FWHM and FWTM values, at the three source-detector distances obtained without and with added scatter, resulted in maximum differences of 0.5±0.18 mm (FWHM) and 1.0 ±0.13 mm (FWTM) between the measured and simulated data. This is small when compared to a typical image pixel size of 4.8 x 4.8 mm^2. As a result, it is assumed that the spatial resolution of the simulated image will be similar to that of the gamma camera image. This indicates that the simulation results are reliable and can be used to accurately

represent the performance of the gamma camera system. Both the measured and simulated resolution deteriorate with an increase in source-detector distance as expected. The difference in the system spatial resolution values can be attributed to minor inconsistencies between the measurement- and simulation scatter environments. It is important to note that statistical uncertainties are also embedded in the calculation of the FWHM and FWTM values. The observed differences were therefore regarded as acceptable.

The system sensitivity between the measured and simulated data resulted in a 6.3% difference. Activity measurements in the radionuclide calibrator greatly impact the accuracy of sensitivity values. Geometric differences can contribute to radionuclide calibrator uncertainties. According to IAEA standards [38,39] a ±5% uncertainty is acceptable. These geometric uncertainties may contribute to the reported sensitivity difference as was also seen by other authors [20,23].

5.2. Verification of the simulated Cardiac Phantom

Visually, the two 3D printed cardiac phantoms present the ED- and ES phases anatomically correct, with the ventricles and atria filled to maximum capacity during the ED and ES phases, respectively. The chamber volumes listed in Table 2.3 correspond to the clinical volumes obtained using cardiovascular magnetic resonance [40]. Table 2.3 shows the difference in volumes between the actual XCAT volumes, and the volumes obtained through weighing the phantoms. As mentioned, the RV volume in the ED phantom is larger than the XCAT volume, as a part of the pulmonary trunk was included during the process of creating the templates used to print the phantoms. The differences between the weighted and known volumes for the remaining heart chambers may be attributable to the interior support structures added during the 3D printing process. The measured and simulated volumes determined using ImageJ resulted in differences between -12.1% and 0.9%. These differences can be attributed to the uncertainty in the activity measurement (as indicated in the sensitivity results), small geometric differences between the printed and simulated cardiac phantoms as well as the difference in the acquisition and simulated scatter environment.

Visual assessment of the measured and simulated images demonstrates that the simulated images given in Figure 2.3 compare favourably with the measured images. Therefore, the selected acquisition parameters used in the simulation are considered acceptable.

From the measured and simulated images, the 1.23 zoom factor yielded images with less noise than the larger zoom factors. However, due to the smaller pixel size (resulting in poorer spatial resolution), the delineation of the different cardiac chambers becomes more cumbersome with the smaller zoom factor. This may have an impact on the accuracy of EF calculations. The zoom factor of 1.78 results in a better separation of the left and right ventricles. The downside of using a larger zoom factor (better spatial resolution) is that the count statistics decrease, leading to a longer acquisition time to obtain the best image quality (i.e. low noise). The larger zoom factor may also result in truncation of the heart during GBP-S studies in larger patients [41].

The mid-ventricular line profiles (Figure 2.3) show that the simulated data follows the trend of the measured data. The small differences may be attributed to discrepancies in the scatter environment and setup of the measured and simulated studies.

The small but constant difference (average difference of 5.8%) between the count statistics of the measured and simulated cardiac phantoms may be due to the inherent uncertainty of the

radionuclide calibrator as seen for the planar system sensitivity evaluation. Geometric differences between the printed and simulated phantoms may also contribute to these minor discrepancies.

Although the cardiac phantoms were imaged and simulated in air, attenuation and scatter interactions originating inside the phantoms were included in the final images. The differences observed between the measured and simulated cardiac phantom studies were found to be negligible, and the simulated cardiac phantoms were considered verified using the modelled gamma camera and voxelised phantoms for the MC simulation. It is therefore assumed that data from simulated cardiac phantoms in an increased attenuation and scatter environment will compare well with measured data from actual cardiac phantoms.

5.3. Verification of GBP-P and GBP-S XCAT Phantom simulation studies

The absolute difference between the known and the calculated LVEF value obtained using the Alfanuclear software for the planar studies was 2.8%. The minor differences between the known and calculated EF are acceptable and the simulated GBP-P XCAT phantom can be considered verified.

It is important to note that the XCAT study presented in this paper is a preliminary investigation and that further research will involve the creation and use of a database of GBP-P studies that cover a variety of ED and ES volumes based on various XCAT models. As previously stated, the GBP-P studies carried out at our institution primarily aim to examine cardiac dysfunction related to cancer treatment. In a recent article by Printezi [42], a PubMed search resulted in 22 articles comprising 1017 cancer patients who underwent GBP studies for screening. The majority of patients (70%) included in these articles were male patients. For this reason, a male XCAT patient model was selected for our preliminary study.

For the GBP-S studies, our results indicate that the LV ED and ES volumes and LVEF values can be determined with reasonable accuracy using the QBS software with the simulated XCAT cardiac model. The processed volume values were slightly larger than the known values. Similar to the GBP-P study, the calculated LVEF value was slightly lower than the true value.

6. Conclusion and future studies

The significance of modelling gamma cameras using MC simulations has been studied in detail by Zaidi [43]. He stated that MC simulations could be used confidently in Nuclear Medicine imaging as research tools [43]. The SIMIND-modelled Symbia gamma camera has been successfully verified for ^{99m}Tc using the above performance criteria as guidelines.

This study indicated that 3D printing allows researchers to create accurate, clinically realistic phantoms from XCAT models. A variety of different organ phantoms can thus be generated. Simulation studies based on these phantoms are also feasible and allow the user to expand the digital phantom database. Future work will include printing an entire anthropomorphic torso and/or abdominal phantom based on an XCAT model's anatomy with various organ inserts. The final evaluation will therefore include a more realistic attenuation and scatter environment.

The XCAT phantom simulation confirmed a good agreement between the GBP-P and GBP-S known and calculated ventricular parameters (volumes and EF). Future studies will include simulating multiple GBP-P and GBP-S studies of male and female XCAT models to create a large

clinically relevant study database with a range of ED and ES volume and EF values. The accuracy of commercial cardiac processing software will be evaluated using these simulated studies.

7. References

[1] Daly CA, Abbasi S, Kwong RY. Cardiac Imaging. In: McManus LM, Mitchell RN, editors. Pathobiology of Human Disease: A Dynamic Encyclopedia of Disease Mechanisms. Elsevier Inc.; 2014. p. 4019–45.

[2] Bartlett ML, Srinivasan G, Barker WC, Kitsiou AN, Dilsizian V, Bacharach SL. Left Ventricular Ejection Fraction: Comparison of Results from Planar and SPECT Gated Blood-Pool Studies. J Nucl Med. 1996;37:1795–9.

[3] Sachpekidis C, Sachpekidis V, Moralidis E, Arsos G. Equilibrium radionuclide ventriculography: Still a clinically useful method for the assessment of cardiac function? Hell J Nucl Med. 2018;21:213–20.

[4] Groch MW, Depuey EG, Belzberg AC, Erwin WD, Kamran M, Barnett CA, et al. Planar imaging versus gated blood-pool SPECT for the assessment of ventricular performance: A multicenter study. J Nucl Med. 2001;42:1773–9.

[5] Wright GA, Thackray S, Howey S, Cleland JG. Left Ventricular Ejection Fraction and Volumes from Gated Blood-Pool SPECT: Comparison with Planar Gated Blood-Pool Imaging and Assessment of Repeatability in Patients with Heart Failure. J Nucl Med. 2003;44:494–8.

[6] Maddahi J, Berman DS, Matsuoka DT, Waxman AD, Forrester JS, Swan HJC. Right Ventricular Ejection Fraction During Exercise in Normal Subjects and in Coronary Artery Disease Patients: Assessment by Multiple-gated Equilibrium Scintigraphy. Am Hear Assoc. 1980;62:133–49. https://doi.org/10.1161/01.cir.62.1.133

[7] Marving J, Hoilund-Carlsen PF, Chrammer-Jorgensen B, Gadsboll N. Are right and left ventricular ejection fractions equal? Circulation. 1985;3:502–14. https://doi.org/10.1161/01.cir.72.3.502

[8] Yang SN, Sun SS, Zhang G, Chou KT, Lo SW, Chiou YR, et al. Left ventricular ejection fraction estimation using mutual information on technetium-99m multiple-gated SPECT scans. Biomed Eng Online. 2015;14:119. https://doi.org/10.1186/s12938-015-0117-2

[9] Hacker M, Hoyer X, Kupzyk S, La Fougere C, Kois J, Stempfle HU, et al. Clinical validation of the gated blood pool SPECT QBS® processing software in congestive heart failure patients: Correlation with MUGA, first-pass RNV and 2D-echocardiography. Int J Cardiovasc Imaging. 2006;22:407–16. https://doi.org/10.1007/s10554-005-9031-1

[10] Segars WP, Sturgeon G, Mendonca S, Grimes J, Tsui BMW. 4D XCAT phantom for multimodality imaging research. Am Assoc Phys Med. 2010;37:4902–15. https://doi.org/10.1007/s12350-014-0062-7

[11] De Bondt P, Claessens T, Rys B, De Winter O, Vandenberghe S, Segers P, et al. Accuracy of 4 different algorithms for the analysis of tomographic radionuclide

ventriculography using a physical, dynamic 4-chamber cardiac phantom. J Nucl Med. 2005;46:165–71.

[12] Läppchen T, Meier LP, Fürstner M, Prenosil GA, Krause T, Rominger A, et al. 3D printing of radioactive phantoms for nuclear medicine imaging. EJNMMI Phys. 2020;7:22. https://doi.org/10.1186%2Fs40658-020-00292-0

[13] Filippou V, Tsoumpas C. Recent advances on the development of phantoms using 3D printing for imaging with CT, MRI, PET, SPECT, and ultrasound. Med Phys. 2018;45:e740–60. https://doi.org/10.1002/mp.13058

[14] Kainz W, Neufeld E, Bolch WE, Graff CG, Kim CH, Kuster N, et al. Advances in computational human phantoms and their applications in biomedical engineering - A topical review. IEEE Trans Radiat Plasma Med Sci. 2019;3:1–23. https://doi.org/10.1109%2FTRPMS.2018.2883437

[15] Lee C, Lodwick D, Hasenauer D, Williams JL, Lee C, Bolch WE. Hybrid computational phantoms of the male and female newborn patient: NURBS-based whole-body models. Phys Med Biol. 2007;52(12):3309–33. https://doi.org/10.1088/0031-9155/52/12/001

[16] The National Library of Medicine. The Visible Human Project, https://www.nlm.nih.gov/research/visible/visible_human.html; 2019 [accessed 14 Aug 2022].

[17] ThePro3DStudio. NURBS: An Introduction, https://professional3dservices.com/blog/nurbs-modeling.html; 2023 [accessed 24 Oct 2022].

[18] Demirkaya O, Al-Mazrou R. Devices for evaluating imaging systems. In: Bailey DL, Humm JL, Todd-Pokropek A, van Aswegen A, editors. Nuclear Medicine Physics: A Handbook for Teachers and Students. Vienna: IAEA; 2014. p. 550.

[19] Ljungberg M, Strand SE, King MA. Monte Carlo calculations in nuclear medicine. 2nd ed. Florida: Taylor & Francis Group; 2013.

[20] Ramonaheng K, van Staden JA, du Raan H. Validation of a Monte Carlo modelled gamma camera for Lutetium-177 imaging. Appl Radiat Isot. 2020;163. https://doi.org/10.1016/j.apradiso.2020.109200

[21] Ljungberg M, Strand SE. A Monte Carlo program for the simulation of scintillation camera characteristics. Comput Methods Programs Biomed. 1989;29:257–72. https://doi.org/10.1016/0169-2607(89)90111-9

[22] Siemens. Symbia T Series System Specifications. Germany; www.siemens.com/mi; 2013 [accessed 13 May 2022].

[23] Bahreyni Toossi MT, Islamian JP, Momennezhad M, Ljungberg M, Naseri SH. SIMIND Monte Carlo simulation of a single photon emission CT. J Med Phys. 2010;35:42–7. https://doi.org/10.4103/0971-6203.55967

[24] Morphis M, van Staden JA, du Raan H, Ljungberg M. Modelling of energy-dependent spectral resolution for SPECT Monte Carlo simulations using SIMIND. Heliyon.

2021;7(2). https://doi.org/10.1016/j.heliyon.2021.e06097

[25] Laboratoire National Henri Becquerel. Atomic and Nuclear data. http://www.lnhb.fr/nuclear-data/nuclear-data-table/; 2023 [accessed 1 Feb 2023].

[26] Ljungberg M. The SIMIND Monte Carlo Program. Sweden; 2020.

[27] Ljungberg M. Monte Carlo simulations for therapy imaging. J Phys Conf Ser. 2011;317. https://iopscience.iop.org/article/10.1088/1742-6596/317/1/012016

[28] Dong X, Saripan M, Mahmud R, Mashohor S, Wang A. Characterization of SIEMENS Symbia T SPECT camera in Monte Carlo simulation environment. Pakistan J Nucl Med. 2018;18–26. https://dx.doi.org/10.24911/PJNMed.175-1540569779

[29] National Electrical Manufacturers Association. Performance Measurements of Gamma Camera. Virginia; 2007.

[30] Yushkevich PA, Piven J, Hazlett HC, Smith RG, Ho S, Gee JC, et al. User-guided 3D active contour segmentation of anatomical structures: Significantly improved efficiency and reliability. Neuroimage. 2006;31:1116–28. https://doi.org/10.1016/j.neuroimage.2006.01.015

[31] Formlabs. Formlabs Support. https://support.formlabs.com/s/article/Using-Durable-Resin?language=en_US ; 2022 [accessed 27 Jan 2022].

[32] Hesse B, Tägil K, Cuocolo A, Anagnostopoulos C, Bardiés M, Bax J, et al. EANM/ESC procedural guidelines for myocardial perfusion imaging in nuclear cardiology. Eur J Nucl Med Mol Imaging. 2005;32:855–97. https://doi.org/10.1007/s00259-005-1779-y

[33] Hesse B, Lindhardt TB, Acampa W, Anagnostopoulos C, Ballinger J, Bax JJ, et al. EANM/ESC guidelines for radionuclide imaging of cardiac function. Eur J Nucl Med Mol Imaging. 2008;35:851–85. https://doi.org/10.1007/s00259-007-0694-9

[34] Schneider CA, Rasband WS, Eliceiri KW. NIH Image to ImageJ: 25 years of Image Analysis HHS Public Access. Vol. 9, Nat Methods. Maryland; 2012 Jul.

[35] Curium US LLC. Ultratag™ RBCKit for the preparation of Technetium Tc 99m–Labeled Red Blood CellsRx only Diagnostic–For Intravenous Use, https://dailymed.nlm.nih.gov/dailymed/fda/fdaDrugXsl.cfm?setid=9f999b75-8a66-40bf-9352-478850b41225&type=display; 2022 [accessed 14 Apr 2023].

[36] Alfanuclear. IM512P: Data and Image Processor. User's Manual, Argentina: Alfanuclear S.A.I.y C. http://alfanuclear.com/SitioAlfa_3/EnglishSite/index.htm; 2004 [accessed 30 Sep 2022].

[37] Van Kriekinge D, Berman DS, Germano G. Automatic quantification of left ventricular ejection fraction from gated blood pool SPECT. J Nucl Cardiol. 1999;6:498–506. https://doi.org/10.1016/s1071-3581(99)90022-3

[38] IAEA. Quality control of nuclear medicine instruments 1991. Vienna; 1991 May.

[39] IAEA. Quality Assurance For Radioactivity Measurement In Nuclear Medicine. Vienna; 2006 Nov.

[40] Kawel-Boehm N, Hetzel SJ, Ambale-Venkatesh B, Captur G, Francois CJ, Jerosch-Herold M, et al. Reference ranges (“normal values”) for cardiovascular magnetic resonance (CMR) in adults and children: 2020 update. J Cardiovasc Magn Reson. 2020;22. https://doi.org/10.1186/s12968-020-00683-3

[41] Wosnitzer B, Gadiraju R, Depuey G. The truncation artifact. J Nucl Cardiol. 2011;18:187–91. https://doi.org/10.1007/s12350-010-9290-7

[42] Printezi MI, Yousif LIE, Kamphuis JAM, van Laake LW, Cramer MJ, Hobbelink MGG, et al. LVEF by Multigated Acquisition Scan Compared to Other Imaging Modalities in Cardio-Oncology: a Systematic Review. Curr Heart Fail Rep. 2022;19:136–45. https://doi.org/10.1007/s11897-022-00544-3

[43] Zaidi H. Relevance of accurate Monte Carlo modeling in nuclear medical imaging. Med Phys. 1999;26:574–608. https://doi.org/10.1118/1.598559

CHAPTER 3 – ARTICLE 2

ASSESSMENT OF PLANAR GATED BLOOD POOL PROCESSING SOFTWARE USING A SIMULATED PATIENT PHANTOM DATABASE

This paper has been submitted for publication in *Heliyon*

Acknowledgement of submission is shown in Appendix B

Table of Contents

1. Abstract

Introduction: Planar gated blood pool (GBP-P) radionuclide imaging is valuable for the non-invasive assessment of left ventricular ejection fraction (LVEF). Serial cardiac imaging can be performed to monitor the potential decline in LVEF among patients undergoing cardiotoxic chemotherapy. Consequently, accurate LVEF determination becomes paramount. While commercial software programs have enhanced the LVEF values' reproducibility, the accuracy of these software programs has raised concerns. This study aimed to generate a database of GBP-P studies with known LVEF values using Monte Carlo simulations and assess LVEF values' accuracy using four commercial software programs.

Methods: We utilised anthropomorphic 4D-XCAT models to simulate 64 clinically realistic GBP-P studies with Monte Carlo simulations. Four commercial software programs (Alfanuclear, Siemens, General Electric Xeleris, and Mediso Tera-Tomo) were used to process these simulated studies. The accuracy and reproducibility of the LVEF values determined with these software programs and the intra- and inter-observer reproducibility of the LVEF values were assessed.

Results: Our study revealed a strong correlation between LVEF values calculated by the software programs and the true LVEF values derived from the 4D-XCAT models. However, all the software programs slightly underestimated LVEF at lower LVEF values. Intra- and inter-observer reliability for LVEF measurements was excellent.

Discussion: Accurate LVEF assessment is crucial for determining the patient's cardiac function before initiating and during chemotherapy treatment. The observed underestimation, particularly at lower LVEF values, emphasises the need for the accurate and reproducible determination of these values to avoid excluding suitable candidates for chemotherapy. The software programs' excellent intra- and inter-observer reliability highlights their potential to reduce subjectivity when using the semi-automatic processing option.

Conclusion: Our study demonstrated the accuracy and reliability of commercial software programs for determining LVEF values from simulated GBP-P studies. Future research will investigate strategies to mitigate the underestimation biases and generalise findings to diverse patient populations.

2. Introduction

Planar gated blood pool (GBP-P) radionuclide imaging has long proven to be beneficial for the non-invasive assessment of regional wall motion, left ventricular ejection fraction (LVEF), and other indices of ventricular function [1]. LVEF is the ratio of the blood volume (stroke volume) ejected during systole from the left ventricle (LV) to the total volume of blood present at the end of diastole, expressed as a percentage. GBP-P imaging, 2D/3D echocardiography (EC), and cardiac magnetic resonance imaging (CMR) are the modalities most frequently used for determining LVEF [2–4]. Even though 2D/3D EC does not use radiation, it is less favoured because it is operator-dependent and relies on certain geometrical assumptions [2–5]. CMR is often the standard choice for non-invasive cardiac studies because of its outstanding contrast, resolution, and absence of patient radiation exposure [2,4,6]. However, CMR is not suitable for all patients, particularly those with implantable cardioverter defibrillators, most pacemakers, and other implant devices such as metallic and cochlear implants, which can contraindicate its use [2,4,5].

Since the 1970s, GBP-P imaging, a cost-effective, non-invasive, and reproducible procedure to determine LVEF in patients, has gained popularity in evaluating cardiac ventricular function [7,8]. The EANM guidelines for radionuclide imaging of cardiac function included reference LVEF values [9]. LVEF is widely used to assess the risk of cardiotoxicity[2,4,7,8,10] in chemotherapy patients [2–5,8,11–16]. It is widely agreed that chemotherapy treatment will be discontinued if the LVEF value before chemotherapy is less than 50% or decreases by more than 10% post-treatment [17]. Therefore, the calculated LVEF value must be accurate and reliable to guarantee the best possible patient care, avoiding complications [2,3,7,8,11].

Sachpekidis et al. and Foley et al. [4,5] have reported that GBP-P studies offer distinct advantages over other imaging modalities regarding ease of use. These studies have indicated that GBP-P imaging exhibits a high accuracy and reliability comparable to CMR imaging. Their findings also highlight the potential of GBP-P imaging as a promising and robust technique for non-invasive assessments of LVEF values, emphasising its value in clinical practice and research settings [4].

Ensuring accurate, repeatable, and reproducible LVEF results from GBP-P studies obtained with commercial software programs is crucial. However, validating these software programs using human subjects or animal studies poses challenges due to ethical and radiation concerns and the lack of known cardiac volumes for confirming the calculated LVEF values. The utilisation of physical phantoms [16,18] has been proposed to overcome these limitations. However, their inability to accurately replicate patient organ shapes and spatial relationships, and the prohibitive cost of creating a set of physical phantoms that mimic various patient and organ sizes, have limited the use of physical phantoms.

In a previous article [14], we proposed the use of hybrid phantoms, in particular, the 4D-XCAT phantom developed by Segars et al. [19,20], to create human cardiac models to assess LVEF values determined with commercial software programs. The XCAT phantom software is a computer model that enables users to create digital patient phantoms mimicking human anatomy and physiology [20] for biomedical research [21]. The unmatched level of detail and anatomical realism in the 4D-XCAT model contributes to the usefulness of digital phantoms generated with the XCAT software [21,22]. It contains a population of male and female anatomies varying in age, height, and weight, allowing for phantom variability [21–23].

The 4D-XCAT phantom is a valuable resource in imaging research for assessing imaging devices and techniques. Commercial software programs are frequently used to process GBP-P studies to determine LVEF values. Software updates, including the introduction of semi-automatic and automatic processing methods, have improved the reliability of LVEF values by reducing the risk of variance. These advancements aim to enhance the accuracy and consistency of LVEF calculations. However, validating the accuracy and precision of LVEF values obtained with new and existing software programs remains crucial to ensure accurate and reliable LVEF results [11]. Fair et al. [12] and De Bondt [16] pointed out that software programs are often not extensively tested before clinical implementation. To address this, the emergence of digital hybrid phantoms provides an opportunity to evaluate and compare the accuracy of LVEF values determined with various software packages by employing hybrid phantoms with known input values. This study aimed to generate a database of GBP-P studies with known LVEF values using Monte Carlo (MC) simulation of digital hybrid patient phantoms. Furthermore, the accuracy of the LVEF values obtained from the simulated GBP-P studies was assessed using four commercial software programs.

3. Materials and Methods

3.1 4D-XCAT Models and Monte Carlo Simulations

A database of six anthropomorphic 4D-XCAT models (three male- and three female models) [19] was used to simulate clinically realistic GBP-P studies [14] with the SIMIND MC program [24]. These models include a wide range of ventricular end-diastolic (ED), end-systolic (ES), and stroke volumes to obtain a comprehensive set of LVEF values. The accuracy of four commercially available software programs for determining LVEF values was assessed using the simulated GBP-P studies. The information regarding the selected 4D-XCAT models is presented in Table 3.1.

Table 3.1: Demographic and biometric data of the six 4D-XCAT models.

	Model 1	Model 2	Model 3	Model 4	Model 5	Model 6
Gender	Male	Female	Male	Female	Male	Female
Age	36	59	52	54	60	51
Ethnicity	Caucasian	Caucasian	Caucasian	Unknown	African	Unknown
Weight (kg)	75.60	63.70	108.00	87.00	81.50	59.25
Height (cm)	176.1	162.7	183.2	161.0	175.0	158.0
Body Mass Index (BMI)	24.38	24.06	32.18	33.56	26.61	23.73

Each of the six 4D-XCAT models was scaled to create a database with additional models with varying ES cardiac volumes, resulting in different EF values. Cardiac scaling factors were introduced to generate different clinically realistic phantoms. Figure 3.1 illustrates a flowchart of the database generation. Left and right ventricular and atrial volumes were kept in clinically acceptable ranges [25], and models not complying were excluded.

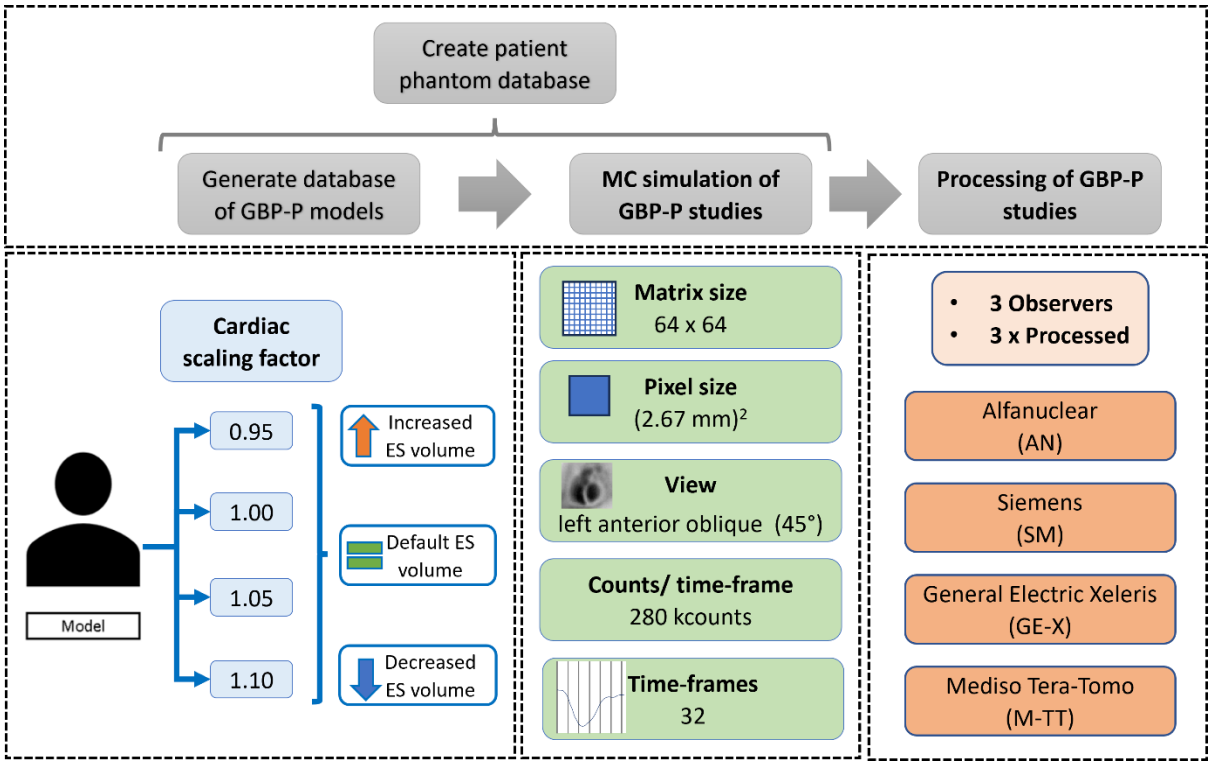

Figure 3.1: Flowchart illustrating the creation of the patient phantom database by generating GBP-P models and MC simulation of the GBP-P studies. Processing of the GBP-P studies is also shown.

A summary of the parameters used to create the 4D-XCAT models is as follows:

- All models were generated to include cardiac and respiratory motion [19,21–23]. The entire heart was translated and/or rotated to mimic respiratory motion.
- Thirty-two time-frames were generated over the cardiac cycle for all models, as stated by guidelines [9,26,27] implemented at our institution.
- No other scale factor was introduced to any of the organs besides the heart scale factor.
- Segmented activity maps and the density maps used for the simulation were generated as 512 x 512 image matrixes with a voxel size of 0.98 × 0.98 × 0.98 mm^3 (Figure 3.2).

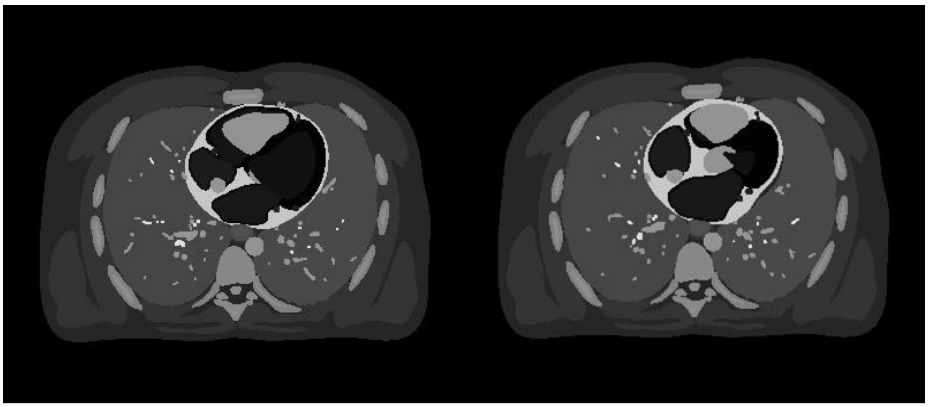

Figure 3.2: Sample transaxial images of the 4D-XCAT phantom's segmented activity map during the end-diastolic (ED) and end-systolic (ES) phases.

The Siemens Symbia gamma camera model used to simulate the GBP-P studies was described in our previous article [14]. The XCAT software was used to create 32 time-frames of the 4D-XCAT phantom for each patient model. Due to factors such as breathing, cardiac rotation, and the fluctuating cardiac cycle, the heart's location within the thoracic cavity changes at each of the 32 time-frames. The attenuation- and activity maps generated with the XCAT software for the 32 time-frames of the 4D-XCAT models were used as input files for the MC code SIMIND. The phantoms' activity distributions (also referred to as activity maps) were based on data from GBP-P studies of patients from our clinic. The simulations were performed with the assistance of the High-Performance Cluster of the University of the Free State with 280 kcounts per time frame for 200 million photon histories per image to limit the MC statistical uncertainty. As recommended by Ljungberg [14,24,29], Poisson noise was incorporated during the simulation process to ensure the noise levels in the simulated images closely resembled those observed in clinical radionuclide images. Other simulation parameters are summarised in the flowchart in Figure 3.1.

The 32 simulated time-frames were concatenated using ImageJ [29] to create GBP-P studies of ~9 000 kcounts mimicking clinically realistic GBP-P studies. These simulated GBP-P studies (Figure 3.3) were converted to DICOM file format using an in-house software program and transferred to the appropriate Nuclear Medicine processing workstations.

3.2 Processing the simulated GBP-P studies

Four different commercial software programs (Alfanuclear (AN), Xeleris by General Electric (GE-X), Siemens (SM), and Tera-Tomo from Mediso (M-TT)) were utilised to process the 64 simulated GBP-P studies (Table 3.2, Figure 3.1). Three independent operators with at least five years of clinical experience blindly processed each GBP-P study three times, allowing the assessment of intra- and inter-observer reproducibility of LVEF calculation. Bunting et al. [30] indicated that the time between repetitions should be long enough to prevent interference from the preceding test. For this reason, the operators in our study were asked to repeat the processing of the GBP-P studies on different days to ensure that the observers were not biased. All GBP-P studies underwent standard processing procedures similar to routine clinical studies. Any modifications to the semi-automated processing were made as required by the user (e.g., adjustment of the region of interest where the processing algorithm failed to

accurately identify the left ventricle) (Figure 3.3). The LVEF was calculated for all processing software after a background correction was applied to the LV counts obtained in the ED and ES phases (Table 3.2).

Table 3.2: Details of the four software programs used in this study.

Software	Company	Processing system	Manufacturing Address	Background ROI definition
AN	Alfanuclear	Data and Image Processor IM512P, version 2.0 [31]	Argentina	Manually drawn background ROI
SM	Siemens	Syngo workstation [32]	Germany	Automatically selected background ROI.
GE-X	General Electric	Xeleris [33]	United States	Automatically selected background ROI.
M-TT	Mediso	Tera-Tomo, version 3.07 [34]	Hungary	Manually drawn ROIs

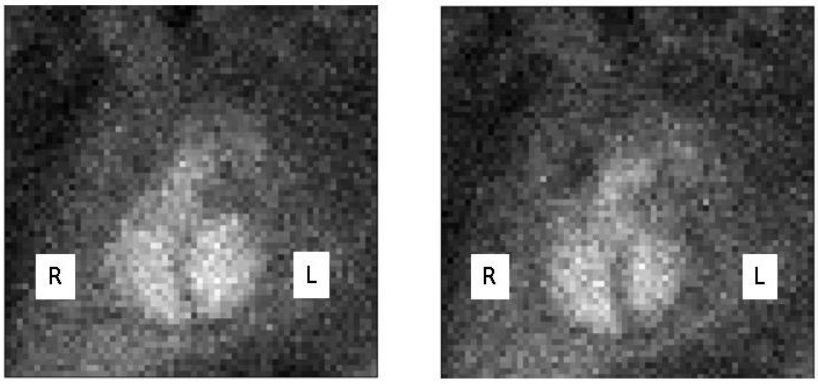

Figure 3.3: Sample of MC simulated images of the ED- and ES-phase of the original 4D-XCAT model 1.

4. Statistical Analysis

LVEF mean and standard deviations of all the models were reported for the 4D-XCAT values and the AN-, SM-, GE-X-, and M-TT calculated values. A one-way analysis of variance (ANOVA) test was performed in Excel to compare the LVEF values obtained with the four different software programs.

Linear regression analysis and the Pearson correlation coefficients (R) were used to evaluate the strength of the relationship and association between calculated LVEF values and the true (or absolute) LVEF values obtained from the 4D-XCAT models. The following guidelines regarding the correlation coefficient, proposed by Chan et al. [35], were used to assess the strength of the linear relationship: poor ($R < 0.3$), fair ($R = 0.3–0.5$), moderately strong ($R = 0.6–0.8$), and very strong ($R \geq 0.8$). The Standard Error of Estimate (SEE) measures the accuracy of the predictions made by the model [36], in this case, the processed LVEF values. The Data

Analysis Toolkit in Excel was used to perform regression analysis on the data and to determine the Pearson coefficient, SEE, and *p* – value.

Bland-Altman analysis assessed the agreement between the LVEF values calculated with commercial software programs and 4D-XCAT models by plotting the difference between LVEF values against the true LVEF values. Any systematic trends in differences were also identified by Bland-Altman analysis. A *p* – value less than 0.05 indicated statistical significance for all statistical tests.

Inter- and intra-observer reliability was assessed by means of an Interclass Correlation Coefficient (ICC) [30,37] and coefficient of variation (CV) using the Real Statistics data analysis toolpack in Excel [38]. An ICC was also obtained to evaluate the agreement between the calculated LVEF using the different software (AN, SM, GE-X, M-TT) and the known 4D-XCAT values. ICC based on a 95% confidence level was used, and the strength of agreement was assessed according to guidelines by Landis and Koch [39], which define agreement as poor (ICC < 0.20), fair (ICC 0.21–0.40), moderate (ICC 0.41–0.60), good (ICC 0.61–0.80), or very good (ICC > 0.80). Koo et al. [37] define an ICC > 0.9 as excellent.

5. Results

5.1 4D-XCAT Models and Monte Carlo Simulations

Table 3.3 displays the left ventricular ED- and ES volumes of the six original XCAT models and their corresponding stroke volumes.

Table 3.3: End-diastolic (ED)-, end-systolic (ES)-, and stroke volumes for the six original models.

	Left Ventricle Volumes (ml)			Right Ventricle Volumes (ml)		
Model number	ED	ES	Stroke (ED – ES)	ED	ES	Stroke (ED – ES)
1	136	71	65	102	71	31
2	109	43	66	82	49	33
3	158	62	97	119	71	48
4	96	37	58	71	43	29
5	117	46	71	87	52	35
6	90	35	55	67	40	27

Eight of the 72 4D-XCAT models were excluded due to inconsistencies and left ventricular ES volumes being too small compared to Kawel-Boehm's reference ranges. [25]. The 64 4D-XCAT models used in this study had a range of ED volumes (159 – 78 ml), ES volumes (94 – 22 ml), and LVEF values (20 – 77%)).

5.2 Left Ventricular Ejection Fraction

The mean and standard deviation of the LVEF calculated from the ED and ES volumes of the 4D-XCAT phantoms as well as the LVEF values determined with the four commercial software programs from the simulated GBP-P studies, are presented in Table 3.4.

Table 3.4: Known LVEF values for the 4D-XCAT models and calculated LVEF values obtained with the four commercial software programs: (AN: Alfanuclear; SM: Siemens, GE-X; General Electric Xeleris; M-TT: Mediso Tera-Tomo) presented as mean ± SD (n = 64).

LVEF	4D-XCAT	AN	SM	GE-X	M-TT
Mean (%)	53.7	50.8	50.7	48.9	52.4
Standard Deviation (%)	13.0	14.5	15.3	15.8	15.5

No significant difference was indicated between the LVEF values calculated by the four programs (one-way ANOVA test, p = 0.64). Furthermore, the agreement between the LVEF values for the 4D-XCAT and the four software programs was excellent (ICC ≥ 0.90, Table 3.5).

Table 3.5: Intra-class correlation for LVEF values between XCAT and the four processing software programs (AN: Alfanuclear; SM: Siemens, GE-X; General Electric Xeleris; M-TT: Mediso Tera-Tomo). Interclass correlation coefficients (ICC) with 95% confidence interval.

		Intra-class correlation between XCAT and the different software			
		AN	SM	GE-X	M-TT
All Operators	*ICC*	0.94	0.94	0.90	0.93
	95% CI	0.90 – 0.96	0.90 – 0.96	0.84 – 0.94	0.88 – 0.95

Linear regression analysis and Bland-Altman plots comparing the LVEF values of the four commercial software programs and the 4D-XCAT phantoms are shown in Figure 3.4. The mean of the operators' data for each software program as well as their respective statistical analysis, are shown in Figure 3.4.

The linear regression analysis showed that the agreement for LVEF values was very strong between 4D-XCAT and AN, SM, GE-X and M-TT (R > 0.94; p <0.1) (Figure 3.4 (a), (c), (e), (g)). The mean difference between the LVEF values for the 4D-XCAT and AN was -2.9±7.9%, between the 4D-XCAT and SM was -3.0±7.8%, between the 4D-XCAT and GE-X was -4.8±9.2% and -1.3±10.6% between the XCAT and M-TT (Figure 3.4 (b), (d), (f), (h)).

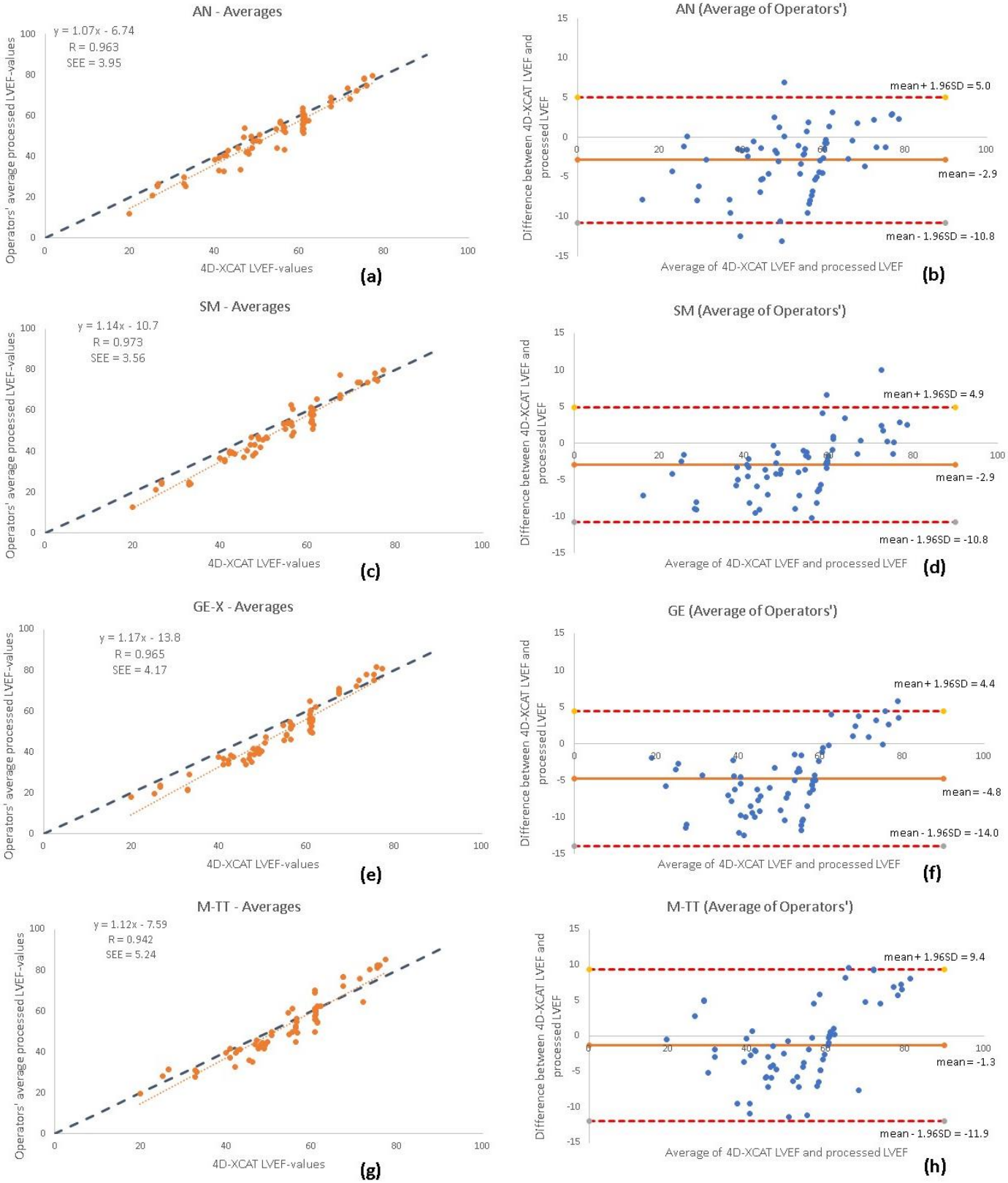

Figure 3.4: Linear regression and Bland-Altman analysis of the four processing software programs (AN: Alfanuclear; SM: Siemens, GE-X; General Electric Xeleris; M-TT: Mediso Tera-Tomo).

5.3 Intra-/inter-observer reliability

No significant difference was indicated between the intra- ($p > 0.61$) and inter-observer ($p > 0.43$) reliability of LVEF values for the four software programs. The intra- and inter-observer reliability of AN, SM, GE-X, and M-TT, as assessed by ICC and CV, is shown in Table 3.6. Both intra- and inter-observer reliability was excellent for all the studied variables (ICC = 0.96–1.00). The CV ranged from 1.1% to 5.8% for intra-observer reliability and 3.2% to 6.6% for inter-observer reliability.

Table 3.6: Intra - and Inter-observer reproducibility results for the four processing software programs (AN: Alfanuclear; SM: Siemens, GE-X; General Electric Xeleris; M-TT: Mediso Tera-Tomo). Interclass correlation coefficients (ICC) with a 95% confidence interval.

		Intra-observer reproducibility			
		AN	SM	GE-X	M-TT
Operator 1	*ICC*	0.99	0.99	0.99	0.96
	CV	2.29	**1.14**	2.96	5.62
Operator 2	*ICC*	0.99	1.00	0.99	0.98
	CV	2.61	1.71	2.34	4.64
Operator 3	*ICC*	0.98	0.98	0.99	0.96
	CV	3.89	3.15	4.38	**5.82**
		Inter-observer reproducibility			
		AN	SM	GE-X	M-TT
All Operators	*ICC*	0.99	0.96	0.99	0.97
	CV	**3.17**	4.64	4.82	**6.59**

6. Discussion

Our study demonstrated the successful creation of a database for simulated GBP-P studies. It was also shown that this database could be used as a valuable tool to assess the performance of new and current cardiac processing software for determining the accuracy and reliability of GBP-P studies. In literature, clinical studies frequently show variations between different operators and software algorithms calculating the LVEF. However, it is essential to acknowledge that the true LVEF value is not known amidst these variations. In our study, the true LVEF values were known; thus, the accuracy of the different software packages could be evaluated.

The MC-generated database was used in this study to assess the accuracy of LVEF values determined with the four commercial software programs. To our knowledge, this is the first study to specifically address the accuracy and reproducibility of commercial software programs for determining LVEF values obtained from MC-simulated GBP-P studies. The study allowed us to evaluate the accuracy of LVEF values determined with commercial software programs without involving human patients, relying instead on clinically realistic simulated studies.

Overall, there was a good correlation between the LVEF values of simulated GBP-P studies determined with the commercial software programs and the true LVEF values calculated from the LV ED and ES volumes of the 4D-XCAT models. The study found no significant difference between the LVEF values determined from the simulated GBP-P studies and those calculated

from the 4D-XCAT models. However, Bland-Altman analysis indicated a slight underestimation of LVEF values by all four software programs at lower LVEF values. This underestimation at lower LVEF values by the commercial software programs is consistent with previous reports and may be attributed to factors such as underestimating the background activity in physical phantoms or self-attenuation of activity in patients with dilated ventricles [40].

The clinical importance of accurate and reliable LVEF values cannot be overstated, particularly in the context of treatment strategies for patients receiving chemotherapy. The accepted threshold for discontinuing chemotherapy is often set at an LVEF value lower than 50%. Therefore, as observed in our study, any bias or systematic underestimation of LVEF values by the software programs could have significant clinical implications. Patients with true LVEF values above the threshold may be erroneously excluded from potentially life-saving chemotherapy regimens due to software-based underestimation. This highlights the critical need for accurate and reliable LVEF measurements, as these measurements directly impact treatment decisions and patient outcomes.

Our study's results also demonstrated very good intra- and inter-observer reliability for determining LVEF values by the four commercial software programs (ICC= 0.96 – 1.00; CV < 5.8% and 6.6%, respectively). The high reproducibility can be attributed to the semi-automatic processing options offered by three of the software programs (AN, SM, and GE-X), reducing the risk of subjective analysis. Similar findings regarding good intra- and inter-observer reliability of LVEF values have been reported in other studies [3,11,41]. The manual analysis employed by the M-TT software program resulted in slightly poorer intra- and inter-observer reliability. This can be ascribed to the increased subjectivity and the potential for larger random errors associated with manually delineating LV ED and -ES regions.

A limitation of this study, pertaining to using 4D-XCAT cardiac models, is that it only provides a single representation of cardiac motion. While the simulated patients encompassed a wide range of LVEF values, caution should be exercised when extrapolating the study's findings to different patient populations characterised by left ventricular dysfunction, as the validity of such extrapolation remains uncertain. Further assessment is needed to address this issue.

A strength of this study lies in the utilisation of 4D-XCAT models to simulate GBP-P studies. In contrast to many physical cardiac phantoms, these models incorporate confounding structures such as great vessels, liver, and spleen, as well as providing a more clinically realistic representation of cardiac and respiratory motion.

7. Conclusion and Future Studies

Our study demonstrated the value of utilising an MC-simulated database of GBP-P studies to evaluate cardiac processing software's performance to accurately determine LVEF values. This research highlights the promising accuracy of commercial software programs in determining LVEF values from simulated GBP-P studies, showcasing their potential practicality in clinical settings. A strong correlation was observed between LVEF values obtained from these software programs and the true LVEF values calculated from the LV volume values from the 4D-XCAT cardiac phantoms. This finding has significant implications for developing new algorithms calculating LVEF from planar radionuclide ventriculography studies. Additionally, these data sets can serve as valuable tools for validating LVEF measurements, training healthcare professionals, and assessing the impact of software upgrades.

It is well recognised that LVEF values and LV volumes hold paramount clinical importance for the diagnosis and prognosis of patients with cardiac diseases. Our study has laid the foundation for future research endeavours. Further investigations can explore the generalisability of our findings to diverse patient populations and delve into strategies to mitigate potential underestimation biases, particularly at lower LVEF values. Additionally, using 4D-XCAT models to simulate gated blood pool SPECT studies could extend our understanding of the accuracy of commercial software programs in determining both right and left ventricular EF and volume values. These studies can reinforce the critical role of accurate LVEF and LV volume assessment in guiding chemotherapy decisions and optimising patient care, ultimately contributing to enhanced clinical outcomes for patients receiving chemotherapy.

8. References

1. Valzania C, Paccagnella A, Spadotto A, Ruotolo I, Bonfiglioli R, Fallani F, Fanti S, Galié N. Early detection of cancer therapy cardiotoxicity by radionuclide angiography: An update. *Journal of Nuclear Cardiology*. Published online 2023. doi:10.1007/s12350-023-03202-w

2. Das GK, Chen Siew NG, Manap MA. Left ventricular ejection fraction by multigated acquisition scan using planar sodium iodide and cadmium-zinc-telluride cameras: a comparison with two-dimensional echocardiography. *Asia Ocean J Nucl Med Biol*. 2023;11(1):55-70. doi:10.22038/AOJNMB.2022.60392.1424

3. Bailey EA, Bailey DL. Results from an Australian and New Zealand audit of left ventricular ejection fraction from gated heart pool scan analysis. *Nucl Med Commun*. 2012;33(1):102-111. doi:10.1097/MNM.0b013e32834c2f0b

4. Sachpekidis C, Sachpekidis V, Moralidis E, Arsos G. Equilibrium radionuclide ventriculography: still a clinically useful method for the assessment of cardiac function? *Hell J Nucl Med*. 2018;21:213-220.

5. Foley TA, Mankad S V, Anavekar NS, Bonnichsen CR, Morris MF, Miller TD, Araoz PA, Araoz P. Measuring Left Ventricular Ejection Fraction-Techniques and Potential Pitfalls. *Citation: European Cardiology*. 2012;8(2):108-122. doi:https://doi.org/10.15420/ecr.2012.8.2.108

6. Marwick TH. Ejection Fraction Pros and Cons: JACC State-of-the-Art Review. *J Am Coll Cardiol*. 2018;72(19):2360-2379. doi:10.1016/j.jacc.2018.08.2162

7. Huang H, Nijjar PS, Misialek JR, Blaes A, Derrico NP, Kazmirczak F, Klem I, Farzaneh-Far A, Shenoy C. Accuracy of left ventricular ejection fraction by contemporary multiple gated acquisition scanning in patients with cancer: Comparison with cardiovascular magnetic resonance. *Journal of Cardiovascular Magnetic Resonance*. 2017;19(1):1-9. doi:10.1186/s12968-017-0348-4

8. Giubbini R, Milan E. The time for radionuclide ventriculography resurrection is coming. *Journal of Nuclear Cardiology*. 2016;23(5):1139-1141. doi:10.1007/s12350-015-0245-x

9. Hesse B, Lindhardt TB, Acampa W, Anagnostopoulos C, Ballinger J, Bax JJ, Edenbrandt L, Flotats A, Germano G, Gmeiner Stopar T, Franken P, Kelion A, Kjaer A, Le Guludec D, Ljungberg M, Maenhout AF, Marcassa C, Marving J, McKiddie F, Schaefer WM, Stegger L, Underwood R. EANM/ESC guidelines for radionuclide imaging of cardiac function. *Eur J Nucl Med Mol Imaging*. 2008;35:851-885. doi:10.1007/s00259-007-0694-9

10. Steyn R, Boniaszczuk J, Geldenhuys T. Comparison of estimates of left ventricular ejection fraction obtained from gated blood pool imaging, different software packages and cameras. *Cardiovasc J Afr*. 2014;25(2):44-49. doi:10.5830/CVJA-2013-082

11. Bresser P, de Beer J, de Wet Y. *A Study Investigating Variability of Left Ventricular Ejection Fraction Using Manual and Automatic Processing Modes in a Single Setting*.; 2015. doi:10.1016/j.radi.2014.10.002

12. Fair JR, Heintz PH, Telepak RJ. Evaluation of new data processing algorithms for planar gated ventriculography (MUGA). *J Appl Clin Med Phys*. 2009;10(3):173-179. doi:10.1120/jacmp.v10i3.2977

13. Mitra D, Basu S. Equilibrium radionuclide angiocardiography: Its usefulness in current practice and potential future applications. *World J Radiol*. 2012;4(10):421-430. doi:10.4329/wjr.v4.i10.421

14. Pieters H, Van Staden JA, Du Plessis FCP, Du Raan H. Validation of a Monte Carlo simulated cardiac phantom for planar and SPECT studies. *Physica Medica*. 2023;111(May). doi:10.1016/j.ejmp.2023.102617

15. Hiscock SC, Evans MJ, Morton RJ, Hall DO. Investigation of normal ranges for left ventricular ejection fraction in cardiac gated blood pool imaging studies using different processing workstations. *Nucl Med Commun*. 2008;29(2):103-109. doi:10.1097/MNM.0b013e3282f20e45

16. De Bondt P. (2005) *Evaluation of Cardiac Volumes by New Scintigraphic Techniques*. PhD Thesis. University of Ghent.

17. Yang SN, Sun SS, Zhang G, Chou KT, Lo SW, Chiou YR, Li FJ, Huang TC. Left ventricular ejection fraction estimation using mutual information on technetium-99m multiple-gated SPECT scans. *Biomed Eng Online*. 2015;14:119. doi:10.1186/s12938-015-0117-2

18. Simon TR, Walker BS, Matthiesen S, Miller C, Triebel J 0, Dowdey JE, Smitherman TC. *A Realistic Dynamic Cardiac Phantom for Evaluating Radionudide Ventriculography: Description and Initial Studies with the Left Ventricular Chamber*. *J Nucl Med 1989;*30:542-547.

19. Segars WP, Sturgeon G, Mendonca S, Grimes J, Tsui BMW. 4D XCAT phantom for multimodality imaging research. *American Association of Physicists in Medicine*. 2010;37:4902-4915. doi:10.1118/1.3480985

20. Segars WP, Mahesh M, Beck TJ, Frey EC, Tsui BMW. Realistic CT simulation using the 4D XCAT phantom. *Med Phys*. 2008;35(8):3800-3808. doi:10.1118/1.2955743

21. Segars WP, Tsui BMW, Cai J, Yin FF, Fung GSK, Samei E. Application of the 4D XCAT Phantoms in Biomedical Imaging and Beyond. *IEEE Trans Med Imaging*. 2018;37(3):680-692. doi:10.1109/TMI.2017.2738448.Application

22. Segars WP, Bond J, Frush J, Hon S, Eckersley C, Williams CH, Feng J, Tward DJ, Ratnanather JT, Miller MI, Frush D, Samei E. Population of anatomically variable 4D XCAT adult phantoms for imaging research and optimization. *Med Phys*. 2013;40(4). doi:10.1118/1.4794178

23. Segars WP, Veress AI, Sturgeon GM, Samei E. Incorporation of the Living Heart Model into the 4D XCAT Phantom for Cardiac Imaging Research. *IEEE Trans Radiat Plasma Med Sci*. 2019;3(1):54-60. doi:10.1109/TRPMS.2018.2823060

24. Ljungberg M. The SIMIND Monte Carlo Program – Medical Radiation Physics, Lund. Published 2020. Accessed December 4, 2021. https://simind.blogg.lu.se/

25. Kawel-Boehm N, Hetzel SJ, Ambale-Venkatesh B, Captur G, Francois CJ, Jerosch-Herold M, Salerno M, Teague SD, Valsangiacomo-Buechel E, van der Geest RJ, Bluemke DA. Reference ranges ("normal values") for cardiovascular magnetic resonance (CMR) in adults and children: 2020 update. *Journal of Cardiovascular Magnetic Resonance*. 2020;22. doi:10.1186/s12968-020-00683-3

26. Farrell MB, Galt JR, Georgoulias P, Malhotra S, Pagnanelli R, Rischpler C, Savir-Baruch B. SNMMI procedure standard/EANM guideline for gated equilibrium radionuclide angiography. *J Nucl Med Technol*. 2020;48(2):126-135. doi:10.2967/jnmt.120.246405

27. Nicol A, Avison M, Harbinson M, Jeans S, Waddington W, Woldman S. Procedure guideline for planar radionuclide cardiac ventriculogram for the assessment of left ventricular systolic function. *Nucl Med Commun*. 2016;2. doi:10.1097/MNM.0b013e328321cdba

28. Ljungberg M. Monte Carlo simulations for therapy imaging. *J Phys Conf Ser*. 2011;317. doi:10.1088/1742-6596/317/1/012016

29. Schneider CA, Rasband WS, Eliceiri KW. *NIH Image to ImageJ: 25 Years of Image Analysis HHS Public Access*. Vol 9.; 2012.

30. Bunting K V., Steeds RP, Slater LT, Rogers JK, Gkoutos G V., Kotecha D. A Practical Guide to Assess the Reproducibility of Echocardiographic Measurements. *Journal of the American Society of Echocardiography*. 2019;32(12):1505-1515. doi:10.1016/j.echo.2019.08.015

31. Alfanuclear - IM512P Data and Image Processor. Accessed August 15, 2023. http://alfanuclear.com/SitioAlfa_3/EnglishSite/IM/IM512P.htm

32. Siemens Healthineers - syngo.via. Accessed August 15, 2023. https://www.siemens-healthineers.com/medical-imaging-it/advanced-visualization-solutions/syngovia

33. GE HealthCare - Xeleris WS 2.0 | GE HealthCare Service Shop USA. Accessed August 15, 2023. https://services.gehealthcare.com/gehcstorefront/c/DI_CTG_L2_NM_09

34. Mediso - InterView™ FUSION processing software. Accessed August 15, 2023. https://mediso.com/global/en/product/interview-processing-workstation/interview-fusion-processing-software

35. Chan YH. *Biostatistics 104: Correlational Analysis*. Vol 44. 12th ed.; 2003. Clinical Trials and Epidemiology Research Unit; Singapore.

36. Zach. What is the Standard Error of the Estimate? (Definition & Example). Published 2021. Accessed September 9, 2023. https://www.statology.org/standard-error-of-estimate/

37. Koo TK, Li MY. A Guideline of Selecting and Reporting Intraclass Correlation Coefficients for Reliability Research. *J Chiropr Med*. 2016;15(2):155-163. doi:10.1016/j.jcm.2016.02.012

38. Free Download | Real Statistics Using Excel. Accessed August 15, 2023. https://real-statistics.com/free-download/

39. Landis JR, Koch GG. *The Measurement of Observer Agreement for Categorical Data*. *Biometrics* 1977; 33:159-174. http://www.jstor.org/stable/2529310.

40. Krakovich A, Zaretsky U, Gelbart E, Moalem I, Naimushin A, Rozen E, Scheinowitz M, Goldkorn R. Anthropomorphic cardiac phantom for dynamic SPECT. *Journal of Nuclear Cardiology*. 2023;30(2):516-527. doi:10.1007/s12350-022-03024-2

41. Skrypniuk J V, Bailey D, Cosgriff PS, Fleming JS, Houston AS, Jarritt PH, Whalley DR. *UK Audit of Left Ventricular Ejection Fraction Estimation from Equilibrium ECG Gated Blood Pool Images*. Vol 26. Lippincott Williams & Wilkins; 2005.

CHAPTER 4

ASSESSMENT OF SPECT GATED BLOOD POOL PROCESSING SOFTWARE USING A SIMULATED PATIENT PHANTOM DATABASE

This paper is a publishable manuscript and is being finalised for submission for publication.

Table of Contents

1. Abstract

Gated blood pool (GBP) studies provide non-invasive insights into cardiac function, particularly left ventricular ejection fraction (LVEF), which is crucial for cardiotoxicity monitoring during chemotherapy. While planar GBP (GBP-P) imaging is a validated method for LVEF quantification, challenges like anatomical overlap persist. Furthermore, aside from assessing LVEF, measuring left ventricular (LV) volumes holds clinical significance for managing, diagnosing, and prognosing patients with cardiac diseases.

GBP SPECT (GBP-S) studies emerged in the late 1990s, offering volumetric information. Still, they haven't replaced GBP-P imaging, mainly due to limitations in availability and the complexity of processing software. The Quantitative Blood Pool SPECT (QBS) software developed by Cedars-Sinai allows for right and left ventricular volume and EF calculation. This study aimed to assess the accuracy of QBS in calculating LV end-diastolic volume (EDV), end-systolic volume (ESV) and EF values for simulated GBP-S studies based on 4D-XCAT models. The results of the EDV, ESV and LVEF values were compared to the known values derived from the 4D-XCAT models.

Using the SIMIND Monte Carlo code (version 6.2), 64 cardiac models generated with the 4D-XCAT software (described in a previous publication) were simulated by following established guidelines for GBP-S imaging. The simulated studies were reconstructed on a Siemens Syngo processing workstation using Filtered Back Projection (FBP) (Butterworth filter) and the ordered subsets expectation maximisation (OSEM) (8 subsets, 4 iterations, Gaussian filter) reconstruction algorithms. These reconstructed axial images were reorientated to produce short axis images that were analysed automatically with the QBS software. The EDV, ESV and LVEF values determined with QBS were compared to known 4D-XCAT values through linear regression and Bland-Altman analysis.

The 64 models exhibited clinically realistic cardiac chamber volumes. Furthermore, this study demonstrated that the successful processing of the GBP-S studies depends on the filter used by QBS to reconstruct the gated SPECT data. Three of the FBP reconstructed studies in our investigation required a higher-order reconstruction filter. However, the OSEM reconstruction resulted in a 100% processing success rate.

The Pearson Correlation coefficient (R) revealed a moderately strong correlation (R = 0.76) for the calculated EDV and ESV values when processing the FBP-reconstructed data. OSEM reconstruction consistently showed strong correlations (R ≥ 0.86) for all parameters, particularly for EF values (R = 0.91).

Bland-Altman analysis emphasised OSEM's superiority, yielding narrower limits of agreement for LV EDV, ESV and EF. The Standard Error of Estimation indicated higher accuracy for EF values than EDV values. No significant differences were found between known and processed values using FBP or OSEM.

Fully automated QBS demonstrated a strong correlation and close agreement with 4D-XCAT models in measuring LV volumes and EF values and can be applied in clinical practice. The high success rate in automated processing minimises the necessity for manual intervention. Future research would focus on validating manual volume calculations for both left and right ventricles and optimising GBP-S reconstruction filters by comparing QBS-derived volume values to known 4D-XCAT values.

2. Introduction

The importance of gated blood pool (GBP) studies is evident as it is a non-invasive procedure that provides valuable information about myocardial wall motion and cardiac function [1–6]. The measurement of global left ventricular function and cardiac volumes is paramount in the daily practice of cardiologists, as these measurements exhibit a strong correlation with prognosis among patients with cardiac disease. Left ventricular ejection fraction (LVEF) also serves as a key parameter for the timely detection, management, and long-term monitoring of cardiotoxicity in patients undergoing chemotherapy [2,7–9]. Planar GBP (GBP-P) imaging has undergone thorough validation and has long been utilised as a non-invasive method for quantification of LVEF. Despite its merits, there are drawbacks associated with these studies. Challenges such as anatomical overlap and the need for background correction are notable limitations. Furthermore, the procedure can be time-consuming because it requires determining the optimal angle that provides the best view of ventricle separation [2–4,10].

Aside from GBP-P, the two most used methods for determining LVEF are 3D echocardiography and cardiac magnetic resonance imaging (CMR). 3D echocardiography is a valuable and widely used tool for assessing LVEF due to its non-invasiveness, real-time imaging capabilities, and widespread availability. However, its limitations include operator dependence, potential difficulty obtaining clear images in certain patients, and tissue penetration and interference constraints [11–15].

Due to its numerous advantages, CMR may be considered the reference method for obtaining accurate ejection fraction (EF) values. The method offers high-resolution images and excellent soft tissue contrast, enables 3D imaging for volumetric assessment of cardiac function, and avoids ionising radiation [13,16–19]. However, CMR is considered a costly modality, not widely available, and unsuitable for patients with certain metallic implantations [13,16,20].

Gated SPECT studies emerged in the late 1990s and early 2000s to replace planar imaging in blood pool procedures as the preferred technique [2,3,7]. This is mainly because tomographic studies can also provide volumetric information [1–3] and are considered an alternative to CMR studies [1,2,4,6,7,10]. SPECT gated blood pool (GBP-S) studies effectively address the challenge of overlapping anatomies, eliminating the need for background correction [3,4,6,10]. The technique facilitates better separation of the ventricles and, therefore, enhances repeatability [6,7]. Additionally, the automatic calculation of LVEF and volume values is an advantage of the method [21].

Despite the multiple advantages of GBP-S, it has yet to replace the firmly established and validated GBP-P studies [2,4,6,8,10]. The primary hindrance lies in the complexity of the processing software, which is often deemed less user-friendly compared to the GBP-P processing software and may also be more costly. The process involves reconstructing the acquired gated SPECT images to generate 3D representations of the heart at each gated phase of the cardiac cycle. Image reconstruction can be performed through Filtered Back Projection (FBP) using a modified Ramp filter [3,4,22]. Alternatively, an Iterative Reconstruction (IR) algorithm, such as the Ordered Subset Expectation Maximisation (OSEM) algorithm, can be employed with a pre-selected number of iterations, and subsets as well as post-filtering of images. These reconstructed image datasets are re-orientated into short-axis slices by manually selecting left ventricular symmetry axes. Subsequently, the images undergo quantitative analysis, providing crucial information regarding the end-diastolic and end-systolic volumes (EDV and ESV), as

well as the EF of the ventricles. However, the available and intricate nature of the processing software for GBP-S remains a key factor limiting the widespread adoption of GBP-S over its planar counterpart.

One commercially available GBP-S software package is Quantitative Blood Pool SPECT (QBS), which forms part of the Cedars-Sinai Cardiac Suite, developed by QUAD [23]. QUAD was formerly known as the Artificial Intelligence in Medicine (AIM) program, a research program at the Department of Medicine at Cedars-Sinai. The sophisticated algorithm, described in detail by Van Kriekinge and colleagues [2,24], was initially developed for automatic quantitative measurements of the LVEF [2]. Later, it was expanded to encompass the calculation of right ventricular (RV) volume and the EF values [24].

In a nutshell, QBS software employs an automatic analysis of short-axis images, utilising a surface-gradient-based algorithm for the determination of ellipsoidal coordinate systems for the ventricles [4,6,10,25–27]. These coordinate systems are used to compute the endocardial surface for each gating interval, ultimately facilitating the determination of ED and ES ventricle volumes [2,25–27]. These volumes are used to calculate the RVEF and LVEF values. The software automatically calculates these parameters for both the LV and RV. In our clinic, Universitas Academic Hospital in Bloemfontein, South Africa, GBP-S hasn't been a routine patient procedure. To acquaint ourselves with the software package, we focussed solely on LV volumes and EFs in this study.

To validate the software, it is essential to compare the accuracy of the LV volumes and EF values of GBP-S studies obtained with the QBS software with the true volumes and EF values. However, direct comparison with true values can be challenging in a clinical setting. While comparison with CMR studies may be valuable, CMR has its limitations as discussed earlier. A viable alternative is using the 4D-XCAT phantom and the SIMIND Monte Carlo (MC) program to simulate GBP-S studies. These simulated studies are clinically realistic, provide precise cardiac volume and EF values, and can serve as a reliable benchmark for assessing the accuracy of these values determined with the GBP-S processing software.

In our prior research [28,29], the 4D-XCAT models proved to be a valuable substitute for patients, replicating realistic human anatomy without subjecting researchers or patients to radiation exposure. In this study [29], we simulated and processed 64 GBP-P studies using four commercial software programs. Building on this foundation, we used the same 4D-XCAT models to simulate and process 64 GBP-S studies, employing the widely used QBS processing software.

Our primary objective was to evaluate the accuracy of the fully automated QBS processing software in measuring global LV EF, EDV and ESV values for simulated GBP-S studies, with the known values of the 4D-XCAT models regarded as the gold standard in this study.

3. Materials and Methods

3.1. 4D-XCAT Models and Monte Carlo Simulations

The 64 cardiac models generated with the 4D-XCAT software are described in a previous publication [29]. These models were meticulously simulated following the established guidelines of GBP-S studies [30]. A summary of the parameters used to create the models is given below:

- All models were generated to include cardiac and respiratory motion [31–34]. The entire heart was translated and/or rotated to mimic respiratory motion.

- No other factors were used for scaling of any other organs.
- As per guidelines, sixteen time-frames per cardiac cycle were used for all models [30].
- The matrix size of the segmented activity- and density maps used for the simulation were generated as 512 × 512, with a voxel size of 0.98 × 0.98 × 0.98 mm^3.

An example of the 4D-XCAT model's parameter file is shown in Appendix C1, encompassing all necessary parameters for model definition. To generate 64 distinct models, the heart_base file, the organ_file and the gender were configured to specify the model type and gender. Parameters hrt_v1 to hrt_v5 were instrumental in establishing LV volumes throughout the cardiac cycle with adjustments tailored for each model to create a range of EF values. Additionally, the hrt_scale_x, hrt_scale_y, and hrt_scale_z parameters were modified to scale the models' hearts employing the scaling factors of 0.95, 1.00, 1.05, and 1,10. As detailed in a prior article [29], these parameter variations resulted in the generation of 64 different 4D-XCAT models.

The gamma camera model, validated for simulating the GBP-S studies, is described in a previous publication [28]. The 16 time-frame output files created respectively for all 64 models using the 4D-XCAT program, known as the activity- and density maps, were used as input files for the MC simulation code. A segmented map of one of the 4D-XCAT models is shown in Figure 4.1. The images represent the cardiac ED- and ES phases, respectively.

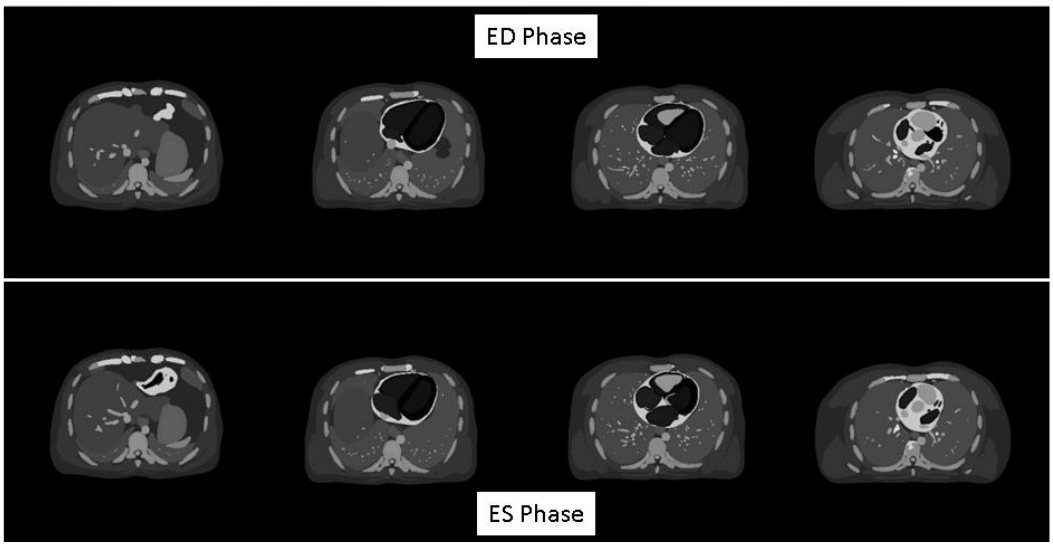

Figure 4.1: A segmented map of a 4D-XCAT model with the heart during ED- and ES phases.

The phantoms' activity distributions were based on bio-kinetic data from a previous article [29]. The activity for the models ranged between 554 MBq and 904 MBq (15 – 25 mCi).

The SIMIND MC version 6.2 program[35] was used to simulate the GBP-S models. For each of the 16 time-frames of the cardiac cycle, 64 projection images were simulated using an energy window of 15%, centred on the 140-keV photopeak of ^{99m}Tc. The simulation of the acquisition was done over a 180° arc around the phantom, mimicking detectors fitted with low energy high resolution (LEHR) collimators. The distance between the collimators and the phantom was maintained at 1 cm. The starting point (Detector 1) was positioned at right anterior oblique, while the endpoint (Detector 2) was at left posterior oblique, as illustrated in Figure 4.2. A montage of a single time-frame comprising 64 projections of one of the 4D-XCAT models is shown in Figure 4.3.

With the matrix size selected as 64 × 64 and a 1.45 zoom factor (as determined according to Pieters et al [28]), the pixel size was 6.59 mm. Poisson noise was added to the simulation process to resemble clinical images, as suggested by Ljungberg [35,36].

The 64 projection images for each of the 16 time-frame were concatenated to mimic a realistic GBP-S study, ensuring compatibility for reconstruction using Siemens Syngo software [37]. Concatenation was done using ImageJ [38], and an in-house program converted images of the GBP-S study to DICOM file format. The simulated GBP-S studies were transferred and processed on the Siemens Syngo processing workstation at the Nuclear Medicine department at Universitas Academic Hospital in Bloemfontein, South Africa.

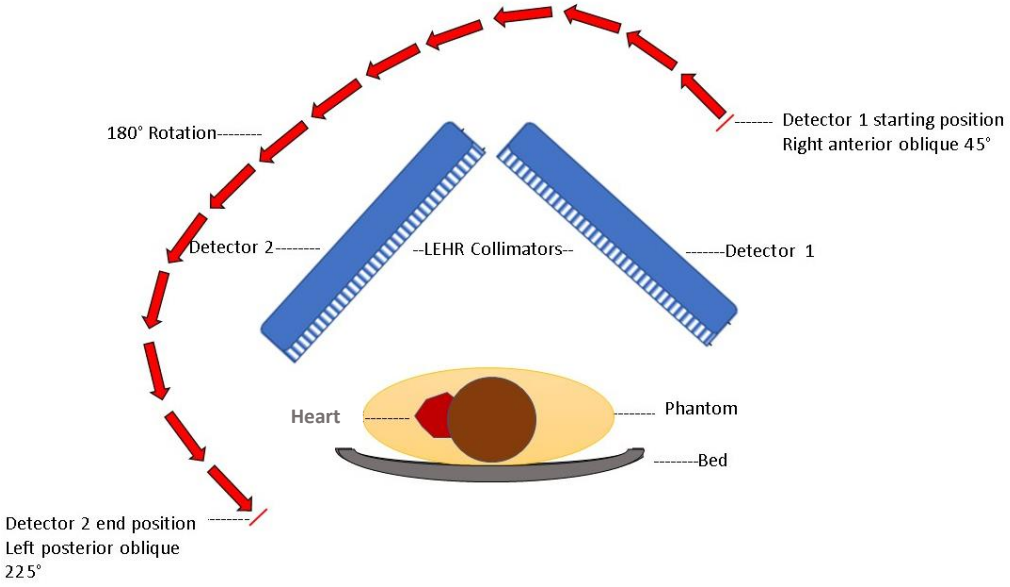

Figure 4.2: Illustration of GBP-S acquisition

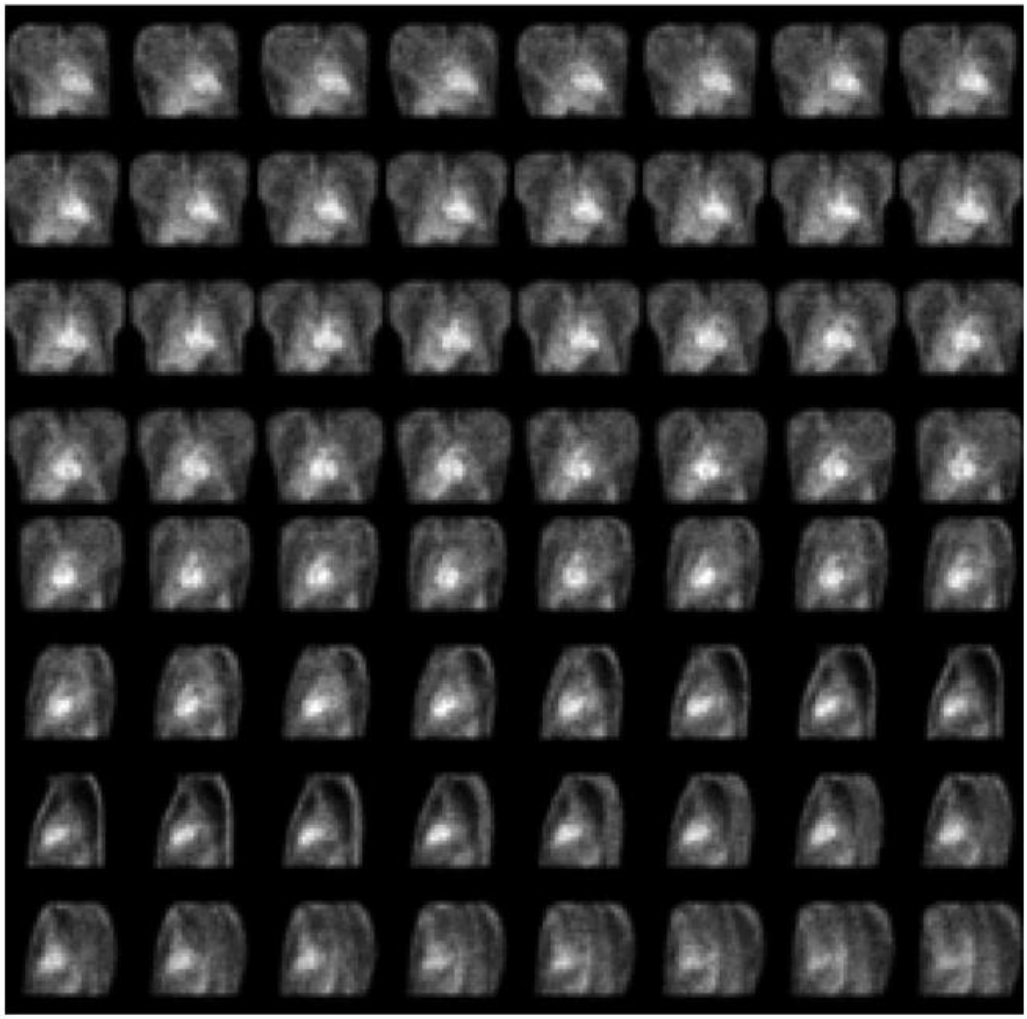

Figure 4.3: A montage of one time-frame of a GBP-S 4D-XCAT model.

3.2. Processing the simulated GBP-S studies

The GBP-S studies were reconstructed using both the FBP and the OSEM reconstruction algorithms. The projection data were reconstructed by FBP with a Butterworth filter (cut-off frequency: 0.5 times the Nyquist frequency, order 5). For OSEM reconstruction, we employed 8 subsets, 4 iterations and applied a Gaussian post-filter (FWHM = 8.4mm). Post reconstruction, the images were reoriented into vertical long-axis, horizontal long-axis and short-axis slices. Subsequently, both FBP and OSEM reconstructed images were analysed with the QBS software, facilitating a comparison of the outcomes generated by the two reconstruction algorithms.

The QBS algorithm used the gated short-axis image data sets as input. It automatically fitted left and right ventricular regions of interest (ROIs) and calculated EDV and ESV, along with the EF values. In this study, we reported results only for the LV. Count-based calculations were performed as recommended by Cedars-Sinai, with a 35% threshold level. The specific 35% count threshold value was also chosen by De Bondt [39] since it had been used successfully in previous studies to derive myocardial surfaces from myocardial perfusion gated SPECT and from GBP SPECT images [27]. We have focused exclusively on the results derived from automatic

processing, foregoing the manual processing option, to enhance our comfort and proficiency in utilising the software.

We recorded the LV volume and LVEF values for all reconstructed studies using the FBP and OSEM algorithms. These values were compared to the true values extracted from the 4D-XCAT log files. The assessment involved a comprehensive analysis through linear regression to evaluate the accuracy and alignment between the simulated, reconstructed data and the ground truth from the 4D-XCAT models.

4. Statistical analysis

The LV EDV, ESV and EF results are presented as mean ± standard deviation (SD). Pearson correlation coefficients (R) expressed the correlations between the calculated and true LV volume and EF values. R values were interpreted as follows: R < 0.3 indicates a poor correlation, R = 0.3–0.5 denotes a fair correlation, R = 0.6–0.8 signifies a moderately strong correlation, and R ≥ 0.8 represents a very strong correlation [40].

The Standard Error of Estimate (SEE) quantifies the variability around the regression line. Bland–Altman analysis, which examines differences between pairs of estimated and reference values, was employed to identify trends and systematic errors. Statistical significance was defined as a *p* – value less than 0.05. Regression analysis, SEE determination, and *p* – value calculations were performed using the Data Analysis Toolkit in Excel.

5. Results

The simulation of the 4D-XCAT models adhered to the parameters outlined in section 2.1. The generated database includes a wide range of LV EDV (78 – 159 ml), ESV (22 – 94 ml) as well as EF values (19.8 – 77.2 %).

The QBS software encountered automatic analysis failure in three of the 64 GBP-S studies (<5%) that were reconstructed using FBP algorithm (QBS_{FBP}). However, after adjusting the Butterworth filter's cutoff frequency from 0.5 cycle/cm to 0.7 cycle/cm, these three studies were analysed successfully using the QBS software. Notably, all GBP-S studies that were reconstructed using the OSEM algorithm (QBS_{OSEM}) were successfully processed using the QBS software. The result page of the QBS software measuring the LVEF for one of the 4D-XCAT models is shown in Figure 4.4.

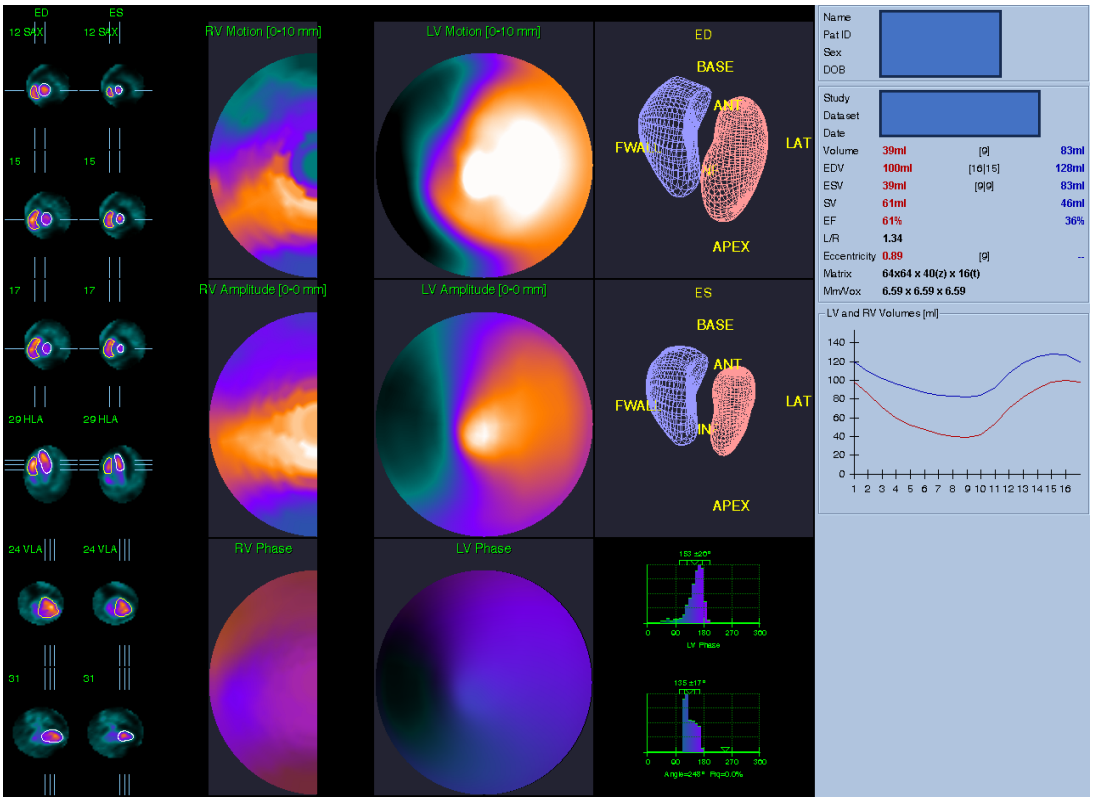

Figure 4.4: QBS software determining the LVEF of this particular 4D-XCAT GBP-S model

The largest differences obtained between the known 4D-XCAT, and processed volume values were as follows: EDV: 41.1 ml (QBS_{FBP}) and 37.0 ml (QBS_{OSEM}); ESV: 48.8 ml (QBS_{FBP}) and 44.8ml (QBS_{OSEM}). The maximum EF differences were 27.2 and 19.2 EF units for the QBS_{FBP} and QBS_{OSEM} data, respectively. Appendix C2 illustrates the differences between FBP and OSEM results over all studies regarding the LV EDV, ESV, and EF values. Table 4.1 reveals that the disparities between the mean known 4D-XCAT values and the mean QBS_{OSEM} values are smaller compared to the differences between the mean known 4D-XCAT values and the mean QBS_{FBP} values.

Table 4.1: Comparison of the mean and standard deviation (SD) of the 4D-XCAT LV volumes and EF values with the QBS results obtained for the FBP and OSEM reconstructed data. Mean and SD were calculated across the results of all 64 models.

	4D-XCAT (known)	**QBS-analysis**	
		QBS_{FBP}	QBS_{OSEM}
EDV (ml)	115.6 ± 24.7 ml	121.8 ± 28.2 ml	113.6 ± 24.2 ml
ESV (ml)	53.7 ± 18.7 ml	51.7 ± 21.6 ml	49.4 ± 18.0 ml
EF (%)	53.7 ± 13.0 %	57.7 ± 14.9 %	56.3 ± 14.1 %

Mean values of LV EDV, ESV and EF values from 4D-XCAT, QBS_{FBP} and QBS_{OSEM} are shown in Table 4.1. No significant difference was found for EDV between the known 4D-XCAT and QBS data (Table 4.2). EDV was slightly over- and underestimated by QBS_{FBP} and QBS_{OSEM},

respectively, when compared to 4D-XCAT [115.6 ± 24.7 (4D-XCAT), 121.8 ± 28.2 ml (QBS_{FBP}), 113.6 ± 24.2 ml (QBS_{OSEM})]. For ESV no significant difference was found between the known 4D-XCAT and QBS data [53.7 ± 18.7 ml (4D-XCAT), 51.7 ± 21.6 ml (QBS_{FBP}), 49.4 ± 18.0 ml (QBS_{OSEM})], (Table 4.2). For LVEF, no significant differences were observed between 4D-XCAT and QBS data [53.7 ± 13.0 % (4D-XCAT), 57.7 ± 14.9 % (QBS_{FBP}), 56.3 ± 14.1 % (QBS_{OSEM})], (Table 4.2).

Table 4.2: P – values obtained in the comparison of the FBP and OSEM reconstructed data with the known data (4D-XCAT)

	QBS_{FBP}	**QBS_{OSEM}**
LV EDV	0.22	0.56
LV ESV	0.53	0.15
LVEF	0.12	0.29

We conducted linear regression and Bland-Altman analyses to compare the QBS results with the known values (4D-XCAT) for the LV EDV, ESV and EFs. The assessment encompassed both the FBP and OSEM reconstructed data. The results of the linear regression and Bland-Altman analyses are visually presented in Figure 4.5 and Figure 4.6, respectively.

The calculated LV EDV using the 4D-XCAT models showed a moderately strong correlation with the corresponding values determined with QBS_{FBP} (R = 0.76 and SEE: 18.30 ml) and a very strong correlation for QBS_{OSEM} (R = 0.88 and SEE: 11.39 ml) (Figure 4.5a and Figure 4.5b, respectively). Similarly, the LV ESV determined with the 4D-XCAT models demonstrated a moderately strong correlation with QBS_{FBP} (R = 0.76 and SEE: 13.73 ml) and very strong QBS_{OSEM} (R = 0.86 and SEE: 9.25 ml) values (Figure 4.5c and Figure 4.5d, respectively). Furthermore, the LVEF values calculated with the 4D-XCAT models correlated very strongly with both QBS_{FBP} (R = 0.87 and SEE: 7.41 ml) and QBS_{OSEM} (R = 0.91 and SEE: 6.01) (Figure 4.5e and Figure 4.5f, respectively).

In the Bland-Altman analysis, the difference (mean ± 1.96SD) of LV EDV obtained from the 4D-XCAT models versus corresponding QBS_{FBP} and QBS_{OSEM} values was -5.7 ± 36.2 ml (Figure 4.6a) and 2.52 ± 23.1 ml (Figure 4.6b), respectively. Similarly, for LV ESV, the difference between the LV ESV values obtained from the 4D-XCAT models and those derived from QBS_{FBP} and QBS_{OSEM} were 2.2 ± 27.3 ml (Figure 4.6c) and 4.7 ± 19.1 ml (Figure 4.6d), respectively. In the case of LVEF, Bland-Altman analysis detected small systematic errors in the LVEF estimation. The mean difference between the LVEF values obtained from 4D-XCAT models and calculated with QBS_{FBP} and QBS_{OSEM} were -3.8 ± 14.5 % (Figure 4.6e) and -2.6 ± 11.7 % (Figure 4.6f), respectively.

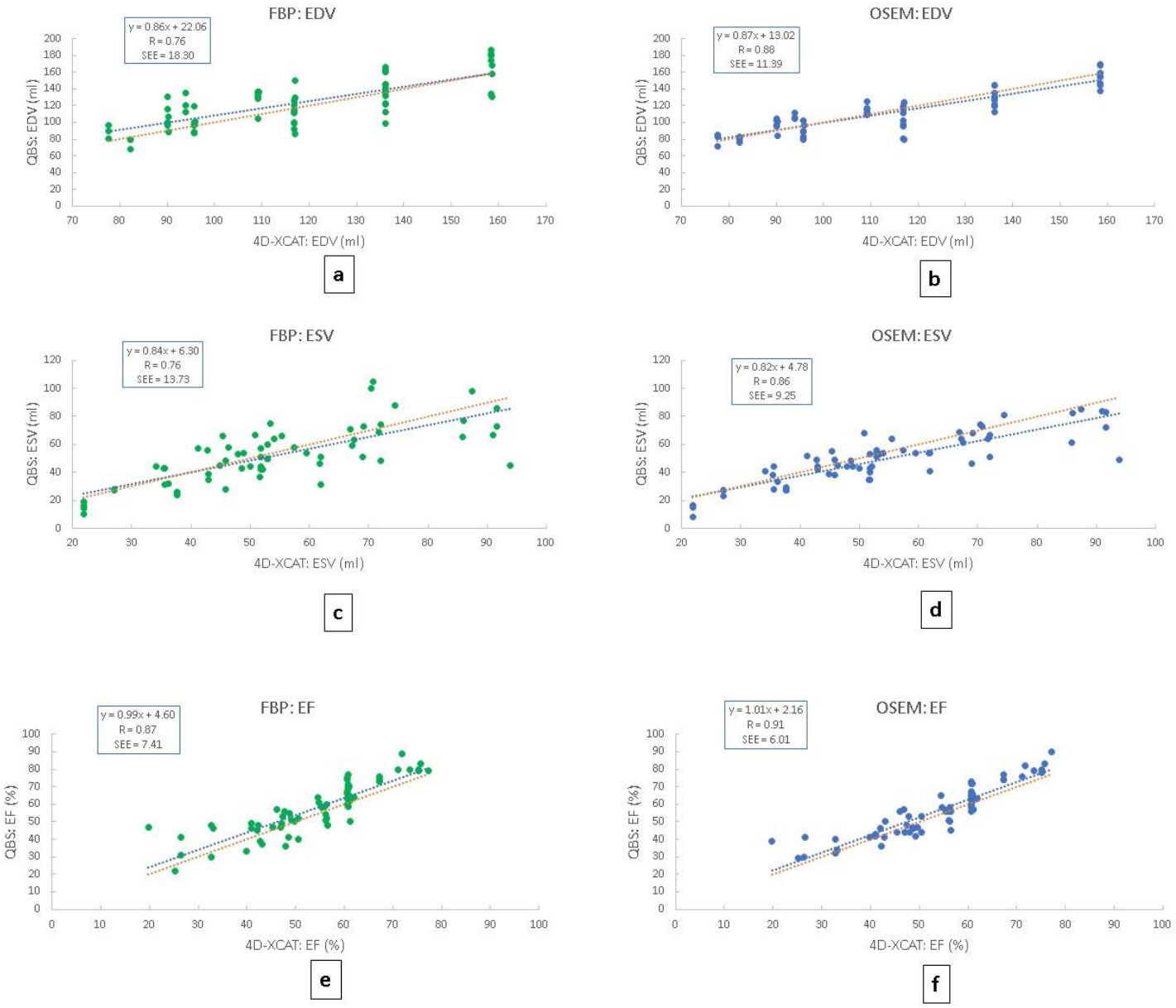

Figure 4.5: Linear regression analysis for comparison of the QBS results with the known 4D-XCAT values for the left ventricle EDV (a & b), ESV (c & d) and EF (e & f) results. The analysis is shown for the FBP (a, c, e) and OSEM (b, d, f) reconstructed data. The blue dotted lines represent the regression lines obtained and the line of identity is shown as an orange dotted line on the graphs.

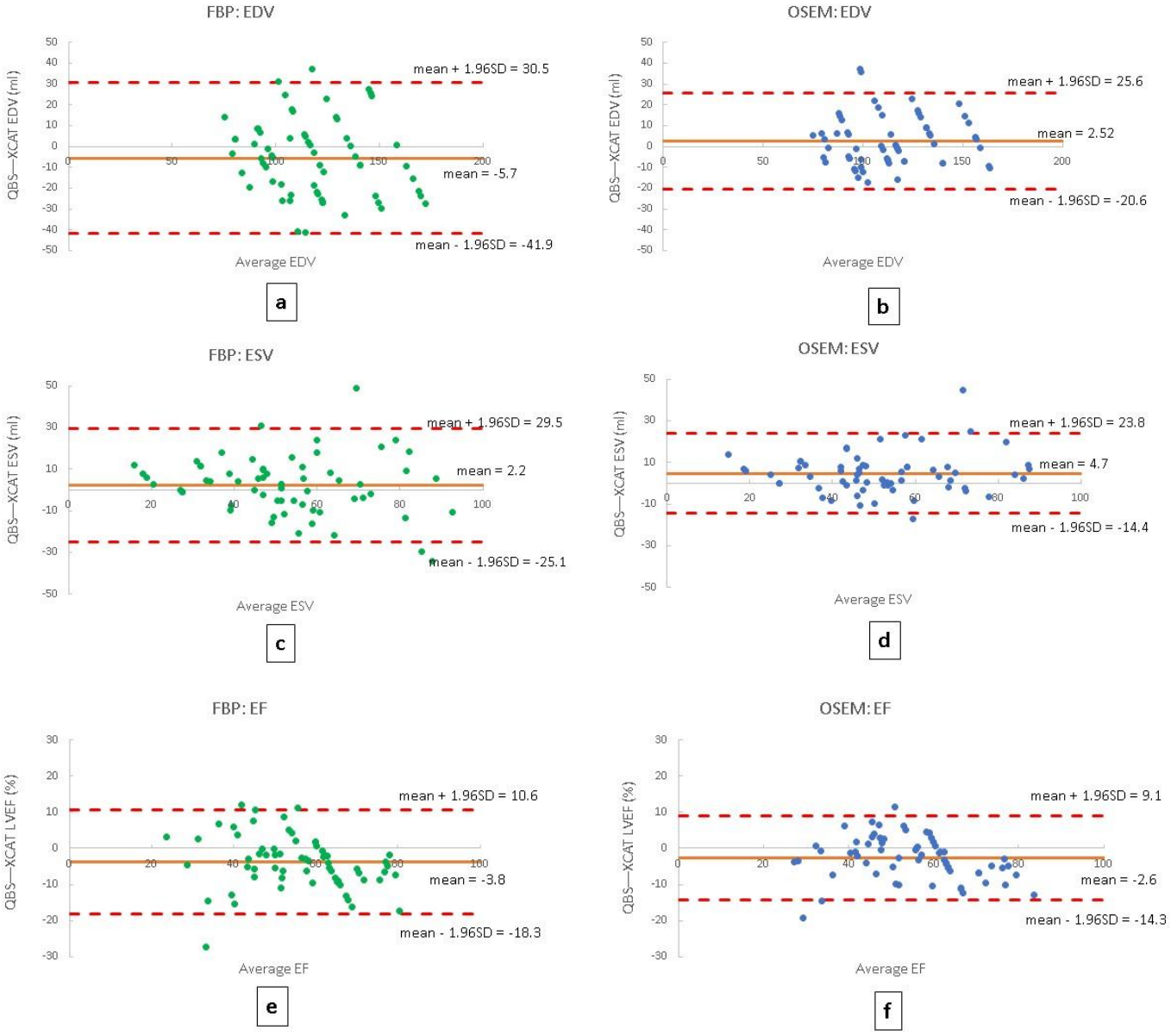

Figure 4.6: Bland-Altman plots for the left ventricular EDV (a & b), ESV (c & d) and EF (e & f) results. The Bland-Altman plots are given for the FBP (a, c, e) and OSEM (b, d, f) reconstructed data. The orange line represents the mean values, while the red dashed lines represent the limits of agreement for the Bland-Altman plots

6. Discussion

The significance of LVEF in comprehending and predicting patient outcomes, particularly in the context of post-chemotherapy follow-up assessments, cannot be overstated. This study not only successfully generated a database of GBP-S studies, but also employed them to validate the accuracy of the commercially available fully automatic processing software, QBS. The estimation of LV EDV, ESV, and EF values were evaluated, using the 4D-XCAT models as the ground truth. Patient study limitations, such as not knowing the true ventricular volumes or the exact EF, the realism of the phantoms, and mimicking true GBP-S in terms of activity and background counts, were all overcome in this study by utilising the digital 4D-XCAT models.

In a previous article, these 4D-XCAT models were also used to simulate 64 GBP-P studies [29]. Each GBP-P study had 32 time-frames, whereas a GBP-S study had 16 time-frames. By comparing the 4D-XCAT models, the largest difference in LVEF values between the GBP-P and GBP-S studies was 0.45%, which can be attributed to the 32 vs 16 time-frames.

The cardiac chambers volume of the 64 models are clinically realistic compared to data from Kawel-Boehm's reference ranges [41]. The unmatched realistic detail of the 4D-XCAT models is evident. It allows for the evaluation of software packages, such as QBS, that utilise complicated algorithms based on anatomical features of the heart to determine LV and RV volumes and EF values. It was demonstrated that the successful processing of the studies depends on the filter used to reconstruct the gated SPECT data. As mentioned before, automatic processing was the primary focus of this study. This study did not involve any manual intervention. The success rate of QBS automatic processing has been described to range from 70% to 89% [2,4,6,8,25,26]. Although three of the FBP reconstructed studies in our investigation required a higher-order reconstruction filter, using the OSEM reconstruction resulted in a 100% processing success rate.

Overall, the Pearson Correlation coefficient (R) was moderately strong (R = 0.76) for the correlation between the known values and the calculated EDV and ESV values, and very strong (R = 0.87) for the EF values obtained from the FBP reconstructed data. For the data reconstructed by OSEM, the R ≥ 0.86 for the EDV, ESV, and EF values, suggest a strong correlation between the known values obtained from the 4D-XCAT model and the processed data. The EF values processed from QBS_{OSEM} correlate better with the known values than those obtained from QBS_{FBP}.

QBS_{FBP} results in an overestimation of smaller volumes for determining LV EDV (Figure 4.5a) and an underestimation of larger volumes for calculating LV ESV (Figure 4.5c). However, QBS_{OSEM} tends to underestimate larger volumes when determining LV EDV and ESV. Both reconstruction methods have a linear correlation in terms of the LVEF.

In terms of the Bland-Altman analysis, for the LV EDV, LV ESV and LVEF, OSEM reconstruction results in narrower limits of agreement, which is suggested by the SEE. The SEE is the highest for EDV values and the lowest for EF values. The study found no significant difference between the known and processed values from either the QBS_{FBP} or QBS_{OSEM} methods.

7. Conclusion and Future studies.

This investigation enhances the significance of 4D-XCAT simulated models in modern-era research, providing a valuable tool for validating software packages without subjecting the researchers or patients to radiation. The importance of these models for GBP-P studies was underscored in a preceding investigation [29].

The reconstructed data plays an immense role in accurately processing GBP-S studies. Due to faster computation times and stronger computation power, IR algorithms such as OSEM have gained popularity. This study demonstrates the difference between FBP and OSEM reconstructed data regarding LV volumes and EFs.

Fully automated QBS demonstrated a strong correlation and close agreement with 4D-XCAT models in measuring LV volumes and EF values, offering a rapid and clinically useful technique. The high success rate observed in the automated processing of GBP-S studies with QBS reduces the necessity for manual intervention. This investigation has laid the foundation for

future research purposes in terms of GBP-S processing. Future research would focus on validating manual volume calculations for both left and right ventricles and optimising GBP-S reconstruction filters by comparing QBS-derived volume values to those from 4D-XCAT studies.

8. References

1. Bartlett ML, Srinivasan G, Barker WC, Kitsiou AN, Dilsizian V, Bacharach SL. Left ventricular ejection fraction: Comparison of results from planar and SPECT gated blood-pool studies. *J Nucl Med*. 1996;37:1795-1799.

2. Van Kriekinge SD, Berman DS, Germano G. Automatic quantification of left ventricular ejection fraction from gated blood pool SPECT. *J Nucl Cardiol*. 1999;6:498-506. doi:10.1016/s1071-3581(99)90022-3

3. Groch MW, Depuey EG, Belzberg AC, Erwin WD, Kamran M, Barnett CA, Hendel RC, Spies SM, Ali A, Marshall RC. *Planar Imaging Versus Gated Blood-Pool SPECT for the Assessment of Ventricular Performance: A Multicenter Study*. *J Nucl Med.* 2001;42:1773-1779.

4. Harel F, Finnerty V, Ngo Q, Grégoire J, Khairy P, Thibault B. SPECT versus planar gated blood pool imaging for left ventricular evaluation. *J Nucl Cardiol*. 2007;14(4):544-549. doi:10.1016/j.nuclcard.2007.04.020

5. Sibille L, Bouallegue F Ben, Bourdon A, Micheau A, Vernhet-Kovacsik H, Mariano-Goulart D. Comparative values of gated blood-pool SPECT and CMR for ejection fraction and volume estimation. *Nucl Med Commun*. 2011;32(2):121-128. doi:10.1097/MNM.0b013e32834155f1

6. Wright GA, Thackray S, Howey S, Cleland JG. *Left Ventricular Ejection Fraction and Volumes from Gated Blood-Pool SPECT: Comparison with Planar Gated Blood-Pool Imaging and Assessment of Repeatability in Patients with Heart Failure*. *J Nucl Med.* 2003;44:494-498. http://www.sghms.ac.uk/depts/phs/staff/jmb/compsd.htm

7. Higuchi T, Taki J, Nakajima K, Kinuya S, Ikeda M, Namura M, Tonami N. Left ventricular ejection and filling rate measurement based on the automatic edge detection method of ECG-gated blood pool single-photon emission tomography. *Ann Nucl Med*. 2004;18(6):507-511. doi:10.1007/BF02984568

8. Hacker M, Hoyer X, Kupzyk S, La Fougere C, Kois J, Stempfle HU, Tiling R, Hahn K, Störk S. Clinical validation of the gated blood pool SPECT QBS® processing software in congestive heart failure patients: Correlation with MUGA, first-pass RNV and 2D-echocardiography. *Int J Cardiovasc Imaging* 2006;22:407-416. doi:10.1007/s10554-005-9031-1

9. Imbert L, Marie PY. Low-dose gated bloodpool SPECT: Is it time to make the shift? *J Nucl Cardiol*. 2021;28(3):951-954. doi:10.1007/s12350-019-01872-z

10. Kim SJ, Kim IJ, Kim YS, Kim YK. Gated blood pool SPECT for measurement of left ventricular volumes and left ventricular ejection fraction: Comparison of 8 and 16 frame gated blood pool SPECT. *Int J Cardiovasc Imaging*. 2005;21(2-3):261-266. doi:10.1007/s10554-004-6133-0

11. Nosir YFM, Fioretti PM, Vletter WB, Boersma E, Salustri A, Postma JT, Reijs AEM, Ten Cate FJ, Roelandt JRTC. Accurate measurement of left ventricular ejection fraction by three-

dimensional echocardiography: A comparison with radionuclide angiography. *Circulation*. 1996;94(3):460-466. doi:10.1161/01.CIR.94.3.460

12. Cwajg E, Cwajg J, Keng F, He ZX, Nagueh S, Verani MS. Comparison of global and regional left ventricular function assessed by gated-SPECT and 2-D echocardiography. *Portuguese journal of cardiology*. Published online 2000.

13. Scatteia A, Silverio A, Padalino R, De Stefano F, America R, Cappelletti AM, Dalla Vecchia LA, Guarini P, Donatelli F, Caiazza F, Dellegrottaglie S. Non-invasive assessment of left ventricle ejection fraction: Where do we stand? *J Pers Med*. 2021;11(11). doi:10.3390/jpm11111153

14. Man SC, van der Wall EE, Swenne CA. Gated SPECT: What's the ideal method to measure LVEF? *Int J Cardiovasc Imaging*. 2008;24(8):807-810. doi:10.1007/s10554-008-9359-4

15. Foley TA, Mankad S V, Anavekar NS, Bonnichsen CR, Morris MF, Miller TD, Araoz PA, Araoz P. Measuring Left Ventricular Ejection Fraction-Techniques and Potential Pitfalls. *Citation: European Cardiology*. 2012;8(2):108-122. doi:https://doi.org/10.15420/ecr.2012.8.2.108

16. Xie BQ, Tian YQ, Zhang J, Zhao SH, Yang MF, Guo F, Wang DY, Wei HX, Chu KW, He ZX. Evaluation of left and right ventricular ejection fraction and volumes from gated blood-pool SPECT in patients with dilated cardiomyopathy: Comparison with cardiac MRI. *J Nucl Med*. 2012;53(4):584-591. doi:10.2967/jnumed.111.096057

17. Kjaer A, Lebech AM, Hesse B, Leth Petersen C. *Right-Sided Cardiac Function in Healthy Volunteers Measured by First-Pass Radionuclide Ventriculography and Gated Blood-Pool SPECT: Comparison with Cine MR*; *Clin Physiol Funct Imaging.* 2005;25:344-349.

18. Huang H, Nijjar PS, Misialek JR, Blaes A, Derrico NP, Kazmirczak F, Klem I, Farzaneh-Far A, Shenoy C. Accuracy of left ventricular ejection fraction by contemporary multiple gated acquisition scanning in patients with cancer: Comparison with cardiovascular magnetic resonance. *J Cardiovasc Magn Reson*. 2017;19(1). doi:10.1186/s12968-017-0348-4

19. Strugnell WE, Hamilton-Craig CR, Parry TA, Bartlett HJG, Slaughter RE. Cardiac MRI is superior to gated blood pool imaging in the assessment of left ventricular function in patients post-cardiac transplantation. *Heart Lung Circ*. 2010;19(7):400-405. doi:10.1016/j.hlc.2010.02.007

20. Verrecchia-Ramos E, Morel O, Retif P, Ben Mahmoud S. Innovative procedure for measuring left ventricular ejection fraction from 18F-FDG first-pass ultra-sensitive digital PET/CT images: evaluation with an anthropomorphic heart phantom. *EJNMMI Phys*. 2021;8(1). doi:10.1186/s40658-021-00387-2

21. Odagiri K, Wakabayashi Y, Tawarahara K, Kurata C, Urushida T, Katoh H, Satoh H, Hayashi H. Evaluation of right and left ventricular function by quantitative blood-pool SPECT (QBS): Comparison with conventional methods and quantitative gated SPECT (QGS). *Ann Nucl Med*. 2006;20(8):519-526. doi:10.1007/BF03026815

22. Dercle L, Ouali M, Pascal P, Giraudmaillet T, Chisin R, Lairez O, Marachet MA, Rousseau H, Bastié D, Bouallègue F Ben, Berry I. Gated blood pool SPECT: The estimation of right ventricular volume and function is algorithm dependent in a clinical setting. *J Nucl Cardiol*. 2015;22:483-492. doi:10.1007/s12350-014-0062-7

23. Cedars-Sinai. QUAD - Quantitative Diagnostic Software Group. 2022. Accessed October 1, 2023. https://www.csaim.com/

24. Daou D, Van Kriekinge SD, Coaguila C, Lebtahi R, Fourme T, Sitbon O, Parent F, Slama M, Le Guludec D, Simonneau G. Automatic quantification of right ventricular function with gated blood pool SPECT. *J Nucl Cardiol*. 2004;11(3):293-304. doi:10.1016/j.nuclcard.2004.01.008

25. Vanhove C, Franken PR. Left ventricular ejection fraction and volumes from gated blood pool tomography: Comparison between two automatic algorithms that work in three-dimensional space. *J Nucl Cardiol*. 2001;8(4):466-471. doi:10.1067/mnc.2001.115518

26. Nichols K, Humayun N, De Bondt P, Vandenberghe S, Akinboboye O, Bergmann S. Model dependence of gated blood pool SPECT ventricular function measurements. *J Nucl Cardiol*. Published online 2004:282-292. doi:10.1016/j.nuclcard.2004.01.007

27. De Bondt P, Claessens T, Rys B, De Winter O, Vandenberghe S, Segers P, Verdonck P, Dierckx RA. Accuracy of 4 different algorithms for the analysis of tomographic radionuclide ventriculography using a physical, dynamic 4-chamber cardiac phantom *J Nucl Cardiol*. 2005;46:165-171.

28. Pieters H, Van Staden JA, Du Plessis FCP, Du Raan H. Validation of a Monte Carlo simulated cardiac phantom for planar and SPECT studies. *Physica Medica*. 2023;111(May). doi:10.1016/j.ejmp.2023.102617

29. Pieters H, Van Staden JA, Du Raan H, Nel MG, Engelbrecht G. (2023) *ASSESSMENT OF PLANAR GATED BLOOD POOL PROCESSING SOFTWARE USING A SIMULATED PATIENT PHANTOM DATABASE* [Manuscript submitted for publication]. Accessed October 12, 2023. https://www.sciencedirect.com/journal/heliyon

30. Hesse B, Lindhardt TB, Acampa W, Anagnostopoulos C, Ballinger J, Bax JJ, Edenbrandt L, Flotats A, Germano G, Stopar TG, Franken P, Kelion A, Kjaer A, Le Guludec D, Ljungberg M, Maenhout AF, Marcassa C, Marving J, McKiddie F, Schaefer WM, Stegger L, Underwood R. *EANM/ESC Guidelines for Radionuclide Imaging of Cardiac Function*. Vol 35.; 2008. doi:10.1007/s00259-007-0694-9

31. Segars WP, Sturgeon G, Mendonca S, Grimes J, Tsui BMW. 4D XCAT phantom for multimodality imaging research. *Med Phys.* 2010;37:4902-4915. doi:10.1118/1.3480985

32. Segars WP, Tsui BMW, Cai J, Yin FF, Fung GSK, Samei E. Application of the 4D XCAT Phantoms in Biomedical Imaging and Beyond. *IEEE Trans Med Imaging*. 2018;37(3):680-692. doi:10.1109/TMI.2017.2738448.Application

33. Segars WP, Bond J, Frush J, Hon S, Eckersley C, Williams CH, Feng J, Tward DJ, Ratnanather JT, Miller MI, Frush D, Samei E. Population of anatomically variable 4D XCAT adult phantoms for imaging research and optimization. *Med Phys*. 2013;40(4). doi:10.1118/1.4794178

34. Kainz W, Neufeld E, Bolch WE, Graff CG, Kim CH, Kuster N, Lloyd B, Morrison T, Segars P, Yeom YS, Zankl M, Xu XG, Tsui BMW. Advances in computational human phantoms and their applications in biomedical engineering - A topical review. *IEEE Trans Radiat Plasma Med Sci*. 2019;3:1-23. doi:10.1109/TRPMS.2018.2883437

35. Ljungberg M. The SIMIND Monte Carlo Program – Medical Radiation Physics, Lund. Published 2020. Accessed December 4, 2021. https://simind.blogg.lu.se/

36. Ljungberg M. Monte Carlo simulations for therapy imaging. *J Phys Conf Ser*. 2011;317. doi:10.1088/1742-6596/317/1/012016

37. Siemens Healthineers. syngo.via - Siemens Healthineers. Accessed August 15, 2023. https://www.siemens-healthineers.com/medical-imaging-it/advanced-visualization-solutions/syngovia

38. Schneider CA, Rasband WS, Eliceiri KW. *NIH Image to ImageJ: 25 Years of Image Analysis HHS Public Access*. Vol 9.; 2012.

39. De Bondt P. *Evaluation of Cardiac Volumes by New Scintigraphic Techniques*. Degree of doctor in medical sciences. University of Ghent; 2005.

40. Chan YH. *Biostatistics 104: Correlational Analysis*. Vol 44. 12th ed.; 2003.

41. Kawel-Boehm N, Hetzel SJ, Ambale-Venkatesh B, Captur G, Francois CJ, Jerosch-Herold M, Salerno M, Teague SD, Valsangiacomo-Buechel E, van der Geest RJ, Bluemke DA. Reference ranges ("normal values") for cardiovascular magnetic resonance (CMR) in adults and children: 2020 update. *J Cardiovasc Magn Reson*. 2020;22. doi:10.1186/s12968-020-00683-3

CHAPTER 5 – Summary and Future Work

Table of Contents

1. Introduction

Gated blood pool (GBP) studies are integral to the field of Nuclear Medicine, providing crucial insight into cardiac function, particularly the left ventricle ejection fraction (LVEF). The LVEF assesses changes in ventricular volume during the end-diastolic (ED) and end-systolic (ES) phases of the cardiac cycle. It plays a pivotal role in detecting, diagnosing, and managing various cardiac diseases. The longstanding preference for GBP planar (GBP-P) methods in measuring the LVEF stems from their validation, non-invasiveness, and straightforward application. Nevertheless, GBP-P studies face challenges such as anatomical overlap, necessitating the use of background correction techniques.

SPECT studies are the three-dimensional (3D) analogue of planar studies. Theoretically, superior, GBP SPECT (GBP-S) studies eliminate some of the GBP-P challenges by being truly volumetric, without the need for any background correction. GBP-S has also been found to enhance the evaluation of regional wall motion by reducing the effects of chamber overlap. Unfortunately, the transition to 3D volumetric studies necessitates the use of more complex algorithms and processing software.

Accuracy and precision are vital in both GBP-P and GBP-S methods to prevent misdiagnosis, ensure appropriate treatment, and avoid negligence. Rigorous testing and comparison to known or true values are imperative for GBP-P and GBP-S processing software programs to meet the general standards as those outlined by regulatory organisations e.g. the Food and Drug Administration. Digital hybrid phantoms, which combine the strengths of voxelised and mathematical phantoms, can accurately mimic human anatomy and physiology. The unparalleled anthropomorphic details of the 4D-XCAT digital hybrid phantom has led to its success in cutting-edge research. These phantoms can be used in conjunction with the Monte Carlo code SIMIND to simulate GBP-P and GBP-S studies, generating databases for testing and validating various GBP-P and GBP-S software packages. The use of 4D-XCAT models to simulate GBP-P and GBP-S studies not only avoids radiation exposure to patients and researchers but also improves the reliability of outcomes of GBP-P and GBP-S software packages by providing benchmark input parameters for evaluation.

2. Study Overview

2.1 Research aim

This study advocates the use of accurate computerised models of human anatomy and physiology, such as the advanced 4D-XCAT phantoms to mimic GBP-P and GBP-S studies. It further emphasises the importance of assessing the accuracy of new and existing processing software packages to determine LVEF values for both GBP-P and GBP-S studies. The study's primary goal was to assess the accuracy of LVEF values of GBP-P and GBP-S studies determined with commercial software programs. This was done by using simulated GBP-P and GBP-S studies of 4D-XCAT patient models with varying cardiac volumes and functions. This chapter (Chapter 5) summarises the outcomes achieved for each objective, offering valuable insight and proposing directions for future research.

2.2 Research objectives

In pursuit of our overarching aim, we established three distinct objectives, outlined in Chapter 1. Each of these objectives was treated as an independent research study, with the findings documented in three separate publishable manuscripts and documented in Chapters 2, 3 and 4.

In Chapter 2, Article 1, titled *"Validation of a Monte Carlo simulated Cardiac Phantom for Planar and SPECT Studies"*, the paramount importance of simulations takes centre stage. Firstly, we validated the modelled Siemens Symbia gamma camera successfully using ^{99m}Tc in accordance with the National Electrical Manufacturers Association (NEMA) guidelines. In the second phase of the study, a stereolithography printer was used to print two 3D cardiac phantoms. These phantoms represented the ED and the ES phases of the heart, respectively. These printed phantoms were filled with radioactivity (^{99m}Tc) and imaged as per published GBP-S guidelines, employing three distinct zoom factors. From the study results, the optimal zoom factor for acquiring GBP-S studies was determined to be 1.45. These acquisitions of the printed cardiac phantoms filled with ^{99m}Tc were also successfully simulated and verified using the SIMIND-modelled Symbia gamma camera.

Acknowledging the constraints associated with physical phantoms, the third aspect of this study focused on assessing and validating the 4D-XCAT model. Segmented images created from the CT images of the two printed cardiac models were used to simulate GBP-P and GBP-S images. Upon individually processing these simulated studies, a remarkable agreement between the known and GBP-P and GBP-S calculated ventricular parameters, specifically LV volumes and LVEF, confirmed the reliability of using the 4D-XCAT model to simulate cardiac imaging. This article was accepted for publication in *Physica Medica* (Appendix A) [1].

The successful simulation of GBP-P studies using 4D-XCAT models paved the way for the investigation detailed in Article 2 titled, *"Assessment of Planar Gated Blood Pool Processing Software using a Simulated Patient Phantom Database"*, elucidated in Chapter 3. A database comprising 64 4D-XCAT models, each featuring diverse cardiac chamber volumes and EF values, was meticulously generated. These models were used to simulate 64 GBP-P studies and served as the foundation for evaluating the accuracy in determining LVEF values across four commercially available GBP-P processing software packages. A strong correlation was found between the calculated LVEF values of the GBP-P studies determined with the processing software packages and the known LVEF values obtained from the 4D-XCAT models, affirming the reliability and accuracy of the four commercially available GBP-P processing software packages. This manuscript has been submitted for review with the intent of publication in *Heliyon* (manuscript number: HELIYON-D-23-48640; Appendix B) [2].

Chapter 4 expands on the research of 4D-XCAT models and GBP-S studies, with the title "Assessment of SPECT Gated Blood Pool Processing Software using a Simulated Patient Phantom Database". This work will be submitted for publication as a third article. The previously generated 4D-XCAT GBP database was this time, simulated according to GBP-S guidelines, laying the foundation for the validation of a commercially available GBP-S processing software, namely QBS (Cedars-Sinai). Notably, this study also shed light on the

possible differences between FBP and OSEM reconstructed data, particularly in relation to LV volumes and EFs.

In this investigation, the fully automated QBS processing software program demonstrated a strong correlation and close agreement with 4D-XCAT models in determining LV volumes and EF values. OSEM reconstructed studies resulted in a slightly better correlation with 4D-XCAT models LV volumes and EF values than the FBP reconstructed studies. The noteworthy success rate of automatically processed GBP-S studies with the QBS software further highlighted the reduced necessity for manual intervention, emphasising the efficiency and reliability of the automatic approach.

3. Future work

The work in Chapter 2 (Article 1) could be expanded by utilising a 3D printer to print an entire anthropomorphic torso and/or abdominal phantom based on a 4D-XCAT model's realistic anatomy with various organ inserts. The final phantom will therefore include a more realistic attenuation and scatter environment. This can be used to evaluate the effect of overlapping anatomies (for example lung, aorta, soft tissue), on the obtained LVEF values in GBP-P studies. The anthropomorphic torso phantom can also contribute to research, quality assurance, and training within the Nuclear Medicine field.

Extending the use of the database of GBP-P studies created from the 4D-XCAT models (as described in Chapter 3) to a multi-centre study opens possibilities to assess the accuracy of LVEF value determination across various commercially available processing software packages and institutionalised protocols. These insights gained from these results can contribute to the development of new algorithms for LVEF calculation. Further investigations can delve into strategies to mitigate potential underestimation biases, particularly evident at lower LVEF values. The models can offer opportunities to develop more practical methods to determine the right ventricle EF from GBP-P studies. The database of GBP-P studies created from the 4D-XCAT models can also be used to assess the accuracy of count-based methods for the calculation of LV volumes using LV volume values of 4D-XCAT models as reference.

Future work will involve optimising reconstruction algorithms (used in Chapter 4), specifically focusing on filters, and number of iterations for iterative reconstruction algorithms. This refining will be achieved through a comparative analysis of volume and EF values obtained from the QBS software and those derived from the 4D-XCAT models. Expanding these investigations will include validating manual calculations for both left- and right ventricle volumes and EF values. Once the validation of QBS is successfully concluded, this investigation can broaden into a multi-centre study, validating other GBP-S processing software packages.

4. References

1. Pieters H, Van Staden JA, Du Plessis FCP, Du Raan H. Validation of a Monte Carlo simulated cardiac phantom for planar and SPECT studies. *Physica Medica*. 2023;111(May). doi:10.1016/j.ejmp.2023.102617

2. Pieters H, Van Staden JA, Du Raan H, Nel MG, Engelbrecht G. (2023) *Assessment Of Planar Gated Blood Pool Processing Software Using A Simulated Patient Phantom Database* [Manuscript submitted for publication]. Accessed October 12, 2023. https://www.sciencedirect.com/journal/heliyon

APPENDICES

Table of Contents

Appendix A: Article 1 – Front page of the published article

Physica Medica 111 (2023) 102617

Contents lists available at ScienceDirect

Physica Medica

journal homepage: www.elsevier.com/locate/ejmp

Validation of a Monte Carlo simulated cardiac phantom for planar and SPECT studies

Hané Pieters *, Johannes A van Staden, Frederik C.P. du Plessis, Hanlie du Raan

Department of Medical Physics, University of the Free State, PO Box 339, Bloemfontein 9301, South Africa

ARTICLE INFO

Keywords:
SIMIND
Stereolithography 3D printed phantom
Gated blood pool studies
4D-XCAT

ABSTRACT

Purpose: This work aimed to validate Monte Carlo (MC) simulated cardiac phantoms for the evaluation of planar- and SPECT-gated-blood-pool (GBP-P and GBP-S) studies.

Methods: A comparison of gamma camera system performance criteria measurements (energy resolution, spatial resolution, sensitivity) with MC simulations was conducted. Furthermore, the accuracy of measured and simulated volumes of two stereolithography-printed cardiac phantoms (based on 4D-XCAT phantoms) was assessed. Finally, the simulated GBP-P and GBP-S XCAT studies were validated by comparing calculated left ventricular ejection fraction (LVEF) and ventricle volume values with known parameters.

Results: The simulated performance criteria compared well with measured values (energy resolution difference: 0.1 ± 0.10%; spatial resolution (full width at half maximum) difference ≤ 0.5 ± 0.8 mm and system sensitivity difference ≤ 6.2 ± 0.62cps/MBq). The measured and simulated cardiac phantoms were in good agreement; the left anterior oblique views compared well. This is supported by line profiles through these phantoms and on average, simulated counts were 5.8% lower than measured counts. The LVEF values calculated from the GBP-P and GBP-S simulated data differ from known values (2.8 ± 0.64% and 0.8 ± 0.52%). The differences between the known XCAT LV volumes and simulated GBP-S calculated volumes were −1.2 ± 1.91 ml and −1.5 ± 0.96 ml for the end-diastolic and end-systolic volumes.

Conclusion: The MC-simulated cardiac phantom has been validated successfully. Stereolithography-printing allows researchers to create clinically realistic organ phantoms and is a valuable tool for validating MC simulations and clinical software. By conducting GBP simulation studies with various XCAT models, the user will be able to generate GBP-P and GBP-S databases for future software evaluation.

1. Introduction

Gated blood-pool (GBP) scintigraphy (planar and SPECT), using ^{99m}Tc pertechnetate labelled red blood cells (RBCs), is commonly used to evaluate the ventricular function of patients due to excellent reproducibility measures [1,2]. Planar gated blood-pool (GBP-P) imaging is often favoured over GBP SPECT (GBP-S) imaging due to the simplified acquisition and processing protocols [3]. GBP-P imaging is a well-established, highly repeatable, non-invasive technique to evaluate ventricular function, particularly the ejection fraction (EF) of the left ventricle (LV) [4,5].

However, a drawback of GBP-P studies is the overlap of anatomical structures resulting in the left ventricular ejection fraction (LVEF) not being calculated as accurately due to activity contribution from the left atria (LA) and/or right ventricle (RV). Furthermore, the accuracy in determining the right ventricular ejection fraction (RVEF) is compromised due to the overlap between the right atrium (RA) and RV in the left anterior oblique (LAO) view [6,7]. The calculation of EF for GBP-P studies also requires a correction for background activity due to over- and underlying tissue such as lung and soft tissues containing radioactive-labelled RBCs. Low count densities and the partial volume effect are two further factors that may compromise the accuracy of LVEF calculations [8].

In contrast, GBP-S imaging can address many of the shortcomings and challenges of GBP-P studies. Wright et al. [5] reported improved repeatability of EF calculation obtained with GBP-S studies due to ideal ventricle separation and eliminating the need for background correction. Furthermore, GBP-S imaging is considered an "all-in-one"

* Corresponding author.
E-mail addresses: pietersh24@gmail.com (H. Pieters), gubijvs@ufs.ac.za (J.A. van Staden), duplessisfcp@ufs.ac.za (F.C.P. du Plessis), duraanh@ufs.ac.za (H. du Raan).

https://doi.org/10.1016/j.ejmp.2023.102617
Received 28 October 2022; Received in revised form 19 April 2023; Accepted 30 May 2023

Appendix B: Article 2 – Acknowledgement of submission

Heliyon

Assessment of Planar Gated Blood Pool Processing Software using a Simulated Patient Phantom Database

–Manuscript Draft–

Manuscript Number:	HELIYON-D-23-48640
Article Type:	Original Research Article
Section/Category:	Medical Sciences
Keywords:	Gated blood pool studies; left ventricular ejection fraction; Monte Carlo simulations; 4D-XCAT models
Manuscript Classifications:	40.180: Medical physics; 40.180.110: Nuclear medicine; 130.110.180: Cardiology Imaging
Corresponding Author:	Hané Pieters, BMedSc.Hons Klerksdorp/Tshepong Hospital Complex Bloemfontein, Free State SOUTH AFRICA
First Author:	Hané Pieters, BMedSc.Hons
Order of Authors:	Hané Pieters, BMedSc.Hons
	Johannes A van Staden, PhD
	Hanlie du Raan, PhD
	Maria G Nel, MBChB
	Gerrit H J Engelbrecht, MBChB MFamMed MMed(Nuclear Medicine)
Abstract:	Introduction: Planar gated blood pool (GBP-P) radionuclide imaging is valuable for the non-invasive assessment of left ventricular ejection fraction (LVEF). Serial cardiac imaging can be performed to monitor the potential decline in LVEF among patients undergoing cardiotoxic chemotherapy. Consequently, accurate LVEF determination becomes paramount. While commercial software programs have enhanced the LVEF values' reproducibility, the accuracy of these software programs has raised concerns. This study aimed to generate a database of GBP-P studies with known LVEF values using Monte Carlo simulations and assess LVEF values' accuracy using four commercial software programs. Methods: We utilised anthropomorphic 4D-XCAT models to simulate 64 clinically realistic GBP-P studies with Monte Carlo simulations. Four commercial software programs (Alfanuclear, Siemens, General Electric Xeleris, and Mediso Tera-Tomo) were used to process these simulated studies. The accuracy and reproducibility of the LVEF values determined with these software programs and the intra- and inter-observer reproducibility of the LVEF values were assessed. Results: Our study revealed a strong correlation between LVEF values calculated by the software programs and the true LVEF values derived from the 4D-XCAT models. However, all the software programs slightly underestimated LVEF at lower LVEF values. Intra- and inter-observer reliability for LVEF measurements was excellent. Discussion: Accurate LVEF assessment is crucial for determining the patient's cardiac function before initiating and during chemotherapy treatment. The observed underestimation, particularly at lower LVEF values, emphasises the need for the accurate and reproducible determination of these values to avoid excluding suitable candidates for chemotherapy. The software programs' excellent intra- and inter-observer reliability highlights their potential to reduce subjectivity when using the semi-automatic processing option. Conclusion: Our study demonstrates the accuracy and reliability of commercial software programs for determining LVEF values from simulated GBP-P studies. Future research would investigate strategies to mitigate the underestimation biases and generalise findings to diverse patient populations.
Suggested Reviewers:	William Paul Segars Associate Professor, Duke University School of Medicine paul.segars@duke.edu

Appendix C: Additional information and results

C1: 4D-XCAT parameter file (parameters used for gated blood pool simulations, rest of parameters were kept at their default settings)

Table C1: Example of the 4D-XCAT parameter file

mode = 0	# program mode (0 = phantom, 1 = heart lesion, 2 = spherical lesion, 3 = plaque, 4 = vectors, 5 = save anatomical variation)
act_phan_each = 1	# activity_phantom_each_frame (1=save phantom to file, 0=don't save)
atten_phan_each = 1	# attenuation_coeff_phantom_each_frame (1=save phantom to file, 0=don't save)
act_phan_ave = 0	# activity_phantom_average (1=save , 0=don't save)
atten_phan_ave = 0	# attenuation_coeff_phantom_average (1=save, 0=don't save)
motion_option = 2	# motion_option (0=beating heart only, 1=respiratory motion only, 2=both motions)
out_period = 1	# output_period (SECS) (if <= 0, then output_period=time_per_frame*output_frames)
time_per_frame = 0.03125	# time_per_frame (SECS) (**IGNORED unless output_period<=0**)
out_frames = 1	# output_frames (# of output time frames)
hrt_period = 1	# hrt_period (SECS) (length of beating heart cycle; normal = 1s)
hrt_start_ph_index = 0.0	# hrt_start_phase_index (range=0 to 1; ED=0, ES=1.0)
heart_base = vmale50_heart.nrb	# basename for heart files (male = vmale50_heart.nrb; female = vfemale50_heart.nrb)
heart_curve_file = heart_curve.txt	# name for file containing time curve for heart
uniform_heart = 0	# sets the thickness of the LV (0 = default, nonuniform wall thickness; 1 = uniform wall thickness for LV)
hrt_v1 = 132.1858	# sets the LV end-diastolic volume (0 = do not change);
hrt_v2 = 72.9832	# sets the LV end-systolic volume (0 = do not change);
hrt_v3 = 93.9268	# sets the LV volume at the beginning of the quiet phase (0 = do not change);
hrt_v4 = 112.5587	# sets the LV volume at the end of the quiet phase (0 = do not change);
hrt_v5 = 122.3835	# sets the LV volume during reduced filling, before end-diastole (0 = do not change);
hrt_t1 = 0.5	# sets the duration from end-diastole to end-systole, hrt_v1 to hrt_v2 (default = 0.5s);
hrt_t2 = 0.192	# sets the duration from end-systole to beginning of quiet phase, hrt_v2 to hrt_v3 (default = 0.192s);
hrt_t3 = 0.115	# sets the duration of quiet phase, hrt_v3 to hrt_v4 (default = 0.115s);
hrt_t4 = 0.193	# sets the duration from end of quiet phase to reduced filling, hrt_v4 to hrt_v5 (default = 0.193s);
hrt_motion_x = 0.0	#hrt_motion_x (extent in cm's of the heart's lateral motion during breathing; default = 0.0 cm)
hrt_motion_y = 1.2	#hrt_motion_y (extent in cm's of the heart's AP motion during breathing; default = 1.2 cm)
hrt_motion_z = 2.0	#hrt_motion_z (extent in cm's of the heart's up/down motion during breathing; default = 2.0 cm)
hrt_motion_rot_xz = 0.0	#hrt_motion_rot_xz (extent in degrees of the heart's xz rotation during breathing; default = 0.0)
hrt_motion_rot_yx = 0.0	#hrt_motion_rot_yx (extent in degrees of the heart's yx rotation during breathing; default = 0.0)

hrt_motion_rot_zy = 0.0	#hrt_motion_rot_zy (extent in degrees of the heart's zy rotation during breathing; default = 0.0)
gender = 0	# male or female phantom (0 = male, 1 = female), be sure to adjust below accordingly
organ_file = vmale50.nrb	# name of organ file that defines all organs (male = vmale50.nrb, female - vfemale50.nrb)
hrt_scale_x = 1.0	# hrt_scale x
hrt_scale_y = 1.0	# hrt_scale y
hrt_scale_z = 1.0	# hrt_scale z
pixel_width = 0.09766	# pixel width (cm);
slice_width = 0.1	# slice width (cm);
array_size = 512	# array size
subvoxel_index = 1	# subvoxel_index (=1,2,3,4 -> 1,8,27,64 subvoxels/voxel, respectively)
startslice = 1220	# start_slice;
endslice = 1520	# end_slice;
myoLV_act = 1	# hrt_myoLV_act - activity in left ventricle myocardium;
myoRV_act = 2	# hrt_myoRV_act - activity in right ventricle myocardium;
myoLA_act = 3	# hrt_myoLA_act - activity in left atrium myocardium;
myoRA_act = 4	# hrt_myoRA_act - activity in right atrium myocardium;
bldplLV_act = 5	# hrt_bldplLV_act - activity in left ventricle chamber (blood pool)
bldplRV_act = 6	# hrt_bldplRV_act - activity in right ventricle chamber (blood pool)
bldplLA_act = 7	# hrt_bldplLA_act - activity in left atria chamber (blood pool)
bldplRA_act = 8	# hrt_bldplRA_act - activity in right atria chamber (blood pool)
coronary_art_activity = 9	# coronary_art_activity - activity in the coronary arteries
coronary_vein_activity = 10	# coronary_vein_activity - activity in the coronary veins
body_activity = 11	# body_activity (background activity);
skin_activity = 12	# skin_activity (used if skin_thickness is > 0)
liver_activity = 18	# liver_activity;
r_lung_activity = 20	# right_lung_activity;
l_lung_activity = 21	# left_lung_activity;
spleen_activity = 36	# spleen_activity;
art_activity = 42	# artery_activity;
vein_activity = 43	# vein_activity;
energy = 140	# radionuclide energy in keV (range 1 - 40MeV, increments of 0.5 keV) ; for attn. map only
atten_table_filename= atten_table.dat	# for attenuation data calculation

C2: Illustrating the differences between FBP and OSEM results for all 64 models regarding the LV EDV, ESV, and EF values.

Figure C2: Differences (y-axis) between FBP and OSEM reconstructed results for all 64 studies (x-axis) in terms of LV a) EDV (ml), b) ESV (ml), and c) EF values (%)

Appendix D: Ethics approval letter

UNIVERSITY OF THE FREE STATE
UNIVERSITEIT VAN DIE VRYSTAAT
YUNIVESITHI YA FREISTATA

UFS·UV
HEALTH SCIENCES
GESONDHEIDSWETENSKAPPE

Health Sciences Research Ethics Committee

10-Mar-2022

Dear **Miss Hané Pieters**

Ethics Clearance: **Assessment of Ventricular Function using Gated Blood Pool Planar and - SPECT Imaging: A Phantom Study**

Principal Investigator: **Miss Hané Pieters**

Department: **Medical Physics Department (Bloemfontein Campus)**

Submission Page

APPLICATION APPROVED

Please ensure that you read the whole document

With reference to your application for ethical clearance with the Faculty of Health Sciences, I am pleased to inform you on behalf of the Health Sciences Research Ethics Committee that you have been granted ethical clearance for your project.

Your ethical clearance number, to be used in all correspondence is:**UFS-HSD2021/1792/2903**

The ethical clearance number is valid for research conducted for one year from issuance. Should you require more time to complete this research, please apply for an extension.

We request that any changes that may take place during the course of your research project be submitted to the HSREC for approval to ensure we are kept up to date with your progress and any ethical implications that may arise. This includes any serious adverse events and/or termination of the study.

A progress report should be submitted within one year of approval, and annually for long term studies. A final report should be submitted at the completion of the study.

Research conducted in any Department of Health facility: Researchers are required to sign and return the HSREC approval letters to the provincial Department of Health where they applied. It is also a requirement for researchers to submit electronic copies of their final research findings, and/or make a presentation of their findings and recommendations at departmental research days when and where indicated.

The HSREC functions in compliance with, but not limited to, the following documents and guidelines: The SA National Health Act. No. 61 of 2003; Ethics in Health Research: Principles, Structures and Processes (2015); SA GCP(2020); Declaration of Helsinki; The Belmont Report; The US Office of Human Research Protections 45 CFR 461 (for non-exempt research with human participants conducted or supported by the US Department of Health and Human Services- (HHS), 21 CFR 50, 21 CFR 56; CIOMS; ICH-GCP-E6 Sections 1-4; International Council for Harmonisation (ICH) Harmonised Guideline, Integrated Addendum to ICH E6(R1), Guideline for Good Clinical Practice (GCP) E6(R2), 2016, SAHPRA Guidelines as well as Laws and Regulations with regard to the Control of Medicines, Constitution of the HSREC of the Faculty of Health Sciences.

Appendix E: Posters and presentations

E1: Poster presentation (SASNM 2023)

VALIDATION OF PLANAR-GBP LVEF PROCESSING USING MONTE CARLO SIMULATED DIGITAL PATIENT PHANTOMS

H Pieters[1], JA van Staden[2], H du Raan[2]
[1]Department of Nuclear Medicine, Klerksdorp Hospital, Klerksdorp,
[2]Department of Medical Physics, University of the Free State, Bloemfontein

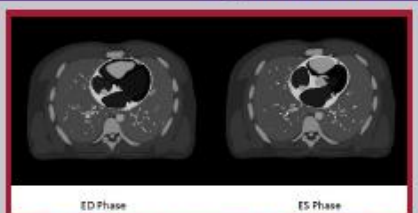

Transaxial slices of the 4D-XCAT phantom during end-diastolic (ED) and end-systolic (ES) phase.

Quantifying left ventricular ejection fraction (LVEF) is important for evaluating cardiac function [1]. Before implementing commercial cardiac processing software programs in clinical practice, it is essential to validate the accuracy and precision of the LVEF values calculated with these programs. The 4D- XCAT software program allows the user to create digital patient phantoms mimicking human anatomy and physiology [2,3].

This study aimed to assess the accuracy of LVEF values obtained with a commercial software program using gamma camera-simulated gated blood pool planar (GBP-P) studies of digital patient models.

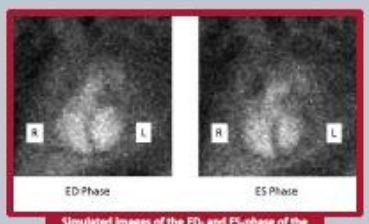

Simulated images of the ED- and ES-phase of the abovementioned model

Digital patient phantoms created with 4D-XCAT and SIMIND Monte Carlo software programs[4] were utilized to simulate 64 male and female gated blood pool planar (GBP-P) studies with a range of LVEF values (19.9% - 77.4%). These simulated GBP-P studies were processed three times by three experienced operators using a commercially available software program, Alfanuclear (AN) [5]. The 'known' LVEF of each 4D-XCAT phantom, determined from the exact volume of the left ventricle in the end-diastolic and end-systolic phases, was considered the gold standard and compared to the calculated LVEF values. Intra- and inter-variability were evaluated using the interclass correlation coefficient (ICC) [6]. Known and calculated LVEF values were compared using regression analysis. Bland-Altman analysis [6] was also used to assess the agreement and identify any systematic trends in differences.

Linear regression of the Alfanuclear calculated data compared to the known values

The intra-observer reliability for all three observers was excellent (ICC_1 = 0.994; ICC_2 = 0.992; ICC_3 = 0.978). The ICC evaluating the interobserver variability was 0.994. The linear regression shows a strong correlation (r = 0.96), with a slight underestimation of the LVEF when the known value is <60%. The Bland-Altman analysis shows that most of the operators' data fall within two standard deviations of the mean, suggesting good agreement between the calculated and known LVEF values. The limits of agreement are narrow, and there is a slight negative bias (-2.9).

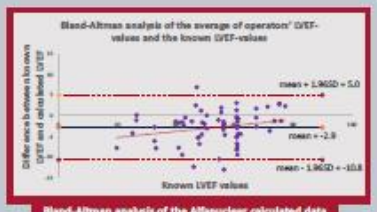

Bland-Altman analysis of the Alfanuclear calculated data compared to the known values

In conclusion, independent processing of GBP-P studies using AN software indicated excellent intra- and interobserver variability. A good agreement was found between the AN calculated LVEF values and the known LVEF of the XCAT simulated images. The digital patient models created with the 4D-XCAT phantom provided a database of studies with known LVEF values whereby AN commercial software was validated. This study will be expanded by evaluating different commercial systems using the same simulated GBP-P studies.

[1] Pieters H, Van Staden JA, Du Plessis FCP, Du Raan H. Validation of a Monte Carlo simulated cardiac phantom for planar and SPECT studies. Phys Medica. 2023;111(May).
[2] Segars WP, Mahesh M, Beck TJ, Frey EC, Tsui BMW. Realistic CT simulation using the 4D XCAT phantom. Med Phys [Internet]. 2008;35(8):3800–8.
[3] Segars WP, Tsui BMW, Cai J, Yin FF, Fung GSK, Samei E. Application of the 4D XCAT Phantoms in Biomedical Imaging and Beyond. IEEE Trans Med Imaging [Internet]. 2018;37(3):680–92.
[4] Ljungberg M. The SIMIND Monte Carlo Program. Sweden; 2020.
[5] Alfanuclear. IM512P: Data and Image Processor. User's Manual. [Internet]. Argentina: Alfanuclear S.A.I.y C.; 2004
[6] Bunting K V., Steeds RP, Slater LT, Rogers JK, Gkoutos G V., Kotecha D. A Practical Guide to Assess the Reproducibility of Echocardiographic Measurements. J Am Soc Echocardiogr [Internet]. 2019;32(12):1505–15

T: +27 51 401 9111 | E: info@ufs.ac.za | www.ufs.ac.za
UFSUV | UFSweb | UFSweb | ufsuv

Inspiring excellence.
Transforming lives.

UNIVERSITY OF THE FREE STATE
UNIVERSITEIT VAN DIE VRYSTAAT
YUNIVESITHI YA FREISTATA
UFS HEALTH SCIENCES

E2: Faculty Forum (UFS Health Sciences) Presentation (Abstract and cover page)

Verification of a 3D Printed Cardiac Phantom with Monte Carlo Simulations for Clinical Validation

Introduction and goal: Gated planar and SPECT blood-pool studies are commonly used to evaluate cardiac ventricular functions. Although SPECT studies have many advantages, it has not yet replaced planar studies, so a thorough evaluation is required. Such an evaluation can be performed using phantoms to avoid radiation hazards to patients and produce reliable outcomes. Physical phantoms are limited due to the fixed size and geometry and are often replaced by digital phantoms. Monte Carlo (MC) simulations of a cardiac phantom were used in this study to provide clinically relevant information. ***The study aimed to verify the MC modelled cardiac phantom by comparing simulated gamma camera images of a digital 3D cardiac phantom with physical measurements of a printed 3D cardiac phantom.***

Method: To verify the modelled gamma camera, NEMA performance criteria measurements were acquired and simulated using the MC code, SIMIND. The results of the simulated and measured data were assessed. SPECT studies of a cardiac phantom, printed using a 3D printer, were acquired and simulated. Both measured and simulated SPECT studies were processed, and the images were compared.

Results: NEMA performance criteria measurements and simulations of the gamma camera compared well. The energy resolution showed a 0.4% difference. For the spatial resolution values, the most significant percentage differences obtained in a scatter medium was 5.1%, and without the scatter medium, 7.9% The sensitivity measurement and simulation resulted in a percentage difference of 6.0%. Acquired and simulated images of the cardiac phantom compared well. The percentage differences between the acquired and simulated average counts for each projection were less than 12%. Line profiles of the measured and simulated projection data showed minor differences.

Conclusion: The modelled gamma camera and cardiac phantom were verified and could be used for further studies.

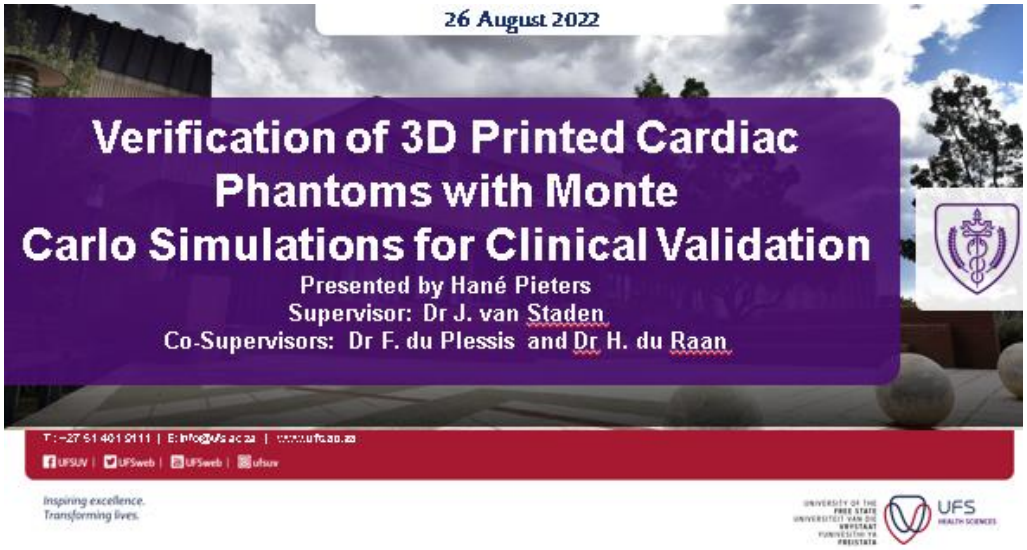

Thesis HPieters

by Hané Pieters

Submission date: 04-Dec-2023 10:50AM (UTC+0200)
Submission ID: 2247272156
File name: Thesis_HPieters_Turmitin.pdf (3.02M)
Word count: 21307
Character count: 117569

UFS

Thesis HPieters

ORIGINALITY REPORT

9%	5%	8%	%
SIMILARITY INDEX	INTERNET SOURCES	PUBLICATIONS	STUDENT PAPERS

PRIMARY SOURCES

1	Zubal, I, and W Segars. "Anthropomorphic Phantoms : Early Developments and Current Advances", Series in Medical Physics and Biomedical Engineering, 2012. Publication	1%
2	Nuclear Medicine Technology Study Guide, 2011. Publication	1%
3	Segars, W. P., Mahadevappa Mahesh, T. Beck, E. C. Frey, and B. M. W. Tsui. "", Medical Imaging 2005 Physics of Medical Imaging, 2005. Publication	1%
4	digital.lib.usu.edu Internet Source	<1%
5	worldwidescience.org Internet Source	<1%
6	"Annual Congress of the European Association of Nuclear Medicine October 13 – 17, 2018 Düsseldorf, Germany", European Journal of Nuclear Medicine and Molecular	<1%